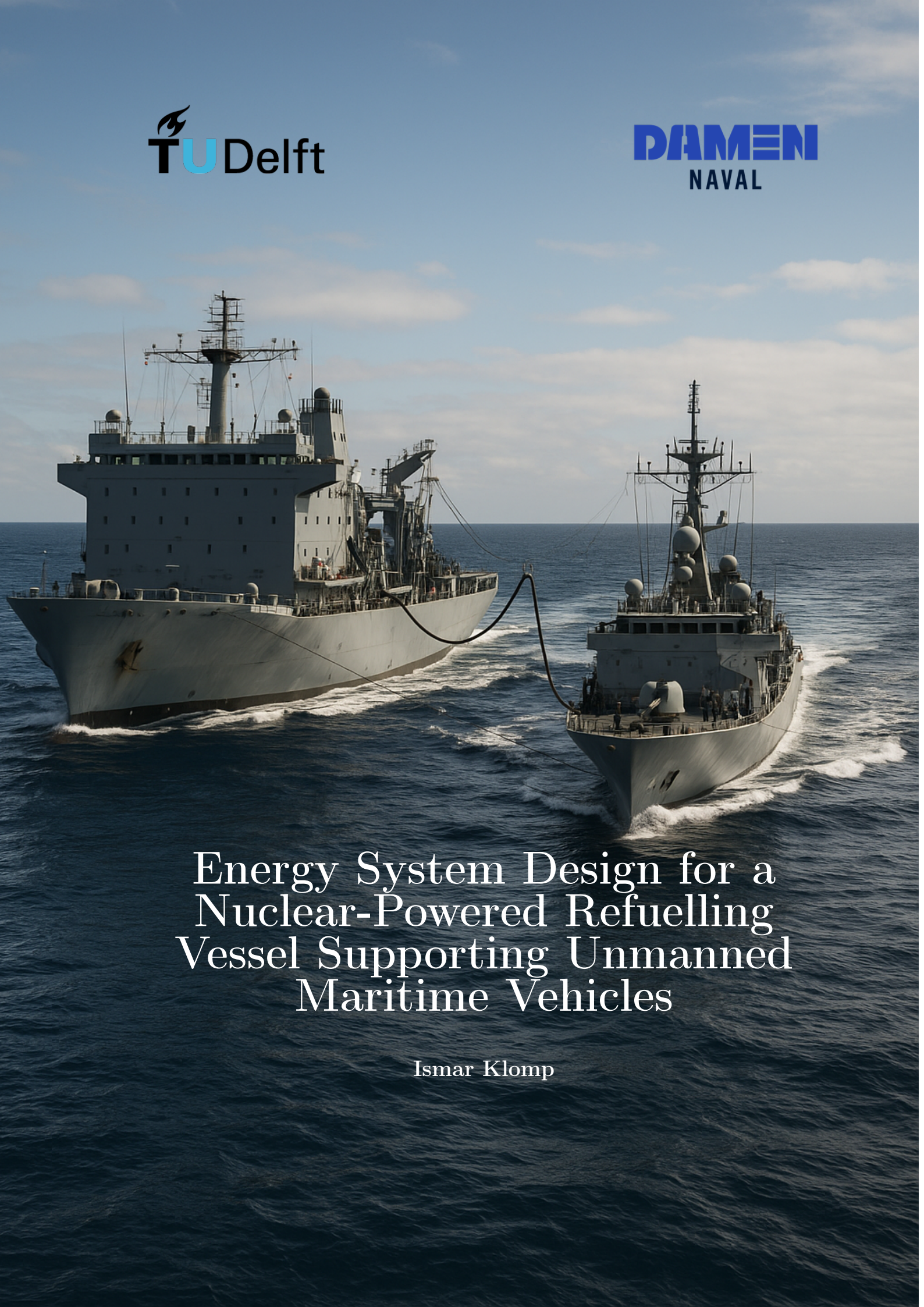

Energy System Design for a Nuclear-Powered Refuelling Vessel Supporting Unmanned Maritime Vehicles

Ismar Klomp

Energy System Design for a Nuclear-Powered Refuelling Vessel Supporting Unmanned Maritime Vehicles

Submitted by

Ismar Klomp

Thesis Report

In fulfilment of the requirements for the degree of
Master of Science
in Mechanical Engineering

at the Department Maritime and Transport Technology of Faculty Mechanical, Maritime and Materials Engineering of Delft University of Technology.

To be defended publicly on Tuesday December 9th, 2025 at 10:00 AM

Student number:	4817761	
MSc track:	Multi-Machine Engineering	
Report number:	2025.MME.9132	
Supervisors:	Dr. Ir. Henk Polinder	TU Delft Supervisor
	Ir. Gert Jan Meijn	Damen Naval Supervisor
	Ir. Sankarshan Durgaprasad	TU Delft Daily Supervisor
Date:	28th November 2025	

TU Delft

DAMEN NAVAL

Preface

I would like to express my gratitude to Gert Jan Meijn for his time and for giving me the opportunity to pursue this Thesis at Damen Naval. I would also like to thank Henk Polinder for supervising me during this process and for introducing me to Sankarshan, who supported me in providing critical and highly valuable feedback throughout the project.

I am also deeply grateful to those closest to me. To my parents, Erik and Judith, whose tireless love and support have allowed me to pursue this academic journey without compromise. And to Eilidh, for all her encouragement and patience during every stage of this thesis.

AI Statement

In this thesis I used Generative AI tools in a supportive manner. AI was used to generate images (such as Figure 2.1 and cover image) and to assist with language improvements, such as grammar and spelling corrections. In addition, an AI-assisted coding tool was used (Matlab Copilot) to help identify errors in MATLAB scripts. In all cases I have reviewed the work and remain fully responsible for the analysis, methods, results, and conclusions presented in this thesis.

Delft, 28th November 2025

Ismar Klomp

Summary

This thesis investigates how a next generation nuclear powered mothership can serve as a self sustaining refuelling hub for a fleet of unmanned maritime vehicles. At its core lies the development of an Energy Management System (EMS) and the first modelling of a fully integrated ship energy architecture capable of producing synthetic fuel for an unmanned fleet. The study connects three fields that are rarely combined: nuclear ship energy systems, onboard fuel production, and autonomous fleet coordination.

Existing research on nuclear propulsion has largely focused on economic feasibility, safety, and reactor lifetime, with limited attention to how such systems could dynamically manage unused power under variable operational loads. In this study, a new concept was developed in which a 140 meter multifunctional support vessel was equipped with a 130 MW_{th} Very High Temperature Reactor serving as the central power source. The reactor's high outlet temperature allows for efficient coupling with process heat systems for onboard fuel synthesis. A complete production chain was modelled, including high-temperature electrolysis for hydrogen generation, Direct Air Capture for CO_2 extraction, and Fischer–Tropsch synthesis for converting syngas into marine diesel (F-76). Together, these subsystems allow the mothership to convert nuclear heat into storable chemical energy, enabling continuous refuelling of its unmanned fleet.

The EMS was developed as the central control layer linking all onboard subsystems while maintaining reactor stability. The rule-based EMS allocates power between propulsion, hotel load, and the fuel production plant, using a 10 MW battery to absorb transient fluctuations and prevent reactor overload. Dynamic simulations confirmed that the system could balance power and mass flows over extended missions, verifying the underlying energy models.

The research then extended the EMS concept beyond internal ship control toward coordinated fleet management. To evaluate this, a series of mission scenarios was modelled for one to six unmanned surface vehicles (USVs), simulating the mothership operating as a refuelling vessel that supports their missions. Initial simulations with a Local EMS coordinating the mothership revealed clear performance limits, as uncoordinated refuelling led to long waiting times and inefficient fuel use. To improve the results the EMS was extended by adding a mixed integer linear optimization framework op top of the mothership internal rule-based EMS. This top optimization layer jointly scheduled refuelling and mission timing for all USVs. This fleet wide EMS enabled sustained operation with six USVs and achieved stable long term mission endurance.

These results show the feasibility of a nuclear powered mothership can acting as the central refuelling hub for an autonomous fleet when governed by a coordinated EMS. The concept demonstrates that with its onboard fuel production system, the mothership requires only a fraction of the fuel normally carried by conventional refuelling ships, and all of it is produced in a carbon-neutral manner. By combining detailed system modelling with optimization driven fleet control, this study outlines a realistic pathway toward persistent and self reliant naval operations independent of traditional logistics support.

Keywords

Energy Management System (EMS); Nuclear-powered mothership; Unmanned Maritime Vehicles (UXVs); Synthetic Fuel Production; Very High Temperature Reactor (VHTR); Fleet-wide Optimization; Dynamic System Modelling; Autonomous Naval Operations

Contents

List of Figures

List of Symbols

Symbol	Description	Units
CO_2	Carbon dioxide	kg, t
H_2	Hydrogen	kg, t
O_2	Oxygen	kg, t
HC	Hydrocarbons	kg, t
CH_4	Methane	kg, t
C_nH_m	Generic hydrocarbon chain	–
η	Efficiency	%
P_x	Power of subsystem x	MW
$\dot{m}_x$	Mass flow rate of stream x	kg/s
E_x	Energy of subsystem x	MWh
M_x	Mass of subsystem x	t
V_x	Volume of subsystem x	m^3
W	Weight or displacement	t
T	Temperature	K, °C
p	Pressure	bar, Pa
ρ	Density	kg/m^3
C_p	Specific heat capacity at constant pressure	kJ/kg·K
$\dot{Q}$	Heat transfer rate	MW
Q_{stored}	Stored heat energy	MJ, MWh
R	Gas constant	J/mol·K
U	Ship speed	m/s, knots
u, v, r	Surge, sway, and yaw velocities	m/s, rad/s
x, y, ψ	Ship position and heading angle	m, rad
F_x, F_y	Forces in surge and sway	kN
N	Yaw moment about the centre	kNm
τ	Torque	Nm
t_{sim}	Simulation time horizon	s, h, day
Δt	Simulation or control timestep	s
α	Reactor ramp-rate coefficient	%/s
μ	Efficiency or penalty multiplier	–
δ	Rudder or thruster angle	deg
SOC	Battery state of charge	%
η_{bat}	Battery round-trip efficiency	–
E_{loss}	Energy losses (conversion or transmission)	MWh
z_i	Binary variable for unit commitment	–
x_i	Continuous decision variable (e.g. power output)	–
J	Objective function value	–
ΔP_{ramp}	Reactor ramp change per time step	MW/s
R_{limit}	Reactor ramp-rate limit	MW/s
L, B, D	Ship length, beam, and draft	m
A_{deck}	Deck surface area	m^2

List of Abbreviations

Abbreviation	Description
UXV	Unmanned "X" Vehicle (generic term for UAV, USV, UUV)
UAV	Unmanned Aerial Vehicle
USV	Unmanned Surface Vehicle
UUV	Unmanned Underwater Vehicle
MUSV	Medium Unmanned Surface Vehicle
SUSV	Small Unmanned Surface Vehicle
LUSV	Large Unmanned Surface Vehicle
AUV	Autonomous Underwater Vehicle
EMS	Energy Management System
MPC	Model Predictive Control
NMPC	Nonlinear Model Predictive Control
PID	Proportional–Integral–Derivative (controller)
LP	Linear Programming
MILP	Mixed-Integer Linear Programming
MINLP	Mixed-Integer Nonlinear Programming
KPI	Key Performance Indicator
TOPSIS	Technique for Order Preference by Similarity to Ideal Solution
VHTR	Very High Temperature Reactor
PWR	Pressurized Water Reactor
MSR	Molten Salt Reactor
LMFR	Liquid Metal Fast Reactor
LFR	Lead-cooled Fast Reactor
SMR	Small Modular Reactor
HTGR	High Temperature Gas-cooled Reactor
SOEC	Solid Oxide Electrolysis Cell
PEM	Proton Exchange Membrane (electrolyser or fuel cell)
DAC	Direct Air Capture unit
RWGS	Reverse Water Gas Shift reactor
FT	Fischer–Tropsch synthesis reactor
ATR	Autothermal Reformer
HTSE	High Temperature Steam Electrolysis
HRS	Heat Recovery System
HRSG	Heat Recovery Steam Generator
HVAC	Heating, Ventilation, and Air Conditioning
SOC	State of Charge (battery)
LHV	Lower Heating Value
HHV	Higher Heating Value
F-76	NATO standard naval diesel fuel
ICE	Internal Combustion Engine
ESS	Energy Storage System
AO	Area of Operation
MATLAB	Matrix Laboratory (numerical software)
Simulink	Dynamic system simulation environment
Gurobi	Commercial optimisation solver
TU Delft	Delft University of Technology

1 | Introduction

Modern warfare is being redefined before our eyes, the battlefield is no longer defined solely by size or tonnage. The war in Ukraine offers a striking demonstration of this truth: low-cost aerial drones and unmanned systems have disrupted traditional army structures and forced a reassessment of how military power is applied. Large surface vessels, once considered the backbone of naval dominance, face a new reality where surprise attacks from unmanned platforms can inflict disproportionate damage. According to one recent assessment, "The last three years have seen navies involved in the most intensive maritime conflict of recent decades... These real-world engagements are reshaping fleet structure, equipment and doctrine for years ahead."[1]

This vulnerability of large battleships has become increasingly apparent and cannot be overlooked. In response to this challenge, new naval concepts have emerged. One proposed strategy is to distribute a large ship's combat and surveillance systems across multiple smaller vessels [1]. By decentralizing these capabilities, a single successful attack would no longer disable the entire system. The use of unmanned support units is considered the most prominent solution in naval applications [2]. The US military has, for this reason, created the term **Unmanned "X" Vehicles (UXVs)**:

- **UAV** – Unmanned Aerial Vehicle
- **USV** – Unmanned Surface Vehicle
- **UUV** – Unmanned Underwater Vehicle

The idea of distributing operational presence over an area comes with significant challenges. One major challenge is that smaller ships have reduced endurance compared to large naval vessels. The fleet must be able to remain in position for extended periods; as stated by the US Navy [3] "up to 8 months without being limited by ships fuel capacity". This requires the availability of refuelling options. Traditionally, refuelling ships must travel long distances and require their own protection, which limits flexibility.

The solution being proposed is a self-sustaining refuelling ship. This concept envisions a mobile fuel-producing vessel capable of replenishing its own energy storage system. The central challenges of this idea lies in the source of energy required to produce fuel onboard and how to manage such a system. The only power source capable of supporting continuous, high-demand production is nuclear power. As shown in Figure 1.1, uranium offers an energy density far greater than that of conventional fossil fuels. This would allow the mothership to generate the power necessary to produce fuel for its fleet.

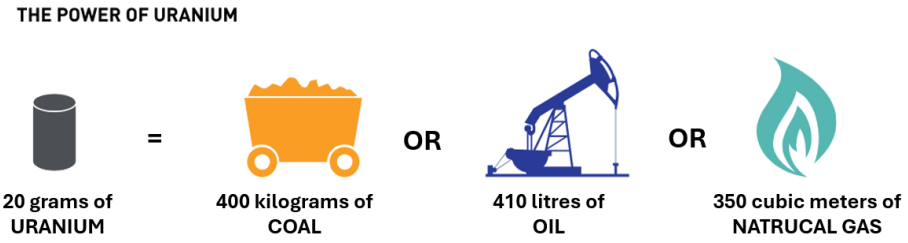

Figure 1.1: Comparison of energy density of uranium versus other fuel types [2]

This thesis focuses on a nuclear powered mothership that functions as a refuelling plant for a fleet of UXVs. These UXVs operate weapon and surveillance systems, thereby enhancing the overall survivability and operational reach of the fleet. Central to the operation of this concept

[1] https://euro-sd.com/2025/03/articles/43406/naval-operations-lessons-from-recent-conflicts
[2] https://cna.ca/reactors-and-smrs/nuclear-fuel/

is an Energy Management System (EMS), which coordinates the distribution of power between propulsion, fuel production, and potentially fleet wide supervision to maintain stable and efficient reactor performance. The work presented here extends ongoing research by developing the first model of a nuclear powered refuelling ship and performing scenario tests to explore how such a mothership could be used and controlled in naval operations. Advancing this concept is essential to keep pace with the rapidly evolving technologies shaping modern conflict.

1.1 Research Questions

The concept of using nuclear-powered ships as refuelling platforms has been explored as early as 1977 [4]. Several studies have proposed component selections and outlined conceptual system designs; however, existing work stops short of developing a complete, verified model that couples onboard fuel production with an integrated energy management system. In particular, the operational behaviour of such a refuelling ship under real-world mission conditions remains largely unexplored.

Based on the literature review in chapter 2, two key research gaps have been identified in the field of nuclear-powered ships and refuelling systems for autonomous fleets:

GAP 1 The integrated modelling and design of a nuclear-powered ship energy system that supports onboard fuel production has not been systematically investigated.

GAP 2 While Energy Management Systems have been studied in isolated ship contexts, their coordinated operation across reactor control, onboard energy distribution, and fleet-level refuelling scenarios has not yet been systematically investigated.

These gaps leads to the central research question of this thesis:

Research Question: "What energy system design is needed for a nuclear-powered naval vessel to function as an independent energy hub for a fleet of unmanned maritime vehicles?"

Answering this research question is done by dividing the problem into a number of sub questions, which, when answered, will form the foundation of the solution to the main research question. These questions are:

Sub-questions:

1. What are the operational requirements and energy demands of the unmanned support units (USVs, UAVs, UUVs) that the mothership must sustain?
2. Which fuel or energy carrier can be practically produced onboard the mothership to meet the UXVs operational constraints?
3. Which reactor type and associated energy conversion technologies are most suitable for providing continuous power to both the mothership's onboard systems and its fuel production plant?
4. How can the energy system architecture (including power distribution, storage, and fuel production subsystems) be modelled to enable the mothership to operate as an independent refuelling hub?
5. What energy management system (EMS) hierarchy can coordinate power generation, storage, and fuel production under varying operational conditions?
6. How does the ship's integrated energy system perform under different EMS strategies (local, mission-aware, and fleet-wide) during realistic refuelling support missions?

1.2 Thesis Outline

This thesis is organized into seven core chapters. Each chapter contributes to answering the sub-questions listed above and builds upon the previous one.

Chapter 2: Literature Review

This chapter reviews literature on nuclear-powered naval systems and autonomous fleet operations. The first three sub-questions guide the review. The main topics explored are:

2.1 **Support Units and Energy Needs:** Classification of UXVs and their energy demands.

2.2 **Naval Energy Carriers:** Assessment of feasible onboard energy carriers.

2.3 **Ship Energy Technologies:** Review of nuclear reactors and Power-to-Liquid systems.

2.4 **Mothership Operations:** Definition of the mothership's role and operating profile.

2.5 **System Scaling:** Initial sizing for shipboard feasibility.

2.6 **Maritime EMS Frameworks:** Review of EMS architectures and control strategies.

2.7 **Research Gap:** Missing integration between onboard fuel production, EMS control, and fleet refuelling.

Chapter 3: Methodology

This chapter outlines the methodological approach taken to ensure future reproducibility.

3.1 **Model Integration:** Bringing all modelling and optimisation components together into a single workflow.

Chapter 4: Modelling of the Ship Energy System Architecture

This chapter models the integrated power and energy system of the mothership. Sub-question four is answered by establishing the baseline model on which all subsequent EMS studies are built.

4.1 **Model Implementation:** Overview of the complete Simulink energy architecture.

4.2 **Power Plant Model:** Representation of reactor, Brayton cycle, and ESS.

4.3 **Fuel Production Plant Model:** Modelling of the full synthetic fuel production chain.

4.4 **Fuel Storage Model:** Representation of onboard fuel storage and refuelling logic.

4.5 **Ship Systems Model:** Modelling of propulsion and hotel loads.

4.6 **Model Verification:** Tests demonstrating correct model behaviour.

Chapter 5: Energy Management System Architecture

This chapter focuses on answering sub-question five by investigating how energy management can be structured to ensure efficient operation under changing mission conditions. The main sections are:

5.1 **Local EMS:** Rule-based EMS implemented in Simulink to manage internal power flows and mission states.

5.2 **Fleet-Wide EMS:** MILP-based optimisation layer using Gurobi to schedule USV refuelling and fleet coordination.

Chapter 6: Model Verification

This chapter verifies that the integrated mothership model behaves realistically by assessing numerical response, and physical feasibility. The main sections are:

6.1 **Steady-State Consistency Test:** Confirms stable power and mass flows under constant operation.

6.2 **Dynamic Ramp-Up Test:** Evaluates system response to a rapid increase in power demand.

6.3 **Dynamic Ramp-Down Test:** Assesses behaviour during sudden load reduction and shutdown.

6.4 **Mission Profile Test:** Validates system performance during a representative refuelling operation.

6.5 **Physical Feasibility Assessment:** Checks whether all subsystems fit within the proposed hull layout.

6.6 **Verification Discussion:** Summarises findings and evaluates overall model feasibility.

Chapter 7: Scenario Testing and Results

This chapter evaluates the performance of the ship system under various operational scenarios. Sub-question six guides the construction of the tests by comparing both EMS layers under identical conditions.

7.1 **Scenario Design:** Mission setup, assumptions, and KPI definitions.

7.2 **Scenario 1 – Local Ship-Centred EMS:** Baseline performance without mission awareness.

7.3 **Scenario 2 – Local Mission-Aware EMS:** Performance with mothership repositioning.

7.4 **Scenario 3 – Mission-Aware EMS (Varying Tasks):** Impact of staggered task durations.

7.5 **Scenario 4 – Fleet-Wide EMS:** Optimised scheduling using Gurobi.

7.6 **Results Discussion:** Comparison and interpretation across all scenarios.

Chapter 8: Conclusion and Recommendations

The final chapter summarizes the main findings and provides recommendations for future research.

2 | Literature review

The concept of employing nuclear-powered ships as refuelling platforms for other vessels has been explored in research since as early as 1977 [4]. In parallel, the use of unmanned vehicles for surveillance, reconnaissance, and other naval operations has developed rapidly. This literature review seeks to bring these two domains together by examining the current state of research on nuclear-powered refuelling concepts for unmanned maritime systems.

This chapter seeks an answer to four sub-questions defined in section 1.1:

SQ1. What are the operational requirements and energy demands of the unmanned support units (USVs, UAVs, UUVs) that the mothership must sustain?

SQ2. Which fuel or energy carrier can be practically produced onboard the mothership to meet the UXVs operational constraints?

SQ3. Which reactor type and associated energy conversion technologies are most suitable for providing continuous power to both the mothership's onboard systems and its fuel production plant?

SQ5. What energy management system (EMS) hierarchy can coordinate power generation, storage, and fuel production under varying operational conditions?

To address these questions, this chapter examines the operational, technological, and control elements that shape the mothership and fleet energy system. section 2.1 examines the unmanned support units relevant to this study, analysing their operational profiles and energy demands to answer SQ1, while section 2.2 identifies the corresponding fuel or energy carrier required for SQ2. section 2.3 then surveys the technologies that enable a nuclear-powered refuelling mothership, including the reactor system, onboard energy storage, and fuel synthesis processes, addressing SQ2 and SQ3. section 2.4 outlines the resulting mothership architecture and its expected operational profile. Finally, section 2.6 reviews existing energy-management approaches in maritime and hybrid energy systems, identifying control hierarchies capable of coordinating power generation, storage, and fuel production within the mothership and across its fleet, thereby answering SQ5.

2.1 Identification of Support Units

"All tactical elements must fight as a cohesive team, must integrate into the whole, the best that can be brought to bear by individual units. These, in the future, will most likely include land and space assets," a quote from Admiral Hayward in 1986, an expert in naval tactics [5]. As he emphasis, that it is vital in modern day combat to use various different support units. The use of these in combination of each other only strengthens tactical operations.

Using different types of units and coordinating large numbers of them requires extensive communication and interaction. For this reason, making these large fleets autonomous is seen as the most effective solution [6]. The ideal support units, as introduced in chapter 1, are the UXVs. Figure 2.1 illustrates the different types. UAVs in the form we know today have already been operational since the Vietnam War in the 1960s [7], with the UUV and the USV becoming more prominent now.

Using unmanned vehicles requires robust control and communication systems, as their operation depends on strict coordination rules and hierarchical structures [8]. An additional advantage is that, if a support unit comes under threat, no human life is placed at risk.

For this study, UXVs are assumed to remain within operational range of the mothership, ensuring safe operation and enabling refuelling directly from its onboard fuel production system. The preceding literature review [9] identified USVs as the most demanding and relevant UXV type for this investigation. A detailed explanation why is illustrated in subsection 10.1.3, with additional analyses of UAVs and UUVs provided in subsection 10.1.1 and subsection 10.1.2. USVs are particularly suitable because naval weapon systems are primarily designed for deployment from surface platforms, making them unsuitable for underwater use and too heavy for aerial vehicles. Consequently, USVs are expected to carry a substantial portion of the weapon payload, and among the UXV classes they also offer the greatest endurance, independence, and payload capacity [10].

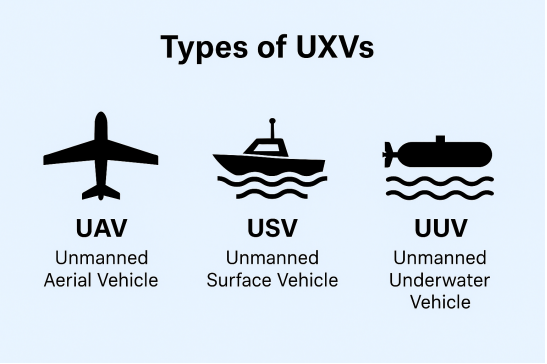

Figure 2.1: UXV types

According to the U.S. Navy [2], there are three classes of USVs that must be considered. These classes are presented in Table 2.1. Relevant examples of each type are shown in Table 10.3 and Table 10.4.

Table 2.1: Overview of USV Sizes and Typical Characteristics as categories by the U.S. Navy[2]

USV Class	**Specifications**	**Power / Endurance**	**Typical Role**
Large (LUSV)	Length: 60–140 m Displacement: >500 t	5–10 MW Endurance: 2–3 weeks	Designed for large payload capacity.
Medium (MUSV)	Length: 25–60 m Displacement: <500 t	0.5–5 MW Endurance: 4–10 days	Versatile multi-role vessel used for patrol and logistics.
Small (SUSV)	Length: <25 m Displacement: <100 t	0.1–1 MW Endurance: 1–2 days	Short-range reconnaissance and coastal operations.

The range of sizes and applications across different USV classes is significant. For this reason, only the segment most relevant to this literature study is considered. Firstly, SUSVs are too small to operate independently on open seas [11]. Their limited size prevents them from carrying substantial weapon systems or keeping pace with the mothership. While one or two SUSVs might be carried onboard for personnel transport, they are not suitable for integration into the mothership's support fleet.

Figure 2.2: The VSX 5209 considered as the reference for MUSV.[12]

LUSVs are also not ideal for the scenarios considered in this study. The main reason is their large size. As explained in chapter 1, the mothership under consideration is a large naval vessel of less than 200 meters in length. A ship of this size would not be able to produce or store sufficient fuel to support the energy demands of multiple LUSVs. Moreover, the low number of LUSVs that could be supported contradicts the concept of operating as a distributed fleet.

This leaves MUSVs as the most suitable USV

type for the intended application. With a typical length of around 50 meters and a minimum endurance of five days as seen in Table 10.3, these vessels are well-suited to carry large naval weapon or surveillance systems. They are also seaworthy and able to maintain formation with the mothership. However, their limited endurance of at most 10-15 days necessitates close proximity to the mothership to ensure regular refuelling.

The VSX 5209 as seen in Figure 2.1 was selected as the reference MUSV for this study. This offshore patrol vessel is designed with a versatile deck layout that allows adaptation to a wide range of operational roles. It features powerful thrusters that provide excellent manoeuvrability for fast responses to emerging situations. Its size and endurance also make it a good benchmark for evaluating the mothership's fuel production capability. The idea is that, if the mothership can meet the energy needs of a fleet of VSX 5209 vessels, it should also be capable of supporting a larger number of smaller units.

To establish realistic energy demands for the VSX 5209, Damen Naval[1] provided an example operational profile. Figure 2.3 shows this profile. The x-axis of the graph represents the vessel's speed, ranging from 0 to 24 knots. The right y-axis shows the propulsion power required for each speed. The left y-axis shows the the typical amount of energy the ship spends at each speed. From this you can deduce how long the ship spends at each speed. This includes not only propulsion energy but also onboard systems such as hotel and combatant loads. From this it can be seen that the ship mainly sails at 12 or 17 knots.

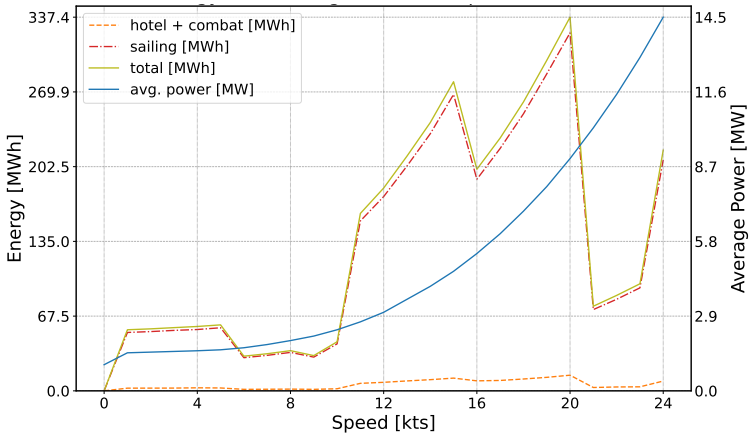

Figure 2.3: Energy spent vs speed (left axis) and average power at each speed (right axis).

For the remainder of this literature study, the VSX 5209 will serve as the representative USV in the fleet. Its operational profile will form the basis for estimating energy demands placed on the mothership.

2.2 Energy Carriers for Naval Refueling

Now that it has been established what type of support units the mothership will provide with energy, it is important to establish the energy carrier medium that will be used by the USVs.

As will be discussed in subsection 2.3.1, nuclear reactors are not easily scaled down to the USV level. This makes the conversion of nuclear energy into another form of energy storage necessary for this system.

The two mediums a nuclear reactor can conventionally convert energy into are thermal energy and electrical energy [13]. A more in depth focus of the nuclear reactor will follow in subsection 2.3.1. The main energy types that can be created from the reactor are demonstrated in Figure 2.4. This graph represents each fuel types energy density vs the power releasing capability with the diagonals showing the duration required to release the energy of one kilogram of the material.

[1] `https://www.damen.com/vessels/defence-and-security/stan-patrol-vessels/vsx-5209-patrol`

The further to the top right, the more suitable the energy carrier is as a fuel type for the USVs. To be considered a feasible fuel source for this application, the energy carrier must have a specific energy of at least 10^2 Wh/kg [15]. This threshold ensures sufficient energy density for long-endurance operations and practical storage on board. Based on this criterion, only fuel cell technology, batteries (specifically lithium-ion batteries), and combustion fuels remain viable candidates. These three fuel sources will now be compared.

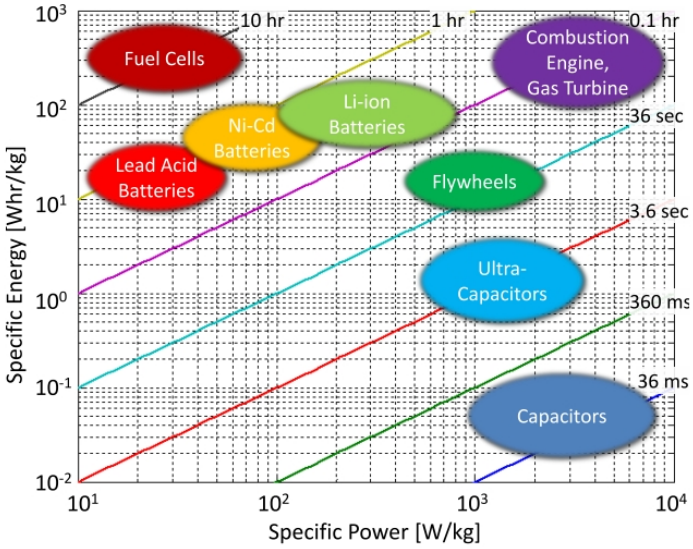

Figure 2.4: Ragone chart of energy storage technologies showing specific power versus specific energy [14].

2.2.1 Lithium Ion Batteries

Lithium-ion batteries remain the industry standard for electrical storage due to their mature supply chains, and extensive commercial deployment. These batteries seem to be a straightforward option for storing reactor generated electricity. However, their suitability rapidly declines when scaled to ship-level energy demands. Despite excellent performance in portable devices and small vehicles [16], lithium-ion systems suffer from low energy density [17]. Even accounting for drivetrain efficiency differences [18], replacing the diesel capacity of the reference USV (section 2.1) would require approximately 3457 m^3 of battery volume and over 3360 tonnes. This is an infeasible size, as illustrated in Figure 2.5. Safety concerns such as thermal runaway under damage or high temperatures further limit military applicability [19]. Charging rates also pose a major constraint: even with 10 MW systems, fully recharging a USV would take more than three days [20]. For these reasons, lithium-ion batteries are unsuitable for long-endurance USVs, though they remain useful for smaller UAVs and UUVs, which can be recharged onboard via an intermediate battery system on the mothership.

2.2.2 Hydrogen Fuel Cell Technology

Since electric batteries are not viable for the USVs, the reactor's electrical output must be converted into a denser chemical fuel. Hydrogen is an attractive option because it can be produced via electrolysis, where electrical energy splits water into hydrogen and oxygen; PEM electrolysers and fuel cells form a common pair for this process [23]. Hydrogen can also be burned directly in combustion engines, though issues such as reduced volumetric efficiency and increased fuel consumption limit its

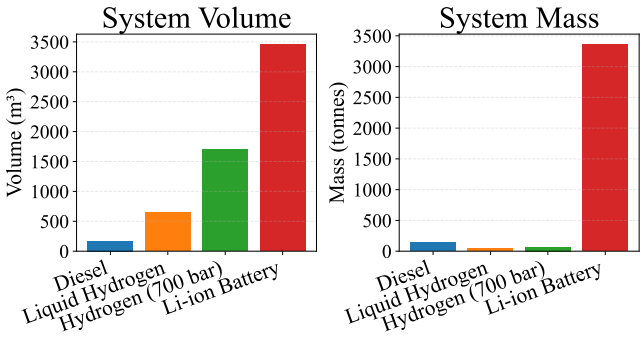

Figure 2.5: USV energy demands converted into equivalent energy carrier volume and mass. Data from [17, 21, 22]

practical performance [21].

Hydrogen storage presents major challenges. At ambient conditions it is extremely energy-sparse, requiring either liquefaction at $-253,^{\circ}$ C or compression to 350–700 bar [24], both of which demand significant energy and complex containment. Although hydrogen is more volumetrically energy dense than batteries, it remains far below diesel, as illustrated in Figure 2.5.

A common strategy to ease storage constraints is to convert hydrogen into ammonia, which liquefies at moderate pressures or at $-33°$C and can later be cracked back into hydrogen. Solid carriers such as metal amine offer additional benefits [24]. However, ammonia is toxic and corrosive, and combustion engine technology for direct ammonia use remains immature. Consequently, the hydrogen–ammonia cycle is noted here for completeness but not considered further.

2.2.3 Combustion Fuels

Given the challenges of storing hydrogen directly, the next step is to convert it into a more stable fuel. Power-to-fuel technology enables this by producing synthetic hydrocarbons. These hydrocarbobs are created through reactions between CO_2 and H_2 using established chemical processes [22].

Candidate fuels include methane, synthetic methanol, and synthetic diesel. Their suitability depends on whether they can be stored for weeks, transferred at sea, and used by different support vessels. LNG methane is compatible with existing engines but requires cryogenic storage at $-163\,^{\circ}$C [25], making it impractical for a refuelling mothership. Methanol is easier to store but is corrosive and only compatible with a limited number of ships [26].

Synthetic diesel emerges as the most practical option: it is non-corrosive, storable at ambient conditions, and already standard across naval fleets. NATO F-76 diesel contains less than 1 percent sulfur [27], and synthetic diesel can be produced to this specification.

The basic steps to convert nuclear energy into synthetic diesel is demonstrated in Figure 2.6. Producing FT diesel requires syngas ($CO + H_2$); hydrogen can be obtained via electrolysis, while CO is produced by reducing CO_2 captured from air or seawater [28]. This is discussed further in section 2.3.

Synthetic diesel is formed via the Fischer–Tropsch (FT) process:

$$(2n+1), \mathrm{H_2} + n, \mathrm{CO} \rightarrow \mathrm{C}n\mathrm{H}2n + 2 + n, \mathrm{H_2O}, \tag{2.1}$$

which converts hydrogen and carbon monoxide into long-chain hydrocarbons [29].

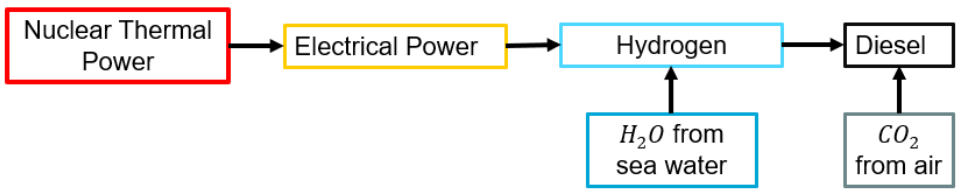

Figure 2.6: energy converging steps from nuclear power to synthetic diesel.

Although the overall efficiency of synthetic diesel production is moderate [29], the aim of this thesis is to determine whether a nuclear-powered mothership can feasibly generate its own fuel to sustain a fleet of USVs. For this purpose, F-76 diesel is selected as the preferred energy carrier.

2.3 Ship Energy System Technologies

The concept of Power-to-Fuel refers to the process of converting electrical energy into a fuel, enabling the storage and transport of energy in chemical form. As discussed in subsection 2.2.3, F-76 is the preferred fuel type to be produced in this system. The idea of generating hydrocarbon fuels from nuclear energy aboard ships has received academic and military attention for several decades. Therefore, this literature study included a keyword-based search to identify relevant research in this domain.

Keywords: Small Modular Reactor, Generation IV Reactor, Synthetic Fuel, Power-to-Liquids, Fischer–Tropsch, Naval Energy Systems, Maritime Fuel

The literature identified studies in which onboard energy systems are designed to produce synthetic fuels. These are summarized in Table 2.2.

Table 2.2: Summary of Key Literature on Shipboard Synthetic Fuel Production

Reference	**Year**	**Reactor Type**	**Fuel Type**	**Summary of Findings**
Bushore [4]	1977	Naval PWR	JP-5 / Diesel	MIT study exploring nuclear-powered synthetic fuel production on a aircraft carrier.
Terry [30]	1995	Naval PWR	JP-5 / Diesel	Designs nuclear naval aircraft carrier for fuel synthesis, suggests all naval ships and aircraft run on a single fuel.
Bogart [31]	2006	HTGR / VHTR	Jet Fuel / Diesel	Proposes mobile and land-based production using HTGRs on a oil tanker sized ship.
Galle-Bishop [32]	2011	MSR (Conceptual)	Synthetic Diesel	Describes a nuclear tanker producing fuels from air and seawater using futuristic components.
Comidy et al. [33]	2019	PWR	Jet Fuel	Evaluates feasibility of onboard synthetic jet fuel using electrolysis and co-electrolysis.
Kapoor and Pawling [34]	2024	Modular Microreactor VHTR	Diesel	Explores compact marine fuel production using a mobile micro nuclear plant.

Each study in Table 2.2 provides detailed analysis of the components involved in shipboard synthetic fuel production, including efficiencies and power requirements. This design builds on those findings by comparing proposed configurations and selecting the most feasible arrangement for the mothership. Across the literature, there is broad agreement on the core elements: all studies employ Fischer–Tropsch synthesis for hydrocarbon production, with Comidy [33] being the only one to focus on jet fuel rather than diesel(a difference in targeted hydrocarbon chain lengths, discussed further in Equation 2.3.5).

Based on this common foundation, a system architecture has been derived for this study. Figure 2.7 presents the resulting layout, showing the major subsystems and their interconnections

in a full-scale synthetic diesel plant.

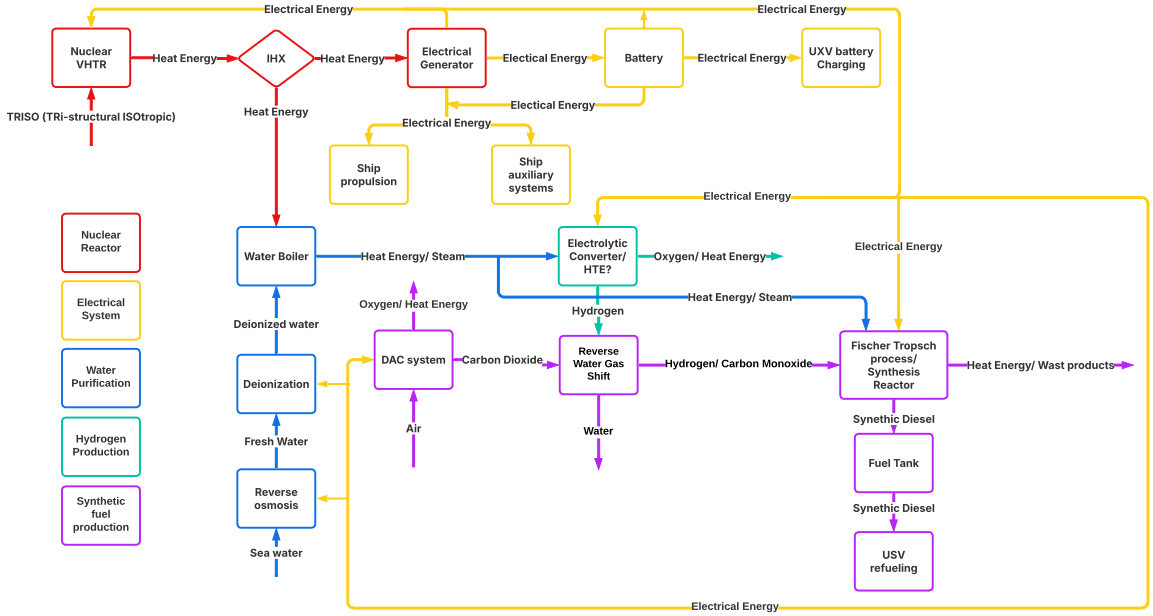

Figure 2.7: Mothership conceptual synthetic diesel production plant subsystem overview

As illustrated in Figure 2.7, the system comprises five main sections: the nuclear reactor, the electrical system, the water purification system, the hydrogen production system, and the synthetic fuel production system. Each section is examined in the following subsections to identify an optimal configuration and determine key performance parameters.

2.3.1 Nuclear Reactor

Nuclear power is the only energy source that can store the power required for long term fuel production as explain in chapter 1. Due to the need to be designed in a ship, the size of the reactors should be Small Modular Reactors (SMRs) [35]. As the name suggests, SMRs are compact reactors that produce up to 300 MW(e) per unit and are designed for modular transport. As of 2024, the IAEA has compiled a comprehensive catalogue of SMRs [35] that are either operational or under development worldwide.

The reactor types fall into two distinct categories, generation III+ which are all Pressurized Water Reactors (PWRs) [36]. The reactors currently used on ships are all PWR. The second category is generation IV reactors which are conceptual designs that aim to minimize safety risks and wastage. While still in development, they offer significant benefits in size and flexibility compared to the PWRs currently in use. One recent publication highlighted each technologies advantages best [37].

Different reactor types considered:

- The Gas Cooled Fast Reactor (GFR) uses helium as a coolant and operates with fast neutrons, offering high efficiency and good fuel utilization.
- The Lead Cooled Fast Reactor (LFR) uses molten lead or lead bismuth, which provides strong passive safety features and long core lifespans.
- The Molten Salt Reactor (MSR) uses liquid fuel dissolved in molten salt, enabling high operating temperatures and inherent safety.

- The Sodium Cooled Fast Reactor (SFR) benefits from decades of research and allows efficient fuel recycling by using liquid sodium as a coolant.
- The Supercritical Water Reactor (SCWR) achieves high thermal efficiency by using water above its critical point.
- The Very High Temperature Reactor (VHTR) uses graphite moderated fuel and helium coolant, operating at very high outlet temperatures ideal for efficient electricity generation.

Notably, the literature on shipboard fuel production summarised in Table 2.2 does not consider one reactor type as the preferred choice.Bushore (1977) [4] selects a PWR, Bogart (2006) [31] adopts a VHTR, and Galla (2011) [32] proposes an MSR. The fact that so many different ones were stated to be best, indicates that the reactor choice for the mothership must be tailored on system specific choices. To do so, a clear understanding of the onboard synthesis plant's energy demands is needed. These demands are further explained in the rest of this section.

The primary reactor requirements are:

- Power production greater than 60 MW to provide enough power for fuel production
- Reactor outlet temperature exceeding 700°C to support thermal integration with the fuel production plant.
- High efficiency across a wide operational range, including part-load conditions (e.g. 30% to 100% capacity), to accommodate different operational scenarios
- 10-15%per minute ramp-up/ramp-down time, to react to unforeseen combat scenarios
- Compliance with naval safety standards.

The PWR was not chosen because, although proven and compact, it operates at relatively low outlet temperatures and rigid load profiles. This limits their suitability for efficient synthetic fuel production [38]. Molten Salt Reactors (MSRs) promise excellent efficiency and safety, but remain at an early stage of development, with several key technologies still unproven for naval use [39]. Fast Spectrum Reactors (FSRs) achieve higher outlet temperatures and compact designs, yet the use of liquid metal coolants introduces complexity and safety challenges in the maritime environment [40, 41].

In contrast, VHTRs combine high outlet temperatures (700–850°C), inert helium cooling and a modular designs in to an efficient reactor. The VHTR also has many strong passive safety features [42]. These characteristics make VHTRs very efficient with studies showing the efficiencies of these reactors reaching up to 45% efficient when converting nuclear heat energy into electrical energy [43]. This makes them particularly well suited for supporting thermochemical fuel synthesis at sea, while maintaining the flexibility and reliability required in naval operations. For these reasons, the VHTR is selected as the reference reactor for this study. More detail on how this reactor was integrated into the system can be found in subsection 10.1.4.

2.3.2 Electrical System

The motherships systems are designed to be fully electric. Terry (1995) [30] was among the first to propose all electric propulsion as the optimal solution. Nearly three decades later, Kapoor (2024) [34] demonstrated that this has indeed become the most effective solution.

The main advantage of an all-electric system lies in the ease of compartmentalization of its components. Fully electric propulsion enables rapid acceleration and flexible placement of thrusters, as they are not constrained by a direct mechanical connection to an engine. This flexibility significantly simplifies integration and layout [44].

Moreover, since the VHTRs energy is ultimately converted into electricity, it is logical to employ a fully electric architecture. The electricity generated powers not only the synthetic fuel production plant, but also all essential onboard systems ranging from propulsion and battery storage to hotel loads and weapon systems.

2.3.3 Water Purification System

As indicated in Equation 2.1, synthetic diesel production requires large quantities of hydrogen, which in turn demands a substantial supply of fresh water [45]. Seawater cannot be electrolysed directly due to its corrosive nature and release of chloride gas[46]. It must therefore be purified before use. Fortunately, large naval vessels already employ mature and reliable desalination systems capable of producing fresh water onboard [33, 32].

Fresh water is typically produced via reverse osmosis (RO), where a semi-permeable membrane removes salts and impurities [47]. RO water is suitable for general ship operations but not for electrolysis, which requires a further de-ionization step to remove residual ions such as sodium, calcium, and chloride [47].

For high-temperature electrolysis, the purified water must then be converted to high-quality steam at 700–900 °C, well above water's critical temperature of 374 °C [48]. As shown in Figure 2.7, this requires a steam generator to produce saturated steam and a superheater to raise it to reaction conditions. A VHTR using supercritical CO_2 as a heat transfer medium can supply the necessary thermal energy. Similar systems have been demonstrated in high-temperature hydrogen research [48] and in industrial applications such as food processing [49].

2.3.4 Hydrogen Production System

Hydrogen can be extracted from water by electrolysis or via SI thermochemical cycles. The latter method is not suitable for naval applications due to its reliance on heavy metals and corrosive processes [50]. Therefore, three electrolysis methods are available:

- Alkaline Electrolysis (AE) — a mature, low-temperature technology using a liquid alkaline electrolyte; robust but limited by lower efficiency and slower dynamic response [51].
- Proton Exchange Membrane (PEM) — a compact, fast-response electrolyser using a solid polymer electrolyte; offers higher purity hydrogen but requires expensive catalyst materials that degrade faster under higher load [52].
- Solid Oxide Electrolysis (SOEC) — a high-temperature process using a ceramic electrolyte and steam feed; achieves the highest efficiencies when high-grade heat is available [45].

Electrolysis has seen impressive improvements in the last decades. Bogart (2006) [31] stated that AE or PEM were the only feasible method of producing Hydrogen, indicating that high temperature electrolysis such as SOEC was not yet available. Galle-Bishop (2011) [32] introduces the use of SOEC, but highlights this to be theoretical and no actual plants are yet operational. In this setting, SOEC is the prefered method due to its direct use of high temperature steam from reactor and no need of high pressure systems and no nead of large scaleWhen diving into the availability of SOECs today it can be seen that this

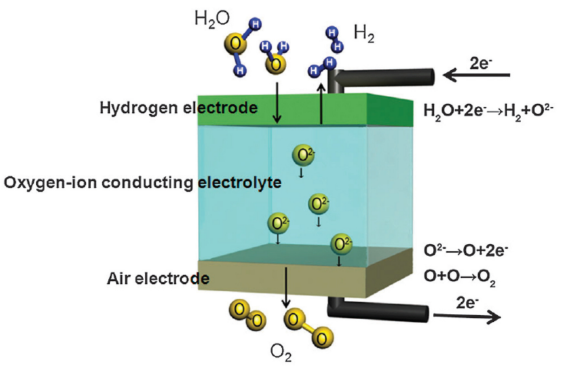

Figure 2.8: Solid Oxide Electrolysis[45]

technology is readily available to be implemented into ships. For this reason SOEC is chosen to be focus on in this literature review.

SOEC is a high-temperature electrolysis process that splits water into hydrogen and oxygen using superheated steam, as shown in Figure 2.8. Operating at 700–800 °C, it uses a solid ceramic electrolyte that conducts oxygen ions (O^{2-}) through the cell [45], leaving hydrogen behind. High-temperature operation reduces electrical demand compared to low-temperature methods and allows efficient integration with a high-grade heat source such as a nuclear reactor.

Two variants exist: High-Temperature Steam Electrolysis (HTSE), which splits only water, and High-Temperature Co-Electrolysis (HTCE), which simultaneously converts H_2O and CO_2 into syngas. Although HTCE offers strong potential for future synthetic-fuel systems, it is still at an early development stage [53]. This study therefore adopts HTSE as the more mature and commercially available option.

Kapoor (2024) [34] did not select SOEC for shipboard hydrogen production because his reactor choice was PWR. This reactor design could not supply the required temperatures. In contrast, the VHTR used for this study makes SOEC both feasible and advantageous.

SOEC systems are now commercially available. Bloom Energy[3] offers the E-5700, producing 2.4 $t_{H_2}\,day^{-1}$ from 4 MW of electricity and achieving an energy demand of 37.5 $kWh\,kg_{H_2}^{-1}$, outperforming other electrolysis technologies, as shown in Figure 2.9.

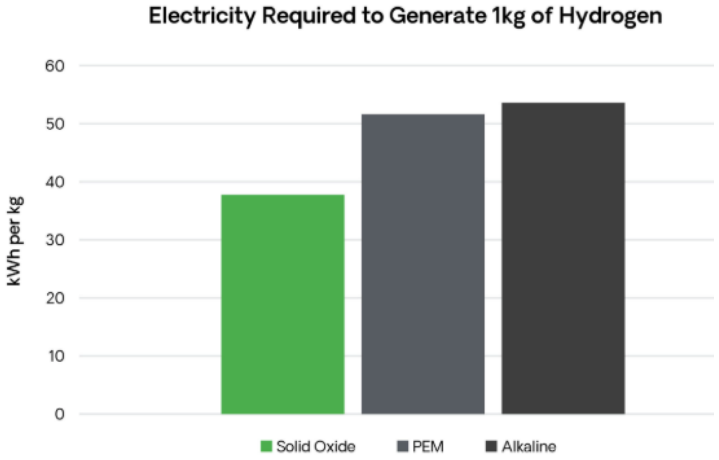

Figure 2.9: Bloom Energy SOEC energy demand compared with other electrolysis technologies [2]

These values already include the heat required for steam generation. When external heat is supplied, for example by the mothership's reactor, the electrical demand can drop by roughly 40%, to around 25 $kWh\,kg_{H_2}^{-1}$. SOEC systems operate at 90–100% LHV efficiency [53, 34]. Since hydrogen comprises roughly one-ninth of the mass of water, a 90%-efficient system requires about 10 L of deionized water per kilogram of hydrogen.

2.3.5 Synthetic Fuel Production System

To produce synthetic diesel, the FT synthesizer is used. This process relies on the chemical reaction shown in Equation 2.2 to convert carbon monoxide and hydrogen into hydrocarbon fuels:

$$(2n{+}1)\ H_2 + n\ CO \rightarrow C_nH_{2n+2} + n\ H_2O \tag{2.2}$$

It is important to note that the FT synthesizer produces hydrocarbon chains of various lengths. This can be seen in Figure 2.10, which shows the range of hydrocarbons produced and highlights

[2] https://www.bloomenergy.com/bloomelectrolyzer/
[3] https://www.bloomenergy.com/bloomelectrolyzer/

the fraction suitable for diesel use (C_{10}–C_{20}). Without further processing, this would result in only 40% efficiency in converting the feedstock into usable diesel [54].

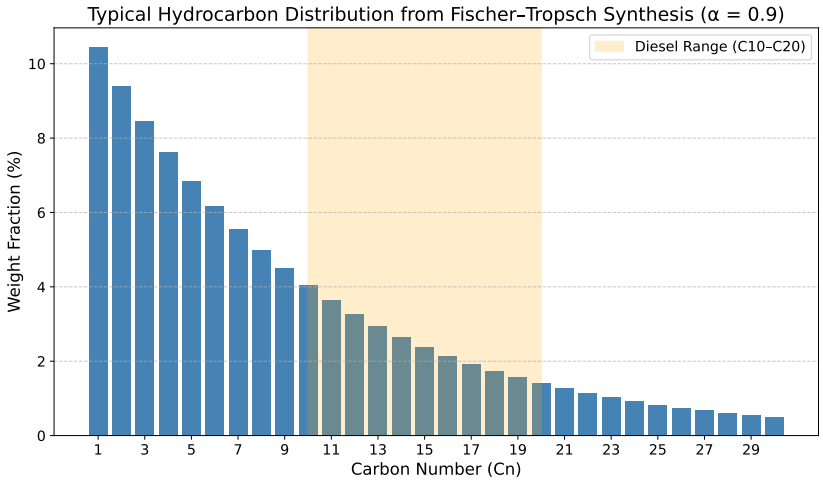

Figure 2.10: FT sythesis production hydrocarbon distribution (alpha = 0.9), data from [33]

To improve this efficiency, two additional systems are incorporated. First, a hydrocracker is used to break down hydrocarbon chains that are too long into chains that fall within the desired diesel range [55]. Second, an autothermal reformer (ATR) is employed to process the hydrocarbon chains that are too short for diesel use [56]. The ATR converts these short hydrocarbons back into syngas, which can then be reused in the FT synthesizer, improving overall fuel yield.

The FT system requires syngas as its input. Syngas is a gas mixture of hydrogen and carbon monoxide. It is produced using the Reverse Water–Gas Shift (RWGS) reaction [57], shown in Equation 2.3:

$$CO_2 + H_2 \rightarrow CO + H_2O \tag{2.3}$$

As seen, the inputs are carbon dioxide and hydrogen, and the outputs are carbon monoxide and steam. The steam produced can be condensed and recycled elsewhere in the system, improving overall efficiency.

The hydrogen required for both reactions is provided by the SOEC, as described in subsection 2.3.4. However, the carbon dioxide input still needs to be sourced from the environment.

CO_2 Extraction

The CO_2 required for the RWGS reactor can be sourced either from seawater or from the atmosphere. Seawater acidification, proposed by Comidy [33], releases dissolved CO_2 by shifting the carbonate equilibrium. Although promising for maritime use, this method has only reached laboratory and pilot-scale maturity and is therefore not considered suitable for implementation as of 2025 [58].

Direct Air Capture (DAC) remains the practical alternative. Its main challenge is the low atmospheric CO_2 concentration of roughly 0.065%, requiring large airflow volumes. Bogart [31] highlighted this constraint in early feasibility studies, and although DAC units have become more compact by 2024, high airflow requirements persist.

A proposed DAC method, described by Kapoor (2024)[34], uses aqueous calcium hydroxide to absorb atmospheric CO_2, forming calcium carbonate that is later calcined to release pure CO_2. The calcium hydroxide loop operates in a closed cycle without continuous reactant consumption [59]. While calcination is heat-intensive, calcium-based DAC remains one of the most scalable options when high-grade nuclear heat is available. Its main drawback is the size and weight of air-handling equipment but, based on Kapoor's comparative assessment [34], this approach is adopted in this thesis.

The DAC system volume can be estimated using:

$$V_{\text{DAC}}\ (\text{m}^3) = 76.406 \cdot (\text{CO}_2\ \text{output}\ (\text{t/day}))^{0.9184} \tag{2.4}$$

with roughly 60% of the system requiring above-deck placement due to intake and ducting.

Electrical and thermal power demands follow [34]:

$$\text{CO}_2\ \text{output}\ (\text{t/day}) = 146.11 \cdot P_{\text{el}}\ (\text{MW}_\text{e}) \tag{2.5}$$

$$P_{\text{th}}\ (\text{MW}_\text{th}) = 5.87 \cdot P_{\text{el}}\ (\text{MW}_\text{e}) \tag{2.6}$$

Syngas production: RWGS

As stated at the start of subsection 2.3.5, carbon dioxide and hydrogen must be fed into the RWGS reactor to produce syngas in the appropriate ratio for use in the FT reactor. The RWGS is a catalytic reaction that requires significant heat input, operating at temperatures between 700–900 °C, as found by Comidy [33]. In this study, Comidy's system configuration is adopted with a $H_2 : CO_2$ molar ratio of 3:1, and methane formation is assumed to be negligible. In mass ration this can be seen as a 1:7.5 kg.

To enable efficient operation of the RWGS reactor, two auxiliary units are considered: a pre-reactor compressor and a post-reactor pressure swing adsorption (PSA) unit. The compressor is used to raise the pressure of the incoming gases to the reactor operating conditions.

After the reaction, the PSA unit is used to separate unreacted CO_2 and H_2 from the product gas stream and recycle them into the reactor inlet. The energy demand, volume and weight of the PSA unit are modelled as functions of the amount of gas being separated, and in this study, it is assumed to operate at 100% separation efficiency [34, 31].

Sythetic Diesel production: Fischer–Tropsch Synthesis

Once syngas (CO and H_2) has been produced via the RWGS reaction, it goes into the FT reactor. Each paper in Table 2.2 uses the FT reactor as the final process to create the synthetic fuel. This reactor converts the syngas into hydrocarbons via catalytic polymerization. The reaction is given in Equation 2.2, where n is the number of carbon atoms in the target molecule:

$$(2n+1)\text{H}_2 + n\text{CO} \rightarrow \text{C}_n\text{H}_{2n+2} + n\text{H}_2\text{O} \tag{2.7}$$

To increase the yield of diesel-range hydrocarbons (F-76) as explain at the start of subsection 2.3.5, two downstream units are included:

- **Hydrocracker**: Used to break down longer-chain hydrocarbons into shorter, diesel-range molecules [55]. As stated in subsection 2.3.5, the hydrocracker increases the proportion of F-76 by converting waxes and heavy ends.
- **Autothermal Reformer (ATR)**: Utilized to convert shorter-chain hydrocarbons and off-spec gas back into syngas [56]. This recycled syngas is redirected into the FT reactor. The ATR is a thermally intensive unit, often integrating partial oxidation and steam reforming.

With the Fischer–Tropsch reactor discussed, all components shown in Figure 2.7 have been evaluated and are considered technologically advanced enough to be realistically implemented in a ship design. This confirms that the literature review can be extended to possible ship and EMS designs.

2.4 Mothership Role and Operational Profile

To establish a realistic foundation for the energy system and EMS design, the operational context and baseline characteristics of the mothership are first defined. The mothership serves as the central refuelling and coordination platform for the USVs, providing fuel, and logistical support during extended missions at sea.

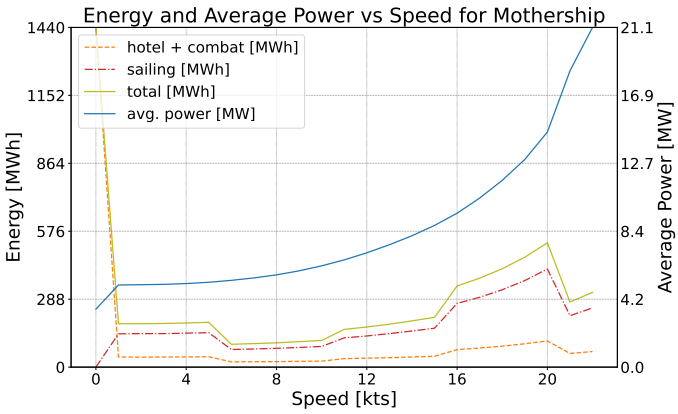

Figure 2.11: Operational profile of the mothership, derived from data of a generic Multi Purpose Support Ship (MPSS).

As a reference, a generic Multi Purpose Support Ship (MPSS) of approximately 140 m in length, provided by Damen Naval[4], was selected as the conceptual baseline. This vessel type closely aligns with the intended operational role of the proposed nuclear-powered mothership. It combines larg deck capacity and refuelling capability, both needed on the mothership.

The operational profile derived from this reference vessel is shown in Figure 2.11. The left vertical axis represents the energy spent at various speeds, while the colours indicate the corresponding loads. The profile illustrates that the ship spends a large proportion of its time stationary or at low speeds, which is typical for support and replenishment operations. The associated average power vs speed can be seen on the left y axis.

2.5 Energy System Scaling

Before the full system model could be implemented, an initial scaling study was performed to determine the approximate power, mass, and volume requirements of each subsystem. The goal was to ensure that the final model implementation operates within physically realistic bounds and reflects feasible shipboard capacities.

Based on the chosen USV, which is estimated to have an endurance of 10-days [60]. the Mothership should be able to produce enough fuel to refuel one USV every 5 days. This translates to a required fuel production capacity of at least 29.5 tonnes per day. This combined with the motherships limited size as shown in section 2.4 means each individual subsystem has been scaled to meet these diesel requirements. The individual subsystem scaling was carried out in detail in the preceding literature study [9], which should be consulted for explanations of the values used in the following table. The resulting system size is summarised in Table 2.3.

Based on the data in Table 2.3, the total system volume of 6498 m^3 falls well within the spatial capacity of the mothership. A vessel measuring approximately 140 m in length, 19 m in beam,

[4] `https://www.damen.com/vessels/defence-and-security/multi-purpose-support-ships`

Table 2.3: System Requirements to Produce 29.5 Tonnes of Synthetic Diesel

Subsystem	**Electric Power** (MW_e)	**Thermal Power** (MW_{th})	**Material Input**	**Material Output**	**Volume** (m^3)	**Weight** (tonnes)
Deionization Unit	0.008	0	285 t fresh water	285 t deionized water	3	3
Steam Superheater	negligible	5.5	285 t water	285 t steam (800 °C)	10	4
SOEC Electrolyzer	17.28	11.52	165.9 t deionized water	16.59 t H_2	537	239.8
DAC Unit	0.66	3.874	306,000 t air	95.9 t CO_2	4908	1960
RWGS Reactor	1	2.5	95.9 t CO_2, 13.1 t H_2	69.9 t syngas, 14.25 t H_2O	15	18
FT Reactor	6.28	0.5	107.6 t syngas	13.8 t F76, 19.4 t long HC, 13.9 t short HC, 60.5 t H_2O	19	25
Hydrocracker	0.2	0.65	19.4 t long HC, 3.49 t H_2	15.5 t F76, 3.88 t short HC	7	11
ATR	0.9	0.4	17.78 t short HC, 20.0 t H_2O	37.7 t syngas	9	13
Total	**26.33**	**24.9**	–	**29.5 t F76**	**6498**	**2274**

and 6.5 m in depth encloses a total hull volume of about 17,300 m^3. This indicates that the integrated energy and fuel production systems would occupy less than half of the available internal space. By weight, the combined mass of 2274 tonnes is also well within the load capacity of the mothership class[5] .

The total power demand of the system is 26.3 MW_e and 24.9 MW_{th}. When combined with the propulsion and hotel loads (approximately 25 MW_e), the mothership requires a continuous electrical supply of roughly 51 MW_e in addition to 24.9 MW_{th} of process heat. Assuming an electrical conversion efficiency of 45% (see section 2.3), the reactor must generate

$$\frac{51\ \mathrm{MW_e}}{0.45} \approx 113\ \mathrm{MW_{th}} \tag{2.8}$$

to meet the electrical demand alone. When the additional 24.9 MW_{th} of thermal process heat is included, the total thermal output required becomes

$$113\ \mathrm{MW_{th}} + 24.9\ \mathrm{MW_{th}} \approx 138\ \mathrm{MW_{th}} \tag{2.9}$$

which justifies selecting a 140 MW_{th} VHTR as sufficient to power the complete mothership energy system.

These estimates confirm that the proposed system is both volumetrically and energetically feasible, providing a realistic foundation for the detailed dynamic modelling that follows.

2.6 Existing EMS Frameworks in Maritime and Energy Systems

With the mothership's energy plant now defined, this section examines how its operation can be coordinated through an EMS. The EMS acts as the supervisory controller governing energy flows across all major subsystems. Its primary objective is to maintain the reactor at near constant output. This maximises efficiency and reduces thermal stress, by scheduling deferrable loads such as fuel production and battery charging to absorb fluctuations.

Although EMS principles are well established in hybrid and all-electric ships, recent developments increasingly incorporate advanced control and artificial intelligence methods [61, 62]. However,

[5] `https://www.damen.com/vessels/defence-and-security/multi-purpose-support-ships`

few studies extend these concepts to nuclear powered vessels, where most research remains centred on safety and feasibility [63]. Studies examining nuclear integration into marine propulsion [64] do not address system wide energy coordination, while economic assessments [65] overlook dynamic control. Comidy (2019)[33] offers the only work linking control of nuclear propulsion to onboard fuel production, but its analysis focuses on costs control rather than EMS.

Recent naval EMS research continues to prioritise submarines [66]. Broader multi-energy reviews [67, 68] discuss EMS strategies for systems combining diesel engines, batteries, and fuel cells, yet none address the dynamic coupling of a nuclear reactor, synthetic-fuel plant, and shipboard loads. Consequently, no verified EMS framework currently exists for a nuclear-powered refuelling vessel.

Given this gap, existing EMS concepts from hybrid and multi-energy ships must be evaluated to determine which architectures and control philosophies best match the operational requirements of this new nuclear configuration.

EMS Control Hierarchies

To understand what the EMS must control, a general shipboard energy management hierarchy is shown in Figure 2.12 [68]. At the lowest level, equipment controllers ensure safe operation of individual components. Subsystem controllers then coordinate groups such as propulsion and the fuel plant. Above these, the EMS governs overall power allocation according to mission priorities, while a command layer defines the broader operational objectives.

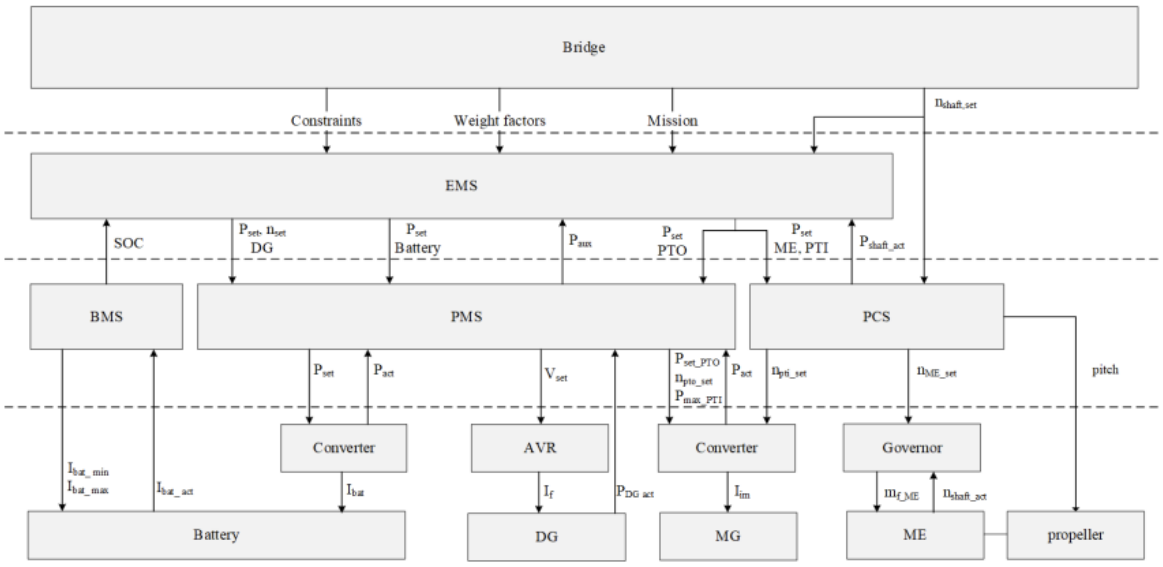

Figure 2.12: Energy system hierarchy on the mothership [68].

Different EMS architectures are described in the literature [69]:

- **Centralised EMS** – a single controller optimises all ship energy flows; efficient but computationally demanding.
- **Hierarchical EMS** – a supervisory layer provides set points to local controllers, offering coordination with responsiveness.

- **Decentralised EMS** – independent subsystem controllers communicate minimally, improving robustness at the cost of global optimality.
- **Multi-agent EMS** – distributed agents negotiate energy use, suitable for multi-vessel or ship to UXV networks.

Given the mothership's integrated but single-vessel design, a **Hierarchical Centralised EMS** offers the best balance of control transparency, coordination, and implementation simplicity. Multi-agent concepts may become relevant for future fleet-wide coordination [70].

EMS Control Strategies

The most common EMS control strategies fall into three categories [67]:

- **Rule-based strategies** use predefined operational logic to manage power flow. They are simple, transparent, and well suited when system behaviour is well understood but limited data exists.
- **Optimisation-based strategies**, including MPC and MILP, compute optimal setpoints in real time but require detailed models and substantial computational resources.
- **Learning-based strategies** rely on data-driven methods or reinforcement learning to adapt control but require extensive training data and validation.

For this literature study, a **Deterministic Rule-based EMS** and a **Global Optimisation EMS** are selected as the most appropriate approaches. Learning-based strategies are not considered due to the absence of sufficient operational data to support training. ZASDF

2.7 Research Gap Formulation

This chapter set out to address four sub-questions:

SQ1. What are the operational requirements and energy demands of the unmanned support units (USVs, UAVs, UUVs) that the mothership must sustain?

SQ2. Which fuel or energy carrier can be practically produced onboard the mothership to meet the UXVs operational constraints?

SQ3. Which reactor type and associated energy conversion technologies are most suitable for providing continuous power to both the mothership's onboard systems and its fuel production plant?

SQ5. What energy management system (EMS) hierarchy can coordinate power generation, storage, and fuel production under varying operational conditions?

The literature reviewed found that for **SQ1**, extensive research exists on the operational use and endurance of unmanned vehicles, particularly USVs [2, 6]. However, no study connects these operational demands to the design of a supporting refueling hub.

In **SQ2**, several works explore the production of synthetic fuels aboard nuclear-powered ships [4, 30, 31, 32, 33, 34], but these focus primarily on feasibility and component design, rather than system-level integration or control.

For **SQ3**, comparisons of reactor types show that small modular and high-temperature reactors could enable efficient fuel synthesis at sea, yet the literature does not extend to dynamic modelling of VHTR systems converting power into other energy carriers.

Finally, **SQ5** highlights the need for an EMS that can manage both shipboard and fleet-level energy flows. While EMS strategies are well developed for conventional hybrid ships [67, 68], none of the reviewed studies address the integrated control of an internal nuclear reactor and synthetic fuel production plant in combination with external refuelling operations for unmanned systems.

Combining these findings reveals that current research addresses many of the components individually but rarely considers their interaction within a single operational framework. The integration of a nuclear reactor with onboard Power-to-Liquid fuel synthesis and coordinated EMS control for supporting autonomous vessels remains largely unexplored.

This points to two research gaps being identified:

GAP 1 The integrated modeling and design of a nuclear-powered ship energy system that supports onboard fuel production has not been systematically investigated

GAP 2 While Energy Management Systems have been studied in isolated ship contexts, their coordinated operation across reactor control, onboard energy distribution, and fleet-level refuelling scenarios has not yet been systematically investigated.

Addressing these gaps requires developing the dynamic modelling of the nuclear power plant, energy conversion, and synthetic fuel production processes within a single simulation environment. Building upon this, an EMS architecture must be designed and tested to coordinate both shipboard energy balance and fleet-level refuelling. Together, these efforts form the foundation for this thesis.

3 | Methodology

This chapter presents the methodological approach used to develop and evaluate the first complete energy system model of a nuclear-powered refuelling mothership. Rather than describing each subsystem in detail (as covered in later chapters), the focus here is on outlining the reasoning behind the chosen tools, modelling environments, and workflow used to answer the research questions introduced in section 1.1.

The research spans several technical domains: nuclear heat production, synthetic fuel generation, shipboard energy distribution, and multi-vessel coordination. To manage this complexity, the main research question was divided into sub-questions that served as a roadmap for structuring both the modelling process and the thesis. Figure 3.1 illustrates how these sub-questions shaped the overall research flow, from defining system requirements to developing the EMS and finally testing the full operational concept.

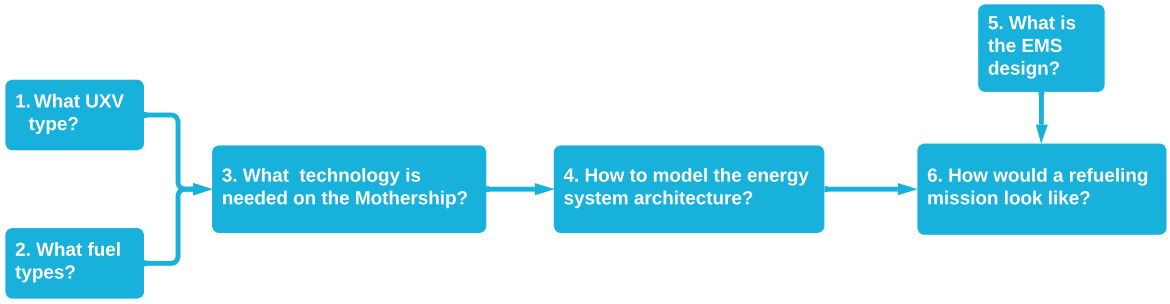

Figure 3.1: Thesis workflow showing the logical connection between sub-questions and the overall research process.

The literature review in chapter 2 first established the foundation for the modelling work by defining the operational context, identifying feasible fuels, and selecting an appropriate reactor and energy-conversion system.

With these choices in place, the next step was to construct the ship's internal energy system model, developed in MATLAB[1]/Simulink as described in chapter 4. Simulink's block-based structure allowed the physical processes (reactor behaviour, hydrogen production, fuel synthesis, and energy distribution) to be represented in a time accurate way.

As the physical model matured, it became clear that the ship's performance could not be assessed without simultaneously developing the EMS. This motivated the EMS design process in chapter 5, where a local rule-based controller was created to stabilise internal power flows. However, adding USV refuelling revealed the need for higher level coordination.

To address this, a global optimisation layer was introduced using a Python Gurobi framework. This optimiser determines when and in what order USVs should be refuelled, allocating limited system resources more effectively than local control alone. Together, the Simulink rule-based EMS and the Python–Gurobi optimiser form the layered EMS architecture used throughout the testing phase in chapter 7.

As shown in the performance evaluation in section 7.6, the introduction of this global scheduling layer significantly improves operational efficiency, coordination behaviour, and overall mission performance, directly addressing the sixth and final sub-question of the thesis.

[1] `https://nl.mathworks.com/products/matlab.html`

3.1 Model Integration

To test the models all components had to be brought together into a single, coherent workflow capable of evaluating the complete mothership concept. Since no existing framework supports a nuclear-powered refuelling vessel of this kind, every element of the workflow (simulation models, optimisation routines, scenario generation, and result processing) had to be build.

Figure 3.2 shows how the different components interact. Mission scenarios are first created in Python using the Scenario Generator, which defines vessel routes, refuelling requests, and overall mission timing. This mission data is then passed to two systems: the Simulink mothership model, which simulates energy flows, fuel production, and refuelling; and, when enabled, the Python–Gurobi fleet scheduling optimiser. The optimiser reviews the initial refuelling requests and generates an improved schedule by optimising the order and timing of refuelling events. This optimised schedule then replaces the original Refuelling request for the mothership energy model before the simulation begins. This ensures that the mothership follows a coordinated plan rather than the initial unoptimised sequence.

After each simulation, all outputs are collected and processed in MATLAB and then visualised using a custom Results Plotter. This allows results from different EMS configurations and scenarios to be compared consistently.

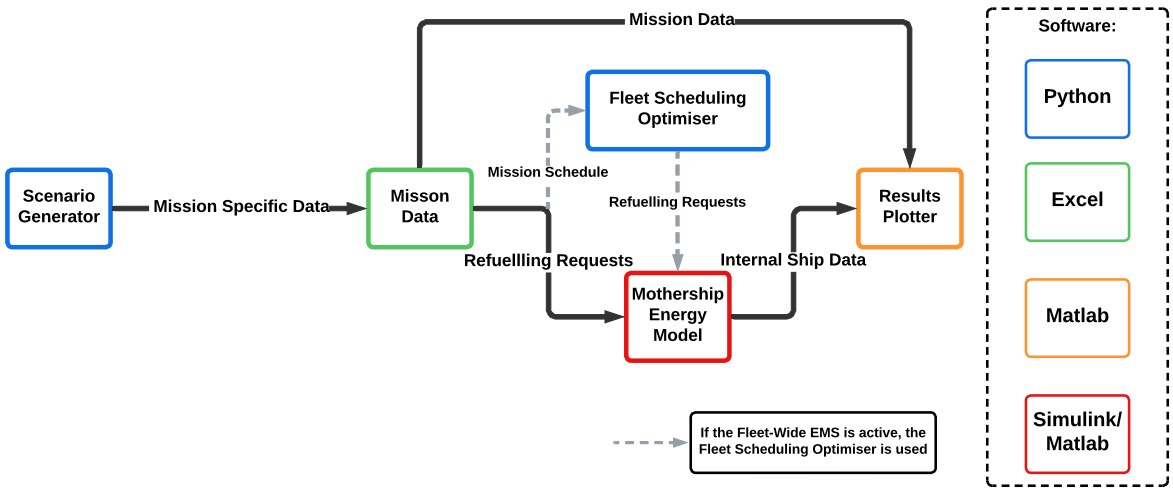

Figure 3.2: Code workflow used during scenario testing showing data exchange between Python, Excel, and MATLAB environments.

Together, this workflow forms a single end-to-end system setup, allowing the internal energy model of the mothership to be tested and to do so using different EMS configurations.

4 | Modelling of the Ship Energy System Architecture

This chapter presents the design of the internal energy system of the mothership. The goal of this model is to represent how energy and mass flow within the mothership when powered by a nuclear power source to produce synthetic diesel. The chapter directly addresses the fourth sub-question of this thesis:

SQ4. What integrated energy system architecture (including power distribution, storage, and fuel production subsystems) best enables the mothership to act as a centralised refuelling hub?

To answer this question, the system was designed using insights from the literature review in chapter 2 on maritime energy systems, nuclear ship propulsion, and synthetic fuel production. As stated in chapter 3, MATLAB/Simulink was chosen for this implementation. The sizing of the subsystems will be based on the system sizing done in section 2.5.

The structure of this chapter is as follows:

The structure of this chapter is as follows:

- **section 4.1** — Provides an overview of the complete Simulink architecture.
- **section 4.2** — Describes the power plant model, including the VHTR reactor, ESS
- **section 4.3** — Explains the fuel production plant
- **section 4.4** — Presents the fuel storage model
- **section 4.5** — Describes how remaining ship systems are modelled.

4.1 Model Implementation

The Simulink model represents the mothership's internal energy system in a modular structure, with each subsystem modelled independently while maintaining a clear overview of their interactions. The complete system layout is shown in Figure 4.1, which divides the architecture into four main parts that together capture the flow of energy and control across the ship. This layout follows the conceptual design introduced in section 2.3.

The first block in Figure 4.1 is the Power Plant, which generates all electrical and thermal power through the nuclear plant and ESS. The second block is the Ship Systems, representing all onboard consumers outside the fuel-production chain, including propulsion and hotel loads. The third block is the Fuel Production Plant, which converts electrical and thermal power into synthetic diesel. Finally, the EMS serves as the supervisory controller that coordinates all subsystems. Its operation is discussed separately in section 5.1.

The model is designed to simulate multi-day mission scenarios. To maintain accuracy during long-duration simulations, all power and mass-flow calculations operate at a one-second time step.

Each subsystem is implemented as a MATLAB function block [1] following a consistent structure. The working principles and governing equations of each individual block are discussed in the following sections. The symbols used in all the equations can be seen in Table 9.1. For full implementation understanding each block has also been summarised according to the structure

[1] `https://nl.mathworks.com/help/simulink/slref/matlabfunction.html`

seen in Table 4.1. For these table summaries of the implemented blocks, the reader is referred to chapter 9.

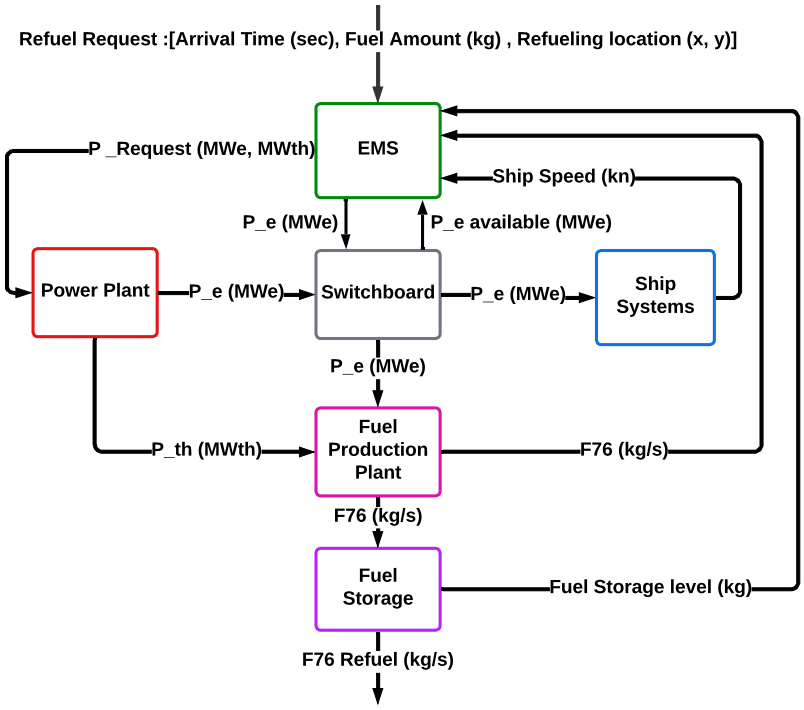

Figure 4.1: Ship Energy System Flow Chart

Table 4.1: Generic structure of summary tables of subsystems implemented into Simulink

Row Type	Purpose and Typical Content
Operational Logic	Describes how the component behaves and how its internal control rules operate during simulation.
Inputs and Outputs	Lists the main input and output variables exchanged with other subsystems.
Fixed Parameters	Summarises constant design or calibration values that define the component's static behaviour.
Delays and Memory	Indicates any temporal behaviour introduced by stored states, feedback terms, or signal delays that preserve physical continuity across timesteps.
Energy Conversion Logic	Explains how energy is transformed within the subsystem. Shows main conversion equations.

4.2 Power Plant Model

The power plant consists of the nuclear reactor, the Brayton-cycle conversion system, and the onboard ESS. These components are controlled by a rule-based controller, which allocates thermal and electrical power according to instantaneous demand from the ship systems and the fuel-production plant. The overall structure implemented in Simulink is shown in Figure 4.2. Power requests from the EMS specify the desired electrical and thermal outputs. The controller first determines whether the nuclear reactor can supply the requested power within its ramp-rate limits; any remaining mismatch is compensated using the ESS.

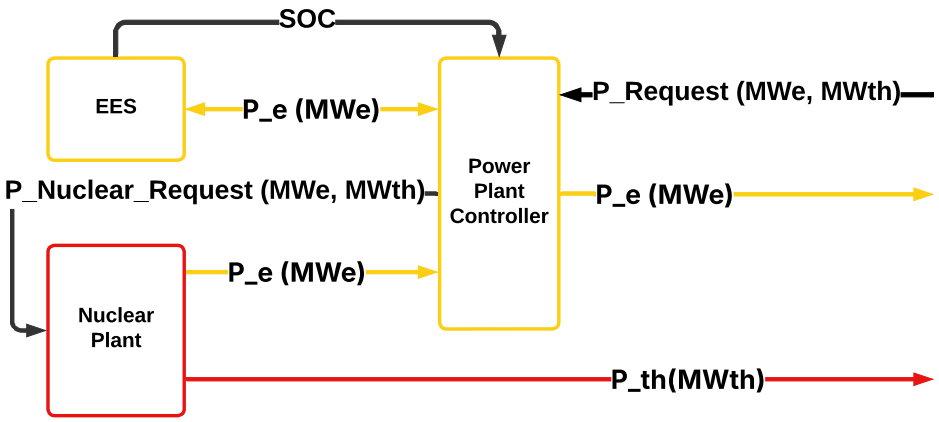

Figure 4.2: Power plant structure implemented into Simulink

4.2.1 Power Plant: Nuclear Plant

As decided on in section 2.3, the nuclear plant uses the VHTR. The design of the VHTR has been vastly investigated [71, 72, 42]. The reactor and plant around it shall not deviate from the designs stated in the literature. The VHTR plant designs all focused massively on the Brayton cycle [73]. This is the gaseous cycle in which the heat from the reactor core is transferred by a gas that is not water vapour. This allows for high temperatures which lead to higher efficiency. The choice of gas was decided on in section 2.3 to be super critical CO_2. A representation of a Brayton cycle integrated with a VHTR is shown in Figure 10.3. The control of the heat flow and power production within the nuclear plant is to be done using control rods [42] in the reactor or by adding control in to the Brayton cycle using bypass control or inventory control [74]. Within this specific system, because the fuel production plant maintains a near continuous electrical load, energy saving safeguards are not needed for this nuclear plant. A cold dump [42] is considered available for emergency yet simple control rod control is considered the main control method.

The sizing study in section 2.5 shows the thermal power required from the reactor was to be 140 MW(th). Simulation results showed that full-capacity operation is uncommon, so the final reactor capacity was set to 130 MW(th), placing the reactor in its high-efficiency region during normal operation.

Based on measured control rod dynamics [71], a 10% per minute ramp limit is imposed in the model. The thermal power available after subtracting fixed direct thermal process heat is

$$P_{\mathrm{th,max}} = \max\big(P_{\mathrm{max}} - P_{\mathrm{th,dir}},\, 0\big), \tag{4.1}$$

which bounds the maximum electrical output through the highest slot efficiency,

$$P_{\mathrm{e,max}} = \eta_{\mathrm{max}}\, P_{\mathrm{th,max}}. \tag{4.2}$$

The allowable change in electrical power per timestep is

$$\Delta P_{\mathrm{e,ramp}} = r\, \frac{\eta_{\mathrm{prev}}}{\eta_{\mathrm{max}}}\, P_{\mathrm{e,max}}\, \frac{\Delta t}{60}, \tag{4.3}$$

where r is the fractional ramp limit (0.10). The updated electrical output is

$$P_{\mathrm{e}} = P_{\mathrm{e,prev}} + \mathrm{clip}(P_{\mathrm{e,target}} - P_{\mathrm{e,prev}},\, -\Delta P_{\mathrm{e,ramp}},\, \Delta P_{\mathrm{e,ramp}})\,, \tag{4.4}$$

and the corresponding thermal output becomes

$$P_{\text{th}} = \frac{P_{\text{e}}}{\eta_{\text{curr}}} + P_{\text{th,dir}}, \tag{4.5}$$

capped at the maximum thermal capacity.

4.2.2 Power Plant: ESS

The reactor's 10% per minute ramp limit means that rapid changes in electrical demand cannot always be met directly. The ESS compensates for these short term imbalances and supports peak loads that exceed the reactor's instantaneous output.

The ESS is not intended for long term storage, as the fuel production plant already functions as the primary energy buffer by continuously drawing power. Instead, the ESS smooths transients and maintains system stability. The chosen configuration provides 10 MWh capacity, with discharge and charge limits of 15 MW and 10 MW respectively.

For a requested power P_{req} (positive for discharge, negative for charge), the exchanged energy is

$$E = |P_{\text{actual}}| \frac{\Delta t}{3600}, \tag{4.6}$$

with power limits

$$P^{\text{dis}}_{\text{actual}} = \min(P_{\text{req}},\, P^{\text{dis}}_{\text{max}}), \tag{4.7}$$

$$P^{\text{ch}}_{\text{actual}} = -\min(|P_{\text{req}}|,\, P^{\text{ch}}_{\text{max}}). \tag{4.8}$$

The state of energy (SOE) evolves as

$$\text{Discharge: } \text{SOE}_{k+1} = \text{SOE}_k - \frac{E}{\eta_{\text{dis}}}, \tag{4.9}$$

$$\text{Charge: } \text{SOE}_{k+1} = \text{SOE}_k + E\,\eta_{\text{ch}}, \tag{4.10}$$

subject to

$$0 \leq \text{SOE}_{k+1} \leq E_{\text{max}}. \tag{4.11}$$

4.2.3 Power Plant controller

The controller determines the power split between the reactor and the battery to meet the system's instantaneous electrical demand. It ensures that the reactor ramps gradually within its defined rate limits, while the battery compensates for temporary power deficits or surpluses. This control logic maintains power stability and prioritises energy flow to the most critical subsystems. The controller operates under rule-based logic, enforcing reactor ramp constraints, battery charge/discharge limits, and a 0.25 MW deadband to prevent oscillation from the battery compensating too early. When power demands can not be met the system is simply push to produce the max power that it can produce.

4.3 Fuel Production Plant Model

To model the ship's fuel production plant, all relevant components identified in section 2.3 are considered. A schematic overview of the fuel production system is shown in Figure 4.3. The system is divided into several main components, each described individually in the following sections. Electrical and thermal power serve as inputs to the plant, which converts the supplied energy into synthetic diesel.

The initial size of each system was placed at the values stated in the scaling section in section 2.5. During testing of the system the different input values where adjusted and corrected to fit the actual transfer relations and to optimise the system further.

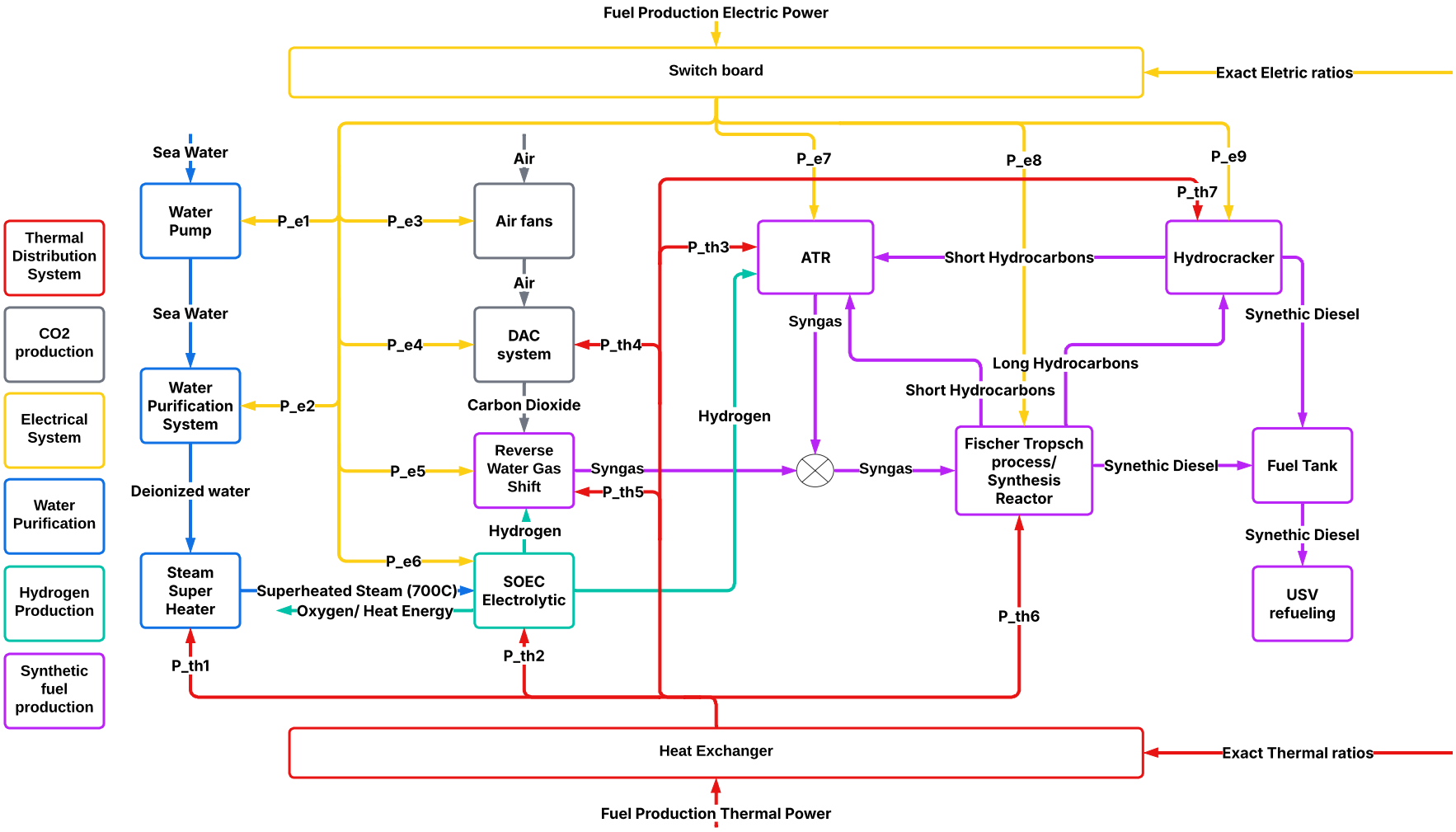

Figure 4.3: Scematic overview of Fuel Production Plant model

The entire fuel-production chain is modelled as a hot-start system, meaning all components operate near their nominal temperatures without cold start-up cycles. This is justified because the nuclear reactor in all scenarios never falls below 30 percent output, providing continuous thermal energy to keep each subsystem within its operating range. High-temperature catalytic processes are also rarely shut down in practice, as thermal cycling leads to long warm-up times, reduced efficiency, and accelerated catalyst degradation. Literature on SOEC operation and FT synthesis supports the use of warm or hot standby as standard practice in continuous plants [75, 76]. Thus, hot-start modelling is a realistic assumption for this study.

4.3.1 Electrical and Thermal Control

The EMS determines the total electrical and thermal power available to the fuel production plant. This power is distributed internally by two proportional switchboards (electrical and thermal), which allocate power to each subsystem based on its instantaneous request.

At every time step, each unit submits a power demand. The switchboard computes a scaling factor on total demand and total supply,

$$\alpha = \frac{P_{\text{available}}}{\sum P_{\text{requested}}}, \tag{4.12}$$

and applies it uniformly to all requests. When sufficient power is available, $\alpha = 1$; otherwise, all subsystems are proportionally reduced.

Although this proportional switchboard is an oversimplification of real industrial control architectures, it remains valid for this system for several reasons. First, all major subsystems already include internal rate limits, thermal inertia, and mass-flow constraints, meaning none can request more power than physically achievable based on the upstream process configuration. Second, in energy-system and process-plant modelling, proportional allocation is a standard practice when units operate in tightly coupled chains and the dominant dynamics are governed by upstream availability rather than local control loops [77]. This approach preserves overall energy balance without requiring fully decentralised PID-style coordination. Finally, the fuel plant behaves as a quasi-steady energy consumer with slow dynamics (DAC, RWGS, FT), making proportional rescaling both numerically stable and representative of supervisory-level behaviour in real chemical-process plants. For these reasons, the proportional switchboard provides an appropriate and computationally efficient approximation for energy-level allocation in the integrated mothership model.

4.3.2 Water Purification System Model

As shown in Figure 4.3, the water purification chain consists of two main components: the seawater pump and the purification unit. Seawater is drawn from the ocean and processed through a combined reverse osmosis and deionisation system, producing freshwater for the electrolyser [47]. A 5000 L freshwater buffer tank ensures uninterrupted electrolyser operation. The purification system is intentionally sized at its optimal efficiency point (see section 2.5), which allows it to produce water much faster than the fuel production chain consumes it. Scaling the unit down to match the downstream demand would reduce its efficiency and increase energy consumption. By using a buffer instead, the system retains high efficiency while supplying the electrolyser with a stable feed. As a result, the purification unit can operate with simple on–off control based solely on the buffer tank level.

4.3.2.1 Seawater Pump

The seawater pump forms the first stage of the purification chain and provides the inflow to the refinery block. Typical of electrically driven centrifugal pumps, it has low inertia and responds

almost instantaneously to shutdown commands while requiring several seconds to ramp up to full operation [47]. This behaviour is captured through a ramp-limited flow rate:

$$\dot{m}_{\mathrm{sw},k+1} = \dot{m}_{\mathrm{sw},k} + \max\Big(-r_{\mathrm{sw}}\Delta t,\ \min\big(\Delta\dot{m}_{\mathrm{sw}},\ r_{\mathrm{sw}}\Delta t\big)\Big), \tag{4.13}$$

where

$$\Delta\dot{m}_{\mathrm{sw}} = \dot{m}_{\mathrm{sw,target}} - \dot{m}_{\mathrm{sw},k},$$

r_{sw} is the pump ramp rate, and $\dot{m}_{\mathrm{sw,target}}$ is the flow permitted by pump power and the on–off command. The pump's rated electrical power is only 0.1 MW and it can supply up to 8 kg/s of seawater, making its energy contribution negligible in the overall ship-level balance.

4.3.2.2 Water Purification

The purification system converts seawater into freshwater using a combined reverse osmosis and deionisation process, modelled as a single block that produces freshwater suitable for electrolysis. Its operation is governed by the freshwater buffer tank: the unit switches on when the volume drops below 5% and shuts down automatically once the tank is full. This simple on–off strategy avoids inefficient part-load operation and stabilises system behaviour.

The electrical demand of the purification block depends on the freshwater mass flow rate and is computed using a specific energy consumption of $E_{\mathrm{spec}} = 0.5\ \mathrm{kWh\,kg^{-1}}$ [47]:

$$P_{\mathrm{elec}} = \dot{m}_{\mathrm{fw}}\frac{E_{\mathrm{spec}}}{3600}, \tag{4.14}$$

where $\dot{m}_{\mathrm{fw}}$ is the freshwater output.

To reflect membrane system dynamics, the freshwater production rate is also ramp-limited:

$$\dot{m}_{\mathrm{fw},k+1} = \dot{m}_{\mathrm{fw},k} + \max(-r_{\mathrm{fw}}\Delta t,\ X)\,, \tag{4.15}$$

$$X = \min(\Delta\dot{m}_{\mathrm{fw}},\ r_{\mathrm{fw}}\Delta t)\,, \tag{4.16}$$

where

$$\Delta\dot{m}_{\mathrm{fw}} = \dot{m}_{\mathrm{fw,target}} - \dot{m}_{\mathrm{fw},k}.$$

The target freshwater flow $\dot{m}_{\mathrm{fw,target}}$ is computed from both the available electrical power and the seawater feed rate. In this formulation, the seawater pump and purification system are represented as demand-driven, low-power subsystems with fast dynamics relative to the downstream hydrogen production and fuel synthesis processes.

4.3.3 Hydrogen Production System

The hydrogen production subsystem consists of a steam superheater and a SOEC, operating sequentially as shown in Figure 4.3. The superheater heats purified water to 700 °C, after which the SOEC converts the resulting steam into hydrogen using both electrical and thermal energy [45]. Their dynamics are tightly linked through mass-flow continuity and coupled electrical/thermal energy constraints.

4.3.3.1 Superheater

Purified water is heated from ambient temperature to 700 °C through three stages [78]: (1) sensible heating of liquid water from 25 to 100 °C, (2) the latent heat of vaporisation at boiling, and (3) superheating of steam from 100 to 700 °C. The total specific energy required per kilogram is

$$E_{\text{per,kg}} = c_{p,\text{liq}}(T_{\text{boil}} - T_{\text{in}}) + h_{\text{vap}} + Z, \tag{4.17}$$

$$Z = c_{p,\text{steam}}(T_{\text{target}} - T_{\text{boil}}). \tag{4.18}$$

The maximum achievable mass flow of 700 °C steam is determined by the thermal power available:

$$\dot{m}_{700^\circ\text{C}} = \frac{P_{\text{thermal}}}{E_{\text{per,kg}}}. \tag{4.19}$$

To represent heat-up delays, transport lags, and the thermal inertia of the real system, the dynamic model applies a first–order ramp limit to the target mass flow:

$$\dot{m}_{k+1} = \dot{m}_k + \max\Big(-r_{\text{sh}}\Delta t,\ \min\big(\Delta\dot{m},\ r_{\text{sh}}\Delta t\big)\Big), \tag{4.20}$$

with

$$\Delta\dot{m} = \dot{m}_{\text{target}} - \dot{m}_k.$$

This ensures the superheater responds realistically to changes in thermal input and upstream water flow.

4.3.3.2 Solid Oxide Electrolyser

The SOEC performs high–temperature electrolysis, using both electrical power and direct thermal energy supplied by the nuclear reactor. This combined energy input increases overall efficiency, expressed as

$$E_{\text{H}_2} = E_{\text{elec}} + E_{\text{thermal}}. \tag{4.21}$$

Hydrogen production at each timestep is jointly constrained by the available electrical power, the available thermal power, and the incoming steam from the superheater:

$$\dot{m}_{\text{H}_2} = \min\left(\frac{P_{\text{elec}}}{E_{\text{elec}}},\ \frac{P_{\text{thermal}}}{E_{\text{thermal}}},\ \frac{\dot{m}_{700^\circ\text{C}}}{9}\right). \tag{4.22}$$

Since 9 kg of water are required per kilogram of hydrogen, the corresponding water consumption is implicit in the final term.

To ensure compatibility with the downstream RWGS reactor, a coordination controller links the SOEC output to the expected CO_2 feed rate. By adjusting hydrogen production toward the required stoichiometric ratio, the system avoids overproduction and maintains stable conditions across the entire fuel-production chain. This predictive coupling keeps both subsystems within their optimal conversion range and improves overall process stability.

4.3.4 Carbon Dioxide Production System

The CO_2 production subsystem consists of an air fan and a DAC unit operating in sequence, as shown in Figure 4.3. The fan provides the bulk airflow, while the DAC extracts CO_2 from ambient air using both electrical and thermal energy. Because atmospheric CO_2 concentration is only 0.065%, very large airflows are required, making DAC the slowest and least mature subsystem within the fuel-production chain [31, 34, 58]. The feasibility of integrating such large-scale DAC equipment on a maritime platform is examined further in chapter 6.

Air Fan System

The air fan converts electrical power into airflow, supplying the DAC unit with the mass flow required for CO_2 capture. The fan follows a linear power–flow relationship:

$$\dot{m}_{\text{air}} = \frac{P_{\text{elec,fan}} \times 10^6}{\text{power}_{\text{per flow}}}, \tag{4.23}$$

The airflow is capped at its rated capacity of 3000 $\text{kg}\,\text{s}^{-1}$, derived from the maximum CO_2 conversion rate of the DAC block. To represent mechanical acceleration limits, the model applies a ramp-rate constraint:

$$\dot{m}_{k+1} = \dot{m}_k + \max\Big(-r_{\text{fan}}\Delta t,\ \min\big(\Delta\dot{m},\ r_{\text{fan}}\Delta t\big)\Big), \tag{4.24}$$

with $\Delta\dot{m} = \dot{m}_{\text{target}} - \dot{m}_k$. This ensures realistic transient fan behaviour.

Direct Air Capture System

The DAC unit extracts CO_2 using three inputs: electrical power, thermal power, and the airflow from the fan. Given the extremely low CO_2 concentration in ambient air, the DAC unit must process very large amounts of air to produce even a small CO_2 stream. The achievable capture rate is constrained by whichever of the three inputs is smallest in relation to one another:

$$\dot{m}_{\text{CO}_2,\text{out}} = \min\left(\frac{P_{\text{elec,in}}}{6.8\times10^{-6}},\ \frac{P_{\text{thermal,in}}}{4.04\times10^{-5}},\ \frac{\dot{m}_{\text{air}}}{1667}\right), \tag{4.25}$$

DAC systems exhibit slow thermal transients due to heating, and desorption dynamics. To model this behaviour, the CO_2 capture rate is updated using ramp-limited dynamics:

$$\dot{m}_{\text{CO}_2,k+1} = \dot{m}_{\text{CO}_2,k} + \Delta\dot{m}_{\text{CO}_2}, \tag{4.26}$$

$$\Delta\dot{m}_{\text{CO}_2} = \max\big(-r_{\text{down}},\ \min\big(\dot{m}^{\max}_{\text{CO}_2} - \dot{m}_{\text{CO}_2,k},\ r_{\text{up}}\big)\big), \tag{4.27}$$

with ramp coefficients selected according to the current utilisation level. Three ramp rates are used to represent slow initial heating, faster mid-range operation, and saturated high-load behaviour [59].

These dynamics ensure that the DAC subsystem correctly governs the overall response speed of the fuel-production chain.

4.3.5 Synthetic Fuel Production System

With hydrogen and CO_2 production established, the final stage of the fuel plant converts these feeds into synthetic diesel, as shown in Figure 4.3. The process chain consists of four reactors operating in sequence: a RWGS reactor, a FT synthesis unit, an ATR, and a hydrocracker. Together these units form a closed recycling loop that maximises carbon utilisation and upgrades the syngas stream into F–76 diesel as the final product.

Reverse Water Gas Shift Reactor

The RWGS unit converts CO_2 and H_2 into CO and H_2O, producing a syngas mixture with a target H_2/CO ratio of approximately 2:1. To achieve this, the inlet $H_2 : CO_2$ ratio is set to 3:1 (molar), equivalent to a mass ratio of roughly $1 : 7.5$ [33]. The reactor exhibits hot start behaviour and ramps gradually due to thermal inertia.

The governing reaction is

$$CO_2 + H_2 \rightarrow CO + H_2O. \tag{4.28}$$

After CO_2 is converted, the achievable syngas mass flow is constrained by reactant availability and power input:

$$\dot{m}_{\text{syngas}} = \min\left(\dot{m}_{\text{CO}} + \dot{m}_{\text{H}_2,\text{left}},\ \frac{P_{\text{elec}}}{E_{\text{elec}}}\right), \tag{4.29}$$

$$\dot{m}_{\text{syngas}} = \min\left(\dot{m}_{\text{syngas}},\ \frac{P_{\text{thermal}}}{E_{\text{thermal}}},\ \dot{m}_{\text{max}}\right), \tag{4.30}$$

$$E_{\text{elec}} = 1.4 \times 10^{-5}\ \text{MW}\,(\text{kg/s})^{-1}, \qquad E_{\text{thermal}} = 3.57 \times 10^{-5}\ \text{MW}\,(\text{kg/s})^{-1}.$$

Dynamic behaviour is captured through a ramp constraint:

$$\dot{m}_{k+1} = \dot{m}_k + \max\Big(-r_{\text{rwgs}}\Delta t,\ \min(\Delta\dot{m},\ r_{\text{rwgs}}\Delta t)\Big). \tag{4.31}$$

Fischer–Tropsch Reactor

The FT reactor converts syngas into long and short chain hydrocarbons following the catalytic polymerisation mechanism

$$(2n+1)\,H_2 + n\,CO \rightarrow C_nH_{2n+2} + n\,H_2O. \tag{4.32}$$

The FT process generates a broad product distribution governed by the Anderson–Schulz–Flory model as explained in section 2.3. Only the C_{10}–C_{20} fraction corresponds to diesel range hydrocarbons; without downstream upgrading this yields roughly 40% diesel [54].

The achievable hydrocarbon production rate is limited by electrical input, syngas availability, and reactor capacity:

$$\dot{m}_{\text{HC}} = \min\Big(P_{\text{elec}}/E_{\text{FT}},\ \eta_{\text{conv}}\dot{m}_{\text{syngas}},\ \dot{m}_{\text{max}}\Big), \tag{4.33}$$

$$E_{\text{FT}} = 1.443 \times 10^{-4}\ \text{MW}\,(\text{kg/s})^{-1}, \qquad \eta_{\text{conv}} = 0.92.$$

The total output is split into short, diesel range, and long hydrocarbons:

$$\dot{m}_{\text{short}} + \dot{m}_{\text{F-76}} + \dot{m}_{\text{long}} = \dot{m}_{\text{HC}}. \tag{4.34}$$

The diesel stream (F–76) leaves the synthesis chain; shorter and longer hydrocarbons are recycled through the ATR and hydrocracker.

Autothermal Reformer

The ATR converts recycled short chain hydrocarbons into syngas, closing the carbon loop and increasing overall diesel yield. The reactor combines partial oxidation and reforming reactions, balancing exothermic and endothermic contributions to maintain autothermal conditions.

The achievable syngas flow is

$$\dot{m}_{\mathrm{ATR}} = \min\Big(0.85\,\dot{m}_{\mathrm{short,tot}},\ P_{\mathrm{elec}}/E_{\mathrm{elec}},\ P_{\mathrm{thermal}}/E_{\mathrm{thermal}},\ \dot{m}_{\max}\Big), \tag{4.35}$$

$$E_{\mathrm{elec}} = 2.3 \times 10^{-5}\ \mathrm{MW\,(kg/s)^{-1}}, \qquad E_{\mathrm{thermal}} = 1.04 \times 10^{-5}\ \mathrm{MW\,(kg/s)^{-1}}.$$

Ramp limits are included to reflect reactor thermal inertia.

Hydrocracker

The hydrocracker upgrades long-chain hydrocarbons ($C_{21}+$) into diesel-range and short-chain fractions through catalytic cracking and hydrogenation. Processing capacity is limited by feed availability, electrical power, thermal power, and reactor design constraints:

$$\dot{m}_{\mathrm{feed}} = \min\left(\dot{m}_{\mathrm{long}},\ \frac{P_{\mathrm{elec}}}{E_{\mathrm{elec}}},\ \frac{P_{\mathrm{thermal}}}{E_{\mathrm{thermal}}},\ \dot{m}_{\max}\right), \tag{4.36}$$

The converted fraction is

$$\dot{m}_{\mathrm{conv}} = 0.9\,\dot{m}_{\mathrm{feed}}. \tag{4.37}$$

with products

$$\dot{m}_{\text{F-76}} = 0.7\,\dot{m}_{\mathrm{conv}}, \qquad \dot{m}_{\mathrm{short}} = 0.3\,\dot{m}_{\mathrm{conv}}. \tag{4.38}$$

Only the diesel fraction leaves the synthesis chain; the short fraction is recycled to the ATR.

4.4 Fuel Storage Model

Once the hydrocarbon stream is converted into F–76 diesel, the product enters the fuel storage block, representing the mothership's internal fuel tanks. The system accumulates fuel continuously from the production plant and discharges it according to scheduled refuelling tasks. The initial fuel level is set to 500 000 kg, representing a realistic partially loaded departure condition that leaves space for fuel production from the very start while still enabling immediate refuelling operations. The maximum capacity is limited to 700 000 kg. This capacity is much smaller than the 5 000 000 kg typical of large naval oilers [79], this was done to emphasise the role of onboard production.

The storage model tracks fuel inventory and authorises new refuelling tasks only when sufficient reserves exist. Refuelling begins once the mothership reaches the scheduled rendezvous point and proceeds at a capped transfer rate of 100 000 kg h^{-1}. This limit is based on typical Replenishment-At-Sea hose and pumping capacities [80].

4.5 Ship Systems Model

The ship systems block, shown in Figure 4.1, represents all non fuel production energy consumers, namely propulsion and hotel loads. The hotel load is modelled as a constant 3 MWe, capturing essential vessel functions such as lighting, HVAC and control systems. This load is assumed to operate continuously throughout the mission.

Propulsion receives the remaining electrical power after hotel demand is met, with the available propulsion power

$$P_{\text{prop}} = \max\big(P_{\text{avail}} - P_{\text{hotel}},\, 0\big). \tag{4.39}$$

The resulting ship speed is obtained from the empirical speed power curve derived from Figure 2.11.

The ship navigates toward an EMS-assigned waypoint. At time step k, with ship position $\mathbf{x}_k$ and target $\mathbf{x}_{\text{tgt}}$, the distance and unit direction are

$$d_k = \|\mathbf{x}_{\text{tgt}} - \mathbf{x}_k\|\,, \tag{4.40}$$

$$\hat{\mathbf{d}}_k = \begin{cases} \dfrac{\mathbf{x}_{\text{tgt}} - \mathbf{x}_k}{d_k}, & d_k > d_{\text{tol}}, \\ \mathbf{0}, & d_k \le d_{\text{tol}}, \end{cases} \tag{4.41}$$

where $d_{\text{tol}} = 0.1$ km avoids oscillation near the target.

The next position is computed by forward integration:

$$\mathbf{x}_{k+1} = \mathbf{x}_k + v_{\text{km s}^{-1}}\, \Delta t\, \hat{\mathbf{d}}_k, \tag{4.42}$$

with the additional constraint that the ship cannot overshoot the destination:

$$\text{if } v_{\text{km s}^{-1}} \Delta t \ge d_k \quad \Rightarrow \quad \mathbf{x}_{k+1} = \mathbf{x}_{\text{tgt}}. \tag{4.43}$$

This subsystem therefore converts electrical power into propulsion output and computes vessel movement at each simulation step, ensuring consistent interaction with the EMS, refuelling logic, and mission control framework.

5 | Energy Management System Architecture

With the mothership's energy system now designed, this chapter describes how these subsystems are coordinated during operation. As outlined in section 2.6, the EMS serves as the supervisory control layer that determines how electrical and thermal power are distributed across the vessel. In traditional marine applications, the EMS focuses on internally balancing power generation, propulsion, and hotel loads. In the mothership this is achieved by coordinating flexible loads such as the synthetic fuel plant and the onboard ESS, which absorb excess energy or supply additional power during peak demand.

For the refuelling mothership, internal energy management alone is insufficient. The vessel functions not only as an energy consumer but also as an energy producer and a mobile refuelling hub for multiple autonomous USVs. To fully exploit the capability of the integrated fuel production plant, the EMS architecture is therefore expanded beyond the vessel itself to include a fleet-wide coordination layer. Because USVs operate with preplanned routes and predictable refuelling needs, this information can be incorporated into the EMS to optimise the mothership's operations.

This chapter answers the fifth sub-question:

6. *What energy management system (EMS) hierarchy can coordinate power generation, storage, and fuel production under varying operational conditions?*

Chapter structure.

- **section 5.1** — Design and implementation of the Local rule-based EMS.
- **section 5.2** — Development of the Fleet-Wide optimization EMS.

Together, these two layers constitute the full EMS architecture of the nuclear-powered refuelling mothership.

5.1 Local Energy Management System

The Local EMS provides the stabilising control layer for the mothership by coordinating reactor output, battery usage, propulsion power, and the synthetic-fuel production chain. A rule-based strategy was selected because it offers fully transparent behaviour and verifiable logic in the absence of empirical data [67]. The EMS continuously allocates power such that the nuclear reactor operates near steady output while ship operations and fuel production remain within physical limits.

5.1.1 Rule-based EMS logic

The hierarchical structure of the EMS, shown in Figure 5.1, places the EMS at the top level, where it issues commands to Level 2 propulsion and fuel-production controllers, which in turn operate their internal subsystems.

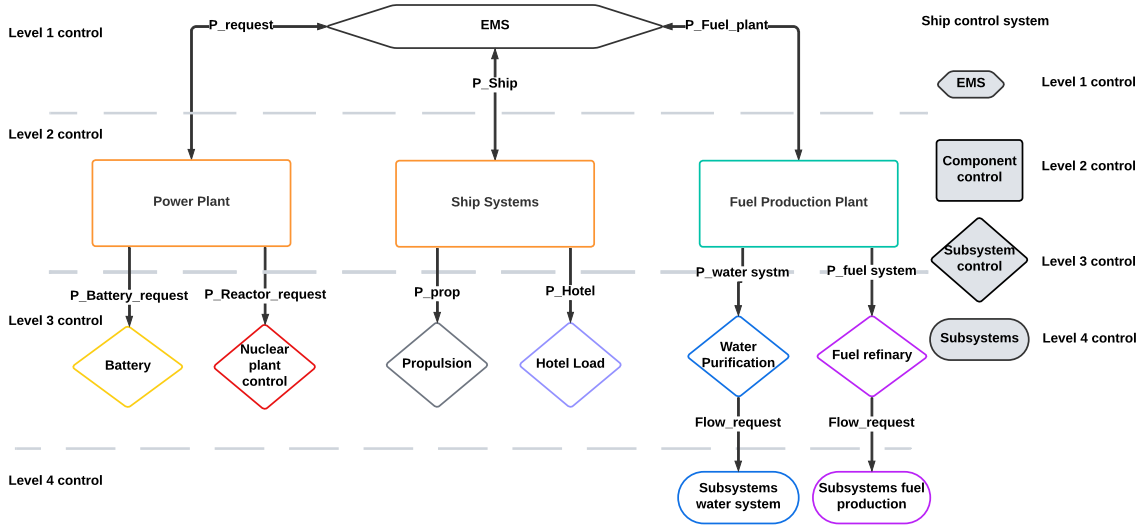

Figure 5.1: Mothership Local Control Levels Hierarchy

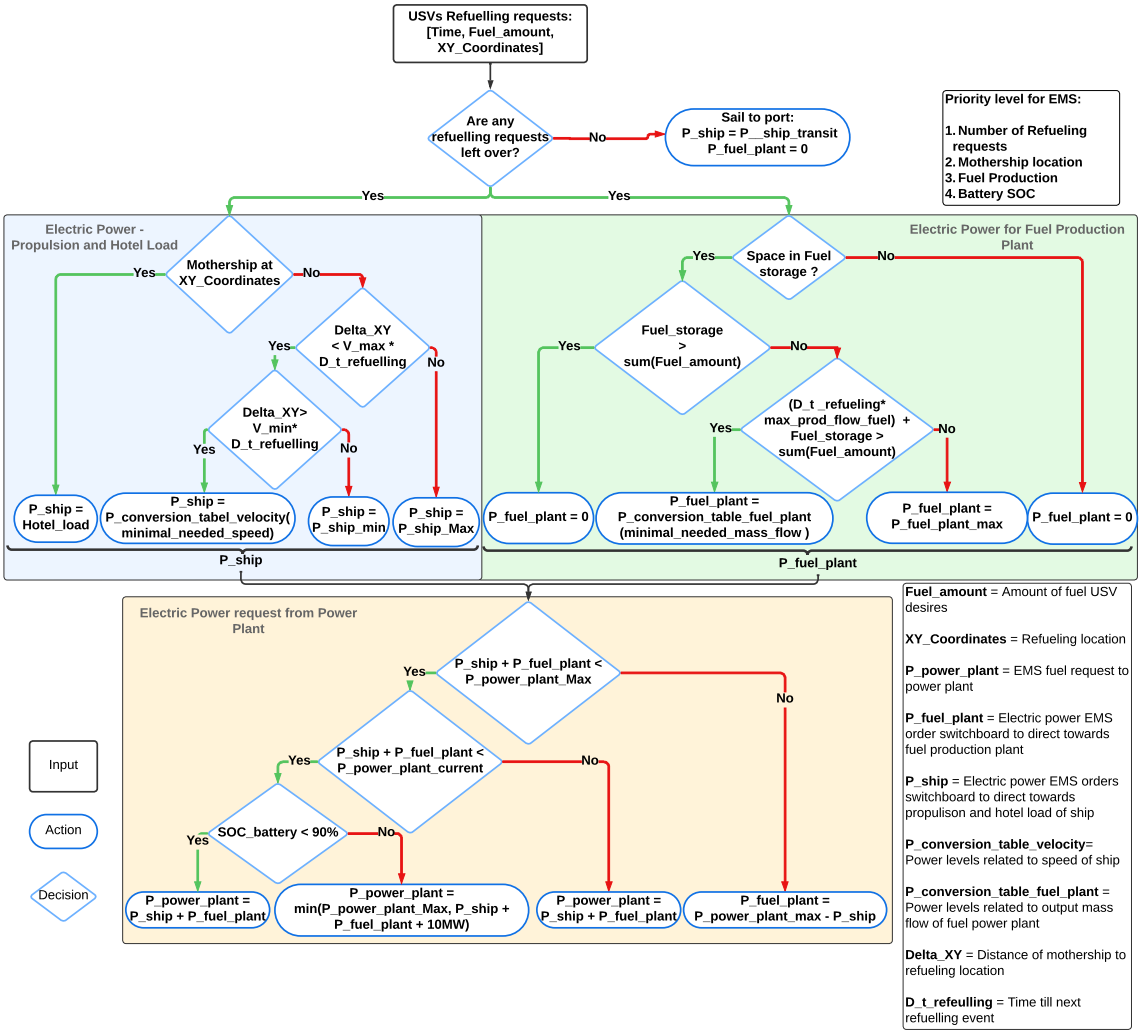

Figure 5.2: Local Rule-based EMS Flowchart

Before implementation, the full control logic was drafted as a detailed flowchart (see Figure 5.2).

Incoming refuelling requests drive all subsequent decisions, which are grouped into three decision branches: navigation, propulsion, and fuel-production commands. Each branch outputs orders to the corresponding Level 2 subsystem.

5.1.2 Simulink Implementation

The Local EMS operates as a finite-state machine that moves the mothership through a set of mission states (transit, refuel, drift, hold, return-to-port). Each state selects a target waypoint $\mathbf{x}_{\text{tgt}}$ and a desired sailing speed v_{cmd}, from which the EMS computes propulsion power. Propulsion power follows the interpolated speed–power curve shown in section 2.4.

The EMS manages the mothership's energy flows according to

$$P_{\text{total}} = P_{\text{ship}} + P_{\text{fuel}}. \tag{5.1}$$

Surplus power is routed to battery charging, while deficits trigger battery discharge. If the battery reaches minimum state of charge, the EMS automatically reduces P_{fuel} to preserve propulsion and essential hotel loads.

To ensure physical behaviour, changes in propulsion power are ramp-limited:

$$\Delta P_{\text{ship}} = \max\big(-r_{\text{prop}},\, \min(P_{\text{ship}} - P_{\text{ship},k},\, r_{\text{prop}})\big), \tag{5.2}$$

with $r_{\text{prop}} = 30\ \text{MW}\,\text{min}^{-1}$, which avoids oscillatory behaviour while appearing instantaneous at the mission timescale.

Given propulsion power, the nominal fuel production power is

$$P_{\text{fuel,nom}} = \max(P_{\text{target}} - P_{\text{ship}},\ 0)\,, \tag{5.3}$$

where the reactor target is held at

$$P_{\text{target}} = 0.95\, P_{\text{max}}. \tag{5.4}$$

To avoid sharp fluctuations entering the thermochemical plant, P_{fuel} is smoothed using a moving-average, first-order low-pass filter:

$$P_{\text{fuel},k+1} = (1-\alpha)\, P_{\text{fuel},k} + \alpha\, P_{\text{fuel,raw}}, \tag{5.5}$$

with

$$\alpha = \frac{\Delta t}{\tau + \Delta t}, \qquad \tau = 5\ \text{s}, \tag{5.6}$$

as recommended for thermochemical process stability [81].

The resulting electrical power demand placed on the reactor is

$$P_{\text{req}} = P_{\text{ship}} + P_{\text{fuel},k+1}, \tag{5.7}$$

and reactor power changes obey a thermal ramp limit:

$$\Delta P_{\text{req}} = \max\big(-r_{\text{rxr}},\, \min(P_{\text{req}} - P_{\text{req},k},\, r_{\text{rxr}})\big), \tag{5.8}$$

with $r_{\text{rxr}} = 0.1\, P_{\text{max}}$ per minute, matching the VHTR characteristics.

For navigation, the EMS computes distance to the target each time step.

$$d_k = \|\mathbf{x}_{\text{tgt}} - \mathbf{x}_k\|\,, \tag{5.9}$$

$$\hat{\mathbf{d}}_k = \begin{cases} \dfrac{\mathbf{x}_{\text{tgt}} - \mathbf{x}_k}{d_k}, & d_k > d_{\text{tol}}, \\ \mathbf{0}, & d_k \le d_{\text{tol}}, \end{cases} \tag{5.10}$$

with $d_{\text{tol}} = 0.1$ km. Position is updated as

$$\mathbf{x}_{k+1} = \mathbf{x}_k + v_{\text{km s}^{-1}}\, \Delta t\, \hat{\mathbf{d}}_k, \tag{5.11}$$

with overshoot prevention:

$$\text{if } v_{\text{km s}^{-1}} \Delta t \geq d_k \quad \Rightarrow \quad \mathbf{x}_{k+1} = \mathbf{x}_{\text{tgt}}. \tag{5.12}$$

The Local EMS forms the stabilising foundation of the intrnal energy system architecture. It regulates power flows, enforces physical ramp limits and governs ship navigation. Verification tests in chapter 6 demonstrate that the rule-based EMS is correctly implemented.

5.2 Fleet-Wide Energy Management System

Testing of the Local EMS revealed as that the mothership's mission performance was limited not by internal power management, but by its inability to use its fuel reserves strategically, this will be demonstrated in chapter 7. In the rule-based configuration, the mothership reacted passively to USV refuelling requests in the order they arrived, without influencing their timing or sequencing. While this behaviour is sufficient for validating physical realism, it does not reflect how real missions operate, since USVs generally follow predictable routes, task sequences, and fuel-use patterns.

To address this limitation, the EMS framework was expanded with a Fleet-Wide EMS. This new layer informs the Local EMS of upcoming refuelling demands and mission timing, enabling the mothership to plan ahead rather than react. The control layer integration is shown in Figure 5.3.The EMS remains the top supervisory controller; however, a new Level 2 "USV Fleet" block provides the Fleet-Wide EMS with the planned USV tasks.

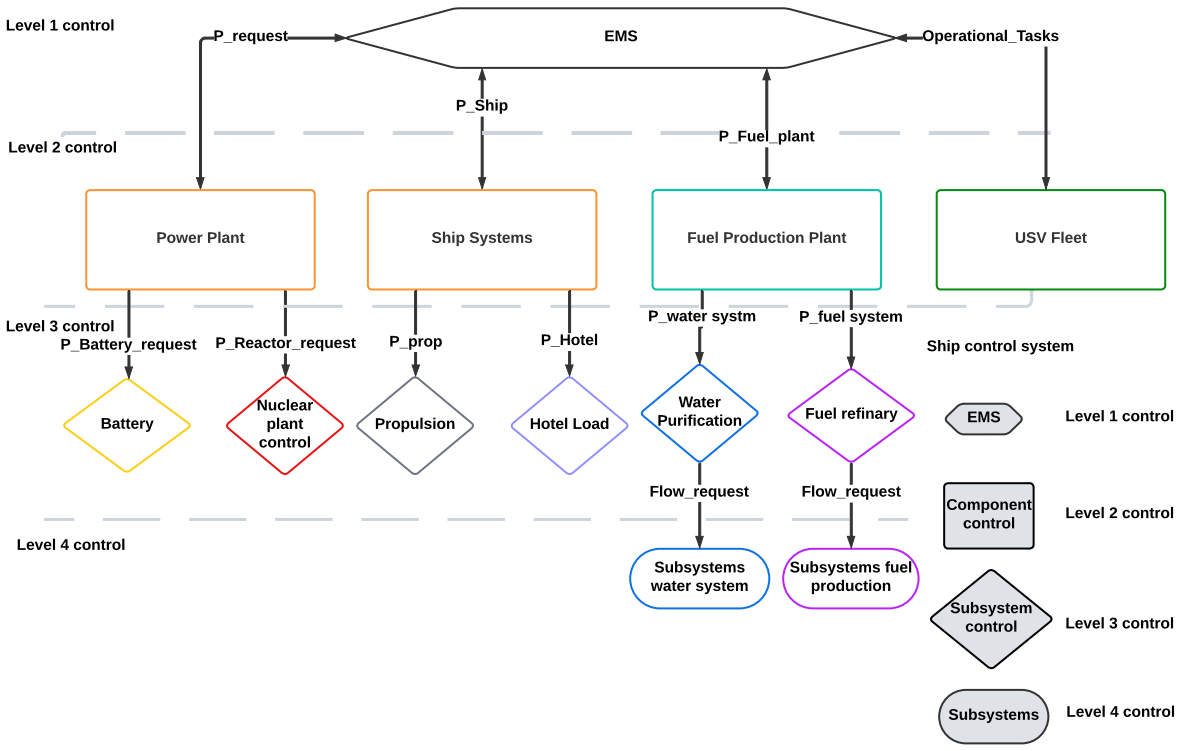

Figure 5.3: Mothership Fleet-Wide Control Levels Hierarchy

The Fleet-Wide EMS is formulated as a Mixed-Integer Linear Program (MILP) [82] and implemented in Python using the Gurobi optimiser. Rather than replacing the Local EMS, it extends it by determining when and where each refuelling event should occur, the optimal order of USVs, the chosen operational areas (AOs), and feasible hub positions for each refuel. The mothership and USVs are treated as a coupled system whose movements and fuel exchange events are optimised to reduce total fuel transferred, thereby extending the mothership's usable reserves.

5.2.1 Optimisation Structure

The mathematical formulation of the MILP defines all components required to construct a feasible refuelling schedule. It outlines the decision space through sets and variables, the objective to minimise fuel transfer, and the constraints that ensure realistic and physically consistent multi-USV operations.

The MILP determines:

- ordering and assignment of tasks,
- selection of refuelling locations,
- USV sailing speeds and route choices,
- timing of all arrivals, departures, and refuelling operations,
- mothership hub position and movement.

Sets

- U : set of USVs.
- $P = \{1, 2, 3\}$: task slots per USV.
- I : set of all tasks across all AOs.
- S : discrete sailing speeds.
- X : candidate refuelling positions for the mothership hub.

Decision Variables

- $a_{u,p,i} \in \{0, 1\}$: task i is assigned to USV u in slot p.
- $t^{\text{start}}_{u,p}$, $t^{\text{AO}}_{u,p}$, $t^{\text{ref}}_{u,p}$, $t^{\text{end}}_{u,p}$: timing of task start, AO arrival, refuel start, and task completion.
- $f^{\text{bef}}_{u,p}$, $f^{\text{aft}}_{u,p}$: USV fuel levels before and after slot p.
- $r_{u,p} \in \{0, 1\}$: refuel decision after slot p.
- $y^{\text{fw}}_{u,p,s}$, $y^{\text{ret}}_{u,p,s}$, $y^{\text{back}}_{u,s}$: one-hot indicators for sailing speeds.
- $x_{u,p} \in X$: selected hub position for refuelling event (u, p).

Objective Function

The optimiser minimises the total refuelled fuel while applying a small penalty to mission duration:

$$\min J = \sum_{u \in U} \sum_{p \in P} \left(f^{\text{aft}}_{u,p} - f^{\text{bef}}_{u,p} \right) \; + \; \varepsilon \sum_{u \in U} t^{\text{end}}_{u,2}, \qquad \varepsilon \ll 1. \tag{5.13}$$

Constraint Structure

The MILP enforces the following families of constraints.

1. *Task assignment:* Each task $i \in I$ must be assigned once, and every USV $u \in U$ must fill all three mission slots $p \in P$. The binary variable $a_{u,p,i}$ indicates whether USV u performs task i in slot p:

$$\sum_{u \in U} \sum_{p \in P} a_{u,p,i} = 1 \qquad \forall i \in I, \tag{5.14}$$

$$\sum_{i \in I} a_{u,p,i} = 1 \qquad \forall u \in U,\ p \in P. \tag{5.15}$$

2. *Travel geometry:* Travel times depend on sailing speed $v(s)$ for speed index $s \in S$. The binary $y_{u,p,s}$ selects the speed, and d denotes the travel distance:

$$t^{\text{in}}_{u,p} = t^{\text{start}}_{u,p} + \sum_{i,s} a_{u,p,i}\, y_{u,p,s}\, \frac{d}{v(s)}. \tag{5.16}$$

3. *AO dwell:* Each operational area $a \in A$ imposes a dwell time $\tau^{\text{AO}}_{a(i),p}$ for task i:

$$t^{\text{out}}_{u,p} = t^{\text{in}}_{u,p} + \sum_{i} a_{u,p,i}\, \tau^{\text{AO}}_{a(i),p}. \tag{5.17}$$

4. *Refuelling:* Only one USV may refuel at a time. Binary $b_{r,s}$ indicates whether refuel event r occurs before s; M is a big-M constant:

$$t^{R}_{s} \geq t^{\text{end}}_{r} - M(1 - b_{r,s}), \tag{5.18}$$

$$t^{R}_{r} \geq t^{\text{end}}_{s} - M b_{r,s}. \tag{5.19}$$

5. *Mothership mobility:* Mothership position during refuelling r is X_r. The Mothership speed limit is $V^{\max}_{\text{hub}}$:

$$|X_s - X_r| \leq V^{\max}_{\text{hub}}\,(t^{R}_{s} - t^{\text{end}}_{r}) + M(1 - b_{r,s}). \tag{5.20}$$

6. *Mothership fuel stock:* Fuel transferred $f^{\text{aft}}_{u,p} - f^{\text{bef}}_{u,p}$ must not exceed the initial store S_0, produced fuel $\eta^{\text{prod}} t^{R}_{u,p}$, and remaining stock after earlier refuels $g_{q,r}$:

$$f^{\text{aft}}_{u,p} - f^{\text{bef}}_{u,p} \leq S_0 + \eta^{\text{prod}}\, t^{R}_{u,p} - \sum_{q<r} g_{q,r}. \tag{5.21}$$

7. *USV fuel feasibility:* Fuel before task p for USV u is $f^{\text{bef}}_{u,p}$, derived from departure fuel $f^{\text{dep}}_{u,p}$ minus: (i) travel burn, (ii) AO dwell burn, (iii) waiting burn. It must stay above the minimum safe fuel F^{minUSV}:

$$f^{\text{bef}}_{u,p} = f^{\text{dep}}_{u,p} - (\text{travel} + \text{dwell} + \text{wait}), \tag{5.22}$$

$$f^{\text{bef}}_{u,p} \geq F^{\text{minUSV}}. \tag{5.23}$$

8. *Return-to-port:* USV must return to port before the mission horizon $T^{\max}$. The time t^{P1}_{u} must account for either Mothership→port distance d^{HP} or AO→port distance $d^{\text{AP}}_{a(i)}$:

$$t^{P1}_{u} \leq t^{P0}_{u} + \frac{d^{\text{HP}}}{v(s)}, \tag{5.24}$$

$$t^{P1}_{u} \leq t^{P0}_{u} + \frac{d^{\text{AP}}_{a(i)}}{v(s)}, \tag{5.25}$$

$$t^{P1}_{u} \leq T^{\max}. \tag{5.26}$$

Solver Configuration

The MILP is solved using Gurobi with the following key parameters:

- `MIPFocus = 1`: prioritise feasible high-quality solutions.
- `MIPGap = 0.10`: terminate when the solution is within 10% of optimality.
- `Presolve = 2`, `Heuristics = 0.25`: balance speed and robustness.

The constraint structure of the Fleet-Wide EMS reflects the operational realities of coordinating an unmanned fleet and ensures that all generated schedules remain physically and logistically feasible. By enforcing all constraints as stated above, the MILP captures the essential rules governing multi USV operations. Discretised refuelling locations, sailing speeds, and precomputed distance maps provide a structured decision space that keeps the optimisation tractable while still representing the key dynamics of USV movement and energy use. These constraints do not restrict the optimiser; rather, they define a realistic and well-bounded problem within which the Fleet-Wide EMS can coordinate USVs effectively, ensuring safe scheduling, predictable interactions, and energy-consistent behaviour across the entire fleet.

The purpose of the Fleet-Wide EMS optimisation is to demonstrate that a feasible and realistic refuelling plan exists for different numbers of USVs, the MILP was not driven to very small optimality gaps. Instead, a GAP of MIPGap = 10% was selected to avoid excessive computation times. This means the solution found was 10% away from the theoretical best solution.

By solving this MILP, the Fleet-Wide EMS generates an optimised schedule of refuelling events that minimises total transferred fuel while ensuring all USVs complete their missions safely. It transforms the mothership's EMS from a purely onboard power manager into a fleet-wide coordination system, enabling synchronised and energy-efficient operation across the entire unmanned fleet. The full mathematical formulation is provided in section 9.3, and results are discussed in section 7.5.

6 | Model Verification

With the complete mothership energy system modelled, the next step is to verify that its power flows, mass flows and subsystem interactions behave in a realistic and consistent manner. Due to no integrated reference model exsiting in literature, external validation is not possible. Instead, internal verification is performed to ensure that all model responses are stable, coherent, and can be explained within realistic limits.

The verification process evaluates both numerical behaviour and physical feasibility. Numerically, the goal is to confirm that the system maintains witin in predefined system limits and responds expectantly during use. Physically, the goal is to determine whether all major subsystems can realistically fit within the proposed hull geometry.

This chapter is organised into the following sections:

Chapter structure.

- section 6.1 — Steady state consistency test.
- section 6.2 — Dynamic ramp up test.
- section 6.3 — Dynamic ramp down test.
- section 6.4 — Mission profile test
- section 6.5 — Physical feasibility Assessment
- section 6.6 — Discussion on feasibility and verification of model

6.1 Steady-State Consistency Test

In this test, the mothership was instructed to sail at 13 kn while the fuel-production plant operated at maximum capacity. The objective is to confirm that all subsystems remain stable under constant power and load. Results are shown in Figure 6.1.

The ship maintains steady operation throughout the test. Plot 1 shows that the reactor supplies the full electrical and thermal demand, producing 45 MWe and 25 MWth (96.1% of reactor max utilization). Since the reactor is allowed to operate between 30% and 100%, these values fall within its realistic range.

Plot 2 confirms that generated power matches total demand. The ship consumes 14.5 MWe in total, split into 3 MWe hotel load and 11.5 MWe propulsion power. Using the power–speed curve from Figure 2.11, this corresponds to a sailing speed of 13 kn, consistent with the test setup.

Plots 3 and 4 show the power and mass flows within the fuel production plant. All power signals remain stable. The SOEC, FT reactor, and hydrocracker dominate electrical consumption, while the Super Heater and DAC unit form the main thermal load. Mass flows behave as expected: purified water flow is higher due to replenishing the water reservoir roughly every 25 minutes at full production, matching the behaviour described in subsection 4.3.2.

Overall, the system remains stable under steady-state conditions, confirming internal consistency of power and mass flows. The next test therefore examines dynamic behaviour.

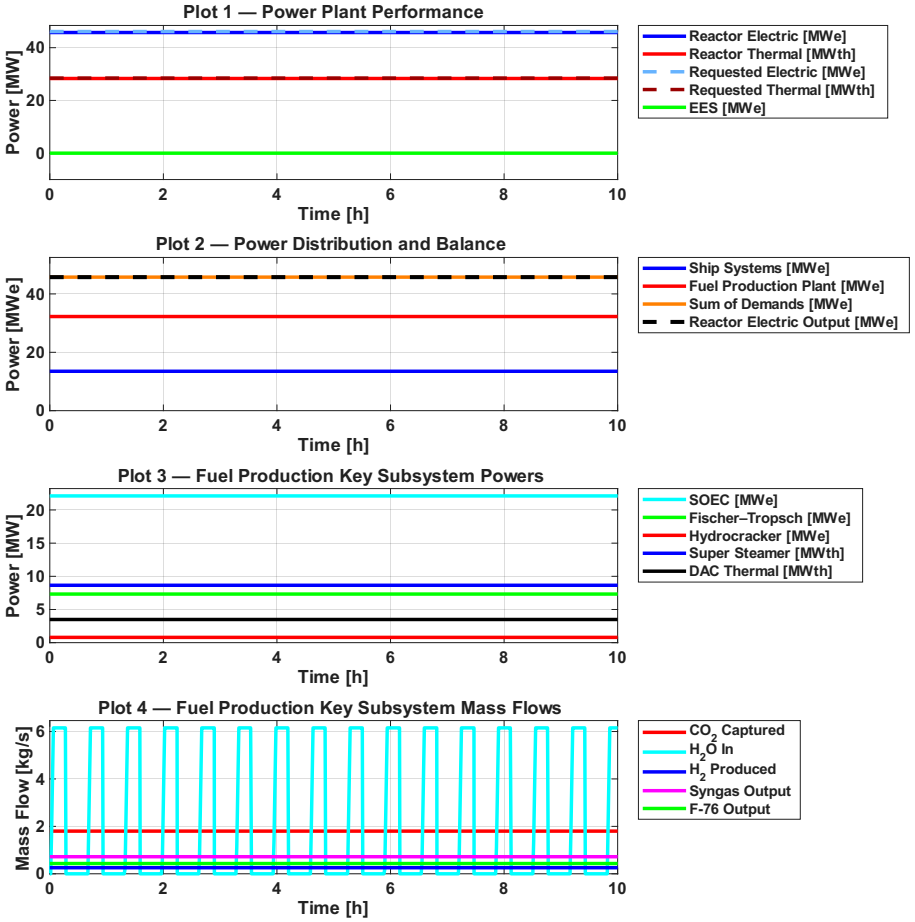

Figure 6.1: Steady-state consistency test showing key model parameters.

6.2 Dynamic Ramp Up Test

In this test, the model response to maximum positive change in power demand is evaluated. For the ramp-up, the reactor begins at its 30% minimum utilization with no battery usage. Propulsion and fuel production are then activated simultaneously to 13 kn and full capacity, with the ESS initially at 50% SOE. The resulting behaviour is shown in Figure 6.2.

At $t = 0$ in plot 1, total power demand jumps to its maximum. Because the reactor is ramp-rate limited as explained in chapter 4, it must increase output at 10% per minute, so the ESS discharges at its full 15 MWe rate to provide immediate propulsion power. A minor modelling inaccuracy appears in the thermal-demand signal: the EMS links thermal and electrical requests, so ESS increased discharge temporarily triggers an oversized thermal request. Once the reactor reaches its thermal cap, this imbalance corrects itself without affecting system performance.

The EMS uses the ESS aggressively, continuing to support system demand for about 20 minutes after the reactor reaches full output. By roughly 30 minutes, the ESS is depleted. A brief negative power dip follows due to the one time step control delay between the EMS and the battery subsystem, which also explains the small oscillations in the total power trace.

The second plot shows that propulsion receives full power from the start, while overall power balance is achieved only once the reactor has fully ramped up. Plots 3 and 4 show power and mass flows within the fuel-production plant. As the ESS depletes, electrical power to the SOEC and FT reactor decreases, while the DAC and superheater powered directly by thermal output—remain unaffected.

As discussed in subsection 4.3.4, the DAC is the slowest-ramping subsystem. It reaches full power within 10 minutes, but its mass flow stabilises only after about 0.45 h, representing thermal inertia into the system. Notably, once the ESS is empty, the CO_2 mass flow remains steady because it is limited by mass inflow rather than power, indicating that additional tuning may further improve model fidelity.

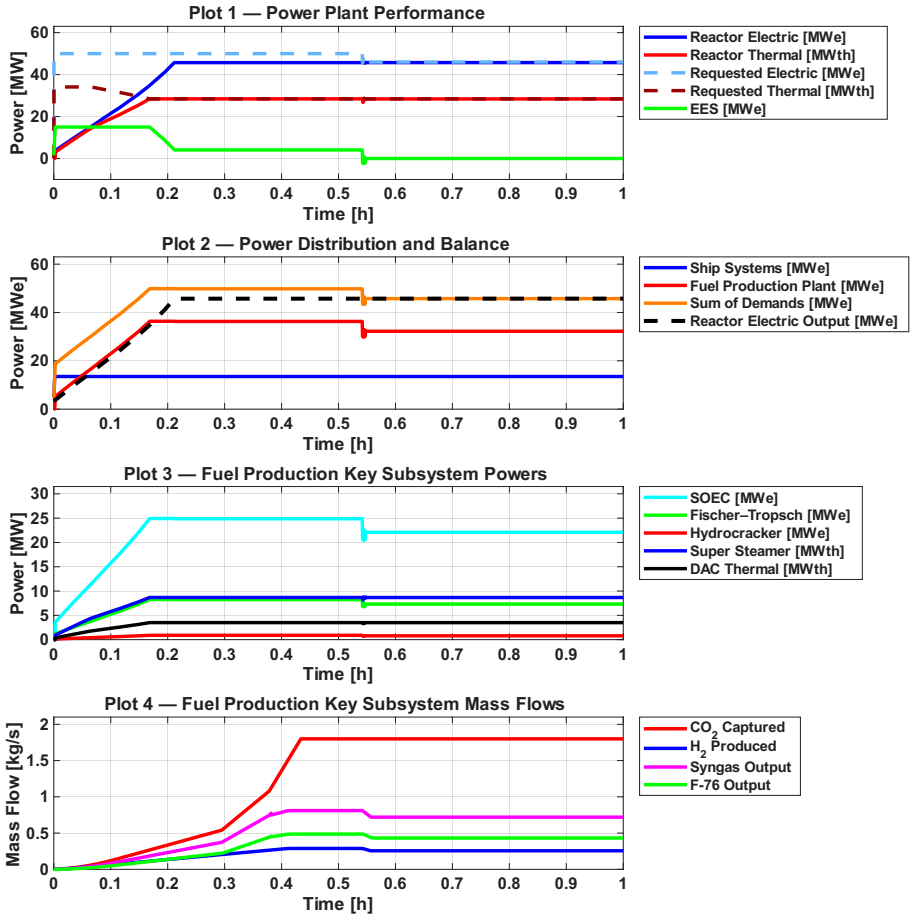

Figure 6.2: Dynamic ramp-up test showing key model parameters.

6.3 Dynamic Ramp-Down Test

The ramp-down test evaluates how quickly the system can reduce power output when demand drops. The model response is shown in Figure 6.3.

Plot 1 shows that power requests fall to their minimum, leaving only the hotel load in the electrical demand. Thermal supply to the fuel-production plant is cut immediately, and the reactor ramps down accordingly. If the ESS is not fully charged, it absorbs excess reactor output to avoid energy wastage. Although excess heat could alternatively be dumped as explained in chapter 4, the EMS instead stores it in the ESS, reflecting a controlled rather than emergency shutdown strategy.

Plot 2 shows that only the 3 MWe hotel load remains active. The reactor electrical output stays at its 30% minimum utilisation limit; while this residual power would not be converted into electricity in reality, it is retained in the model for visual clarity.

Plot 3 illustrates the immediate removal of electrical and thermal power from all production subsystems. In practice, small amounts of power would still be required for control and shutdown,

but these processes fall outside the scope of this work.

Plot 4 shows the gradual decline in CO_2 production, reflecting the DAC's thermal inertia and its intentionally slow ramp rate. An instantaneous drop to zero would be physically unrealistic, whereas the slow decay better represents the subsystem's natural cooldown behaviour. Any excess CO_2 generated during this period could be safely vented through a pressure-release system if the plant were fully shut down.

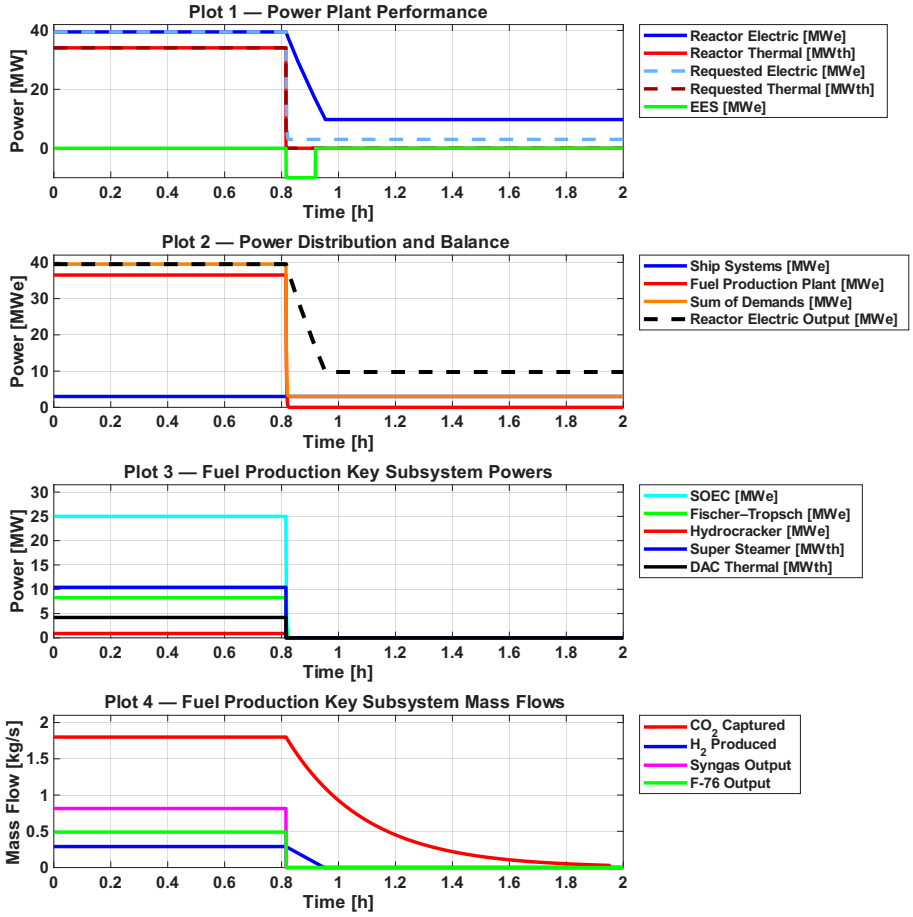

Figure 6.3: Dynamic Ramp-Down Test — Key Model Parameters

6.4 Mission Profile Test (1-Hour Operational Scenario)

This test represents a short operational refuelling cycle. During refuelling, the mothership transitions from stationary waiting to sailing at 10 kn while supplying fuel to a USV. After refuelling, it returns to the refuelling location at 17 kn and waits for the next operation. The system response is shown in Figure 6.4.

Plot 1 shows the ship remaining stationary until roughly 0.8 h, after which it accelerates. Plot 2 indicates propulsion power increasing from the 3 MWe hotel load to 11 MWe, corresponding to a sailing speed of 10 kn. During this ramp-up, the ESS compensates for the reactor's limited ramp rate, ensuring the fuel-production plant remains fully powered. A similar compensation occurs when the mothership sails back after refuelling and propulsion power peaks, maintaining stable plant operation.

Once the ship returns to the refuelling point, propulsion power drops, but the reactor continues producing about 5 MWe more than required. The EMS intentionally maintains this surplus to

recharge the ESS in preparation for the next manoeuvre.

A notable behaviour appears in the thermal power trace: direct thermal supply decreases during this phase. This occurs because the EMS anticipates ESS support on the electrical side but does not adjust the corresponding thermal demand, causing an unintended reduction in total plant heat input. Although physically incorrect, this reduction has minimal impact on mass flows due to the system's existing buffers. Plot 4 confirms that subsystem behaviour remains stable; the DAC in particular has strong thermal inertia, making it insensitive to small heat variations.

While this inconsistency does not affect the validity of the test, refining the EMS coupling between thermal and electrical demand would improve model accuracy in future work.

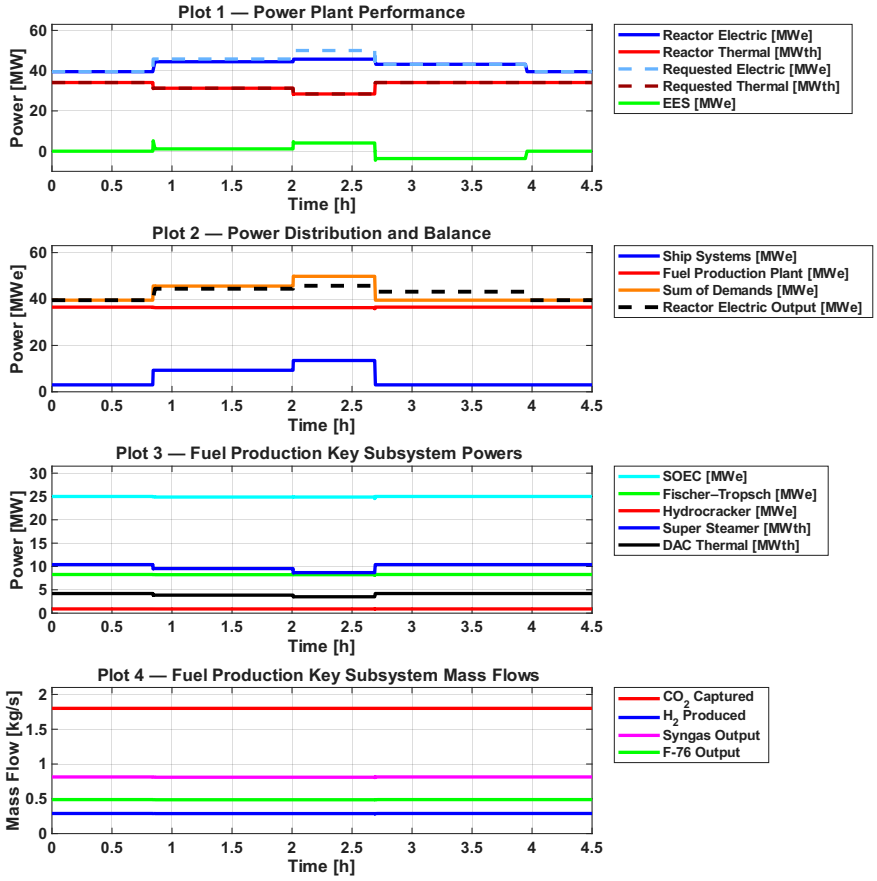

Figure 6.4: Mission Profile Test — Key Model Parameters

6.5 Physical Feasibility Assessment

Beyond numerical verification, the physical feasibility of the energy system depends on whether all subsystems can be accommodated within the mothership's geometry and displacement limits. Although this thesis does not aim to produce a complete ship design, it demonstrates that the motherships fuel producing energy system could be arranged within practical spatial constraints of a ship hull.

An initial dimensional sizing was performed in section 2.5, based on literature for comparable maritime and industrial systems. These values were refined during model development because the subsystems were tuned to each other which altered the power and mass requirements. The resulting subsystem volumes and masses are summarised in Table 10.5, representing the best

estimate of their relative contribution to internal layout and overall mass distribution.

To assess spatial feasibility more concretely, a 3D model of the mothership was created using these updated dimensions. This visualisation illustrates the approximate placement of the primary subsystems within the hull, following the layout principles discussed in chapter 4. The purpose is not detailed naval architecture but to verify that the power plant and fuel-production plant can realistically fit within the proposed hull.

The 3D representation confirms that the integrated systems can be accommodated within the ship's dimensions. The DAC tower has the largest overall volume, as mentioned in section 4.3 60% of its volume must be above deck to facilitate the air fans. The reactor and other fuel-production modules can be positioned easily within the hull. ESS units and fuel tanks are placed low in the hull, providing ballast and structural balance. This demonstrates that the general arrangement is feasible, though a full naval-architectural study would be required to prove any true feasibility.

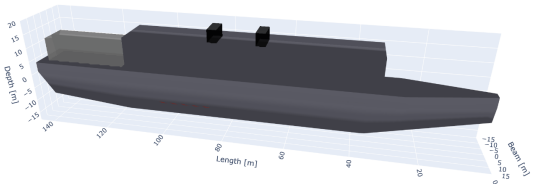

(a) Top view — Full hull and onboard layout

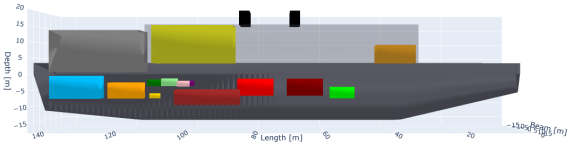

(b) Side view — Draft and deck structure

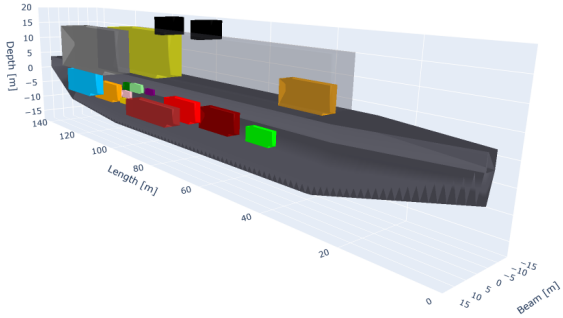

(c) Angled view — Reactor and fuel systems

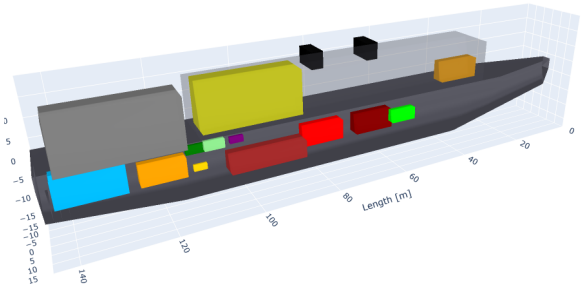

(d) Rear view — Propulsion and DAC zone

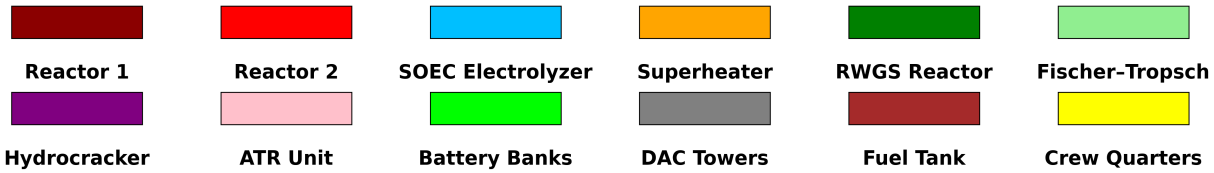

Figure 6.5: Overview of mothership model showing subsystem distribution. The vessel is 145 m in length, 20 m in beam, and 15 m in depth.

6.6 Verification Summary and Discussion

The verification tests confirm that the integrated Simulink model behaves as intended, with only minor and explainable deviations. The system performs reliably under steady state loading, respects the defined reactor ramp rate limits, and correctly identifies the DAC as the slowest-responding subsystem. The ESS exhibits appropriately aggressive dynamic behaviour, effectively compensating for short-term demand fluctuations and maintaining or increasing power levels throughout.

A small inconsistency was observed in the coupling between electrical and thermal power requests within the EMS. During rapid transitions, this coupling will momentarily overestimate thermal demand. However, the reactor's fixed thermal cap prevents this demand to translate into exceeding physical limits, ensuring that the global system response remains valid. When the ESS becomes depleted, brief oscillations appear in the total power trace due to the time step delay between the ESS and the EMS. This causes a single time step spike in power levels of ESS. These effects are minor and can be eliminated in future work by adding a response filter or proportional smoothing to the EMS logic.

During ramp-down events, the ESS correctly transitions into a charging state, absorbing excess reactor output as the system powers off. The residual 30% reactor output shown in the plots represents the modelled utilisation minimum and was retained solely for visualisation; a real reactor would no produce this electrical output if there is no demand. This simplification has no meaningful impact on the refuelling simulations and so is acceptable. A more refined implementation could gradually taper power to slow-reacting components such as the DAC to better capture thermal stabilisation effects.

In the mission-profile test, the system demonstrates consistent power coordination, realistic reactor dynamics, and proper ESS support. The only deviation is a small drop in direct thermal power caused by the EMS allocation logic. The mass flows show no observable influence because of this. This is due to them not being limited by thermal power yet by electrical power.

Beyond numerical verification, the spatial feasibility assessment confirms that the entire energy system can be integrated within the proposed hull envelope. All major subsystems fit within the estimated geometry and mass limits. The DAC system shows to be the largest system yet considering the height of the control tower it would be capable to be fitted into the ship. The total system mass of approximately 6100 tonnes lies within the expected displacement range for a vessel of this scale, indicating that the concept is physically plausible even though several subsystems remain at a conceptual stage.

Overall, the complete Simulink model provides a strong first implementation of a nuclear-powered refuelling mothership. The model is numerically stable and suitable for evaluating the EMS strategies and operational scenarios discussed in the next chapter.

Future refinements could include more detailed thermal modelling, improved structural integration, and higher-accuracy component representations to better assess large-scale onboard fuel synthesis. These additions would further strengthen the realism of the model, but the current implementation offers a reliable foundation for the remainder of this thesis.

7 | Scenario Testing and Results

The complete Simulink model from chapter 4 and the EMS designs from chapter 5 together form the integrated system evaluated in this chapter. The aim of this chapter is to answer the final sub-question (SQ6):

> *How does the ship's integrated energy system perform under different EMS strategies (local, mission-aware, and fleet-wide) during realistic refuelling support missions?*

To evaluate this, four mission scenarios were developed, each representing a step in scenario complexity and EMS capability. This structured approach allows direct comparison across EMS types under equivalent operating conditions. With the use of six Key Performance Indicators (KPIs), the scenarios where compared.

Chapter overview

This chapter is organised as follows:

- section 7.1: Definition of mission scenarios and KPI definitions.
- section 7.2: Results of the Local EMS with constant tasks.
- section 7.3: Performance of the Mission-Aware EMS.
- section 7.4: Performance of the Mission-Aware EMS under varying task lengths.
- section 7.5: Analysis of the Fleet-Wide EMS using Gurobi optimisation.
- section 7.6: Comparison of all EMS strategies using the six KPIs.

7.1 Scenario design

To compare the performance of the two EMS configurations explained in chapter 5, four mission scenarios were created. Each builds upon the previous in terms of situational awareness and coordination complexity. The scenarios are as follows:

- **Scenario 1 — Local Ship-Centred EMS (Constant Tasks):** The mothership is stationary and can only react to incoming refuelling requests. All USVs following identical and predictable mission durations.
- **Scenario 2 — Local Mission-Aware EMS (Constant Tasks):** The EMS gains awareness of USV routes and sets ideal refuelling locations for each USV. Missions remain identical to USVs in scenario 1.
- **Scenario 3 — Local Mission-Aware EMS (Varying Tasks):** The same mission-aware logic is applied as in scenario 2, but USVs now operate with more realistic varying task durations and fuel needs.
- **Scenario 4 — Fleet-Wide EMS (Varying Tasks):** A global optimisation layer (Gurobi) coordinates all refuelling events across the fleet, enabling full multi-USV scheduling under same variable mission conditions as in scenario 3.

These four scenarios are tested using identical mission frameworks. This mission framework was developed with Damen Naval [1] to ensure realistic operational assumptions. The overall concept represents a long-endurance surveillance mission in a large open-water region (e.g., Mediterranean sea), far from external support. Key assumptions include:

[1] `https://www.damen.com/companies/naval`

- A 20-day mission window with continuous USV operation.
- The mothership remains at least 40 NM outside the operational areas as a mobile refuelling ship would.
- The mission begins and ends at a port roughly 300 NM from the operational zone.
- Each USV performs three multi-day tasks inside assigned Areas of Operation (AOs).
- Only one USV refuels at a time for safety and logistical realism.
- During refuelling, the mothership maintains a drift speed of 10 kn.

The spatial setup is illustrated in Figure 7.1.

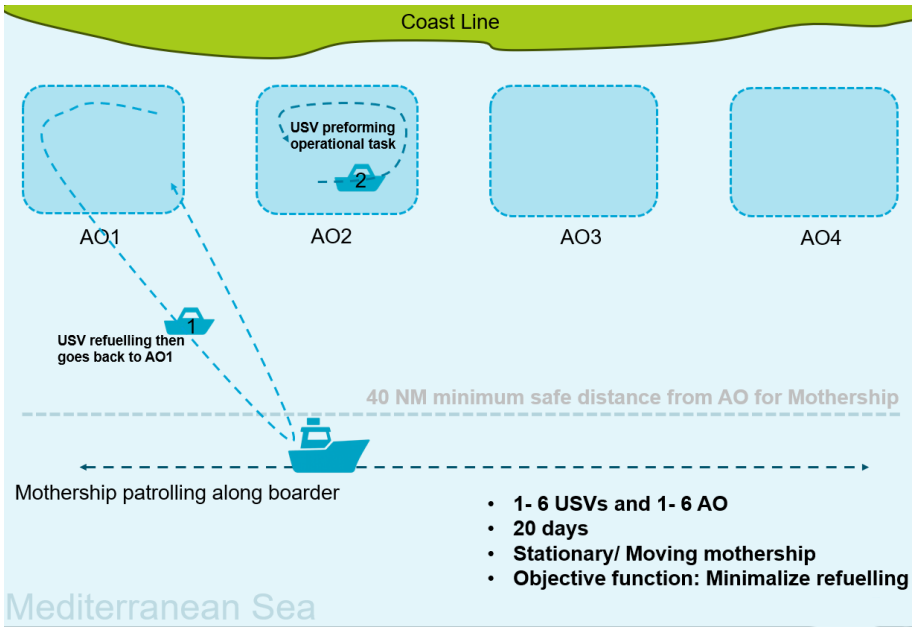

Figure 7.1: Scenario visualisation for two USVs and the mothership.

The number of USVs tested ranges from one to six. Damen Naval identified four USVs as the most likely operational fleet size, and the mothership design was initially sized according to 4 USVs as explained in section 2.5. Extending the scenarios to six USVs enables evaluation of the EMS's ability to make effective refuelling decisions under increased coordination load.

To allow a fair and quantitative comparison across all EMS types, six KPIs were defined. These metrics evaluate internal reactor and energy behaviour, coordination across the fleet, fuel usage patterns, and overall mission success. The KPIs are summarised in Table 7.1.

The first two KPIs in Table 7.1 reflect internal mothership performance and are expected to show little variation across scenarios. This is because they depend on the Local EMS, which manages the ship's internal systems in all four scenarios and therefore operates with the same control logic each time. η_{reactor} measures total thermal power capacity of the reactor is utilized, while η_{energy} quantifies how effectively reactor heat is converted into useful onboard power. Useful onboard power is simplified to hotel and propulsion load and energy stored into synthetic diesel.

Table 7.1: Key Performance Indicators (KPIs) for EMS Evaluation

KPI Name	Symbol	Description	Interpretation (Larger = Better)
Reactor Utilization	η_{reactor}	Average reactor P_{th} output relative to its maximum thermal rating.	Higher means steadier, more efficient reactor use.
Mothership Energy Efficiency	η_{energy}	Fraction of reactor thermal power converted into useful energy (hotel load, propulsion, or synthetic diesel).	Higher means less energy lost.
Fleet Coordination Efficiency	η_{coord}	Inverse of total USV idle/waiting time relative to mission duration.	Higher means better fleet synchronisation.
Fuel Level Retention Ratio	η_{fuel}	Final vs initial diesel volume in the mothership's fuel tanks.	Above 1 indicates long-term refuelling capability.
USV Fuel Utilization	$\eta_{\text{usv fuel}}$	Total fuel consumed by all USVs relative to available fuel.	Higher means more USV fuel effectively used.
Mission Completion Rate	η_{mission}	Fraction of USV tasks successfully completed.	Must be ≥ 1 for full mission success.

The remaining KPIs describe mission level behaviour. η_{coord} measures how much of the total USV time is spent performing mission tasks; values below 1 indicate that waiting time occurred during the operation. η_{fuel} indicates whether the mothership can sustain long-term refuelling operations, with values above 1 implying continuous operation without external support. $\eta_{\text{usv fuel}}$ captures how much of the fuel supplied to the USVs is actually utilised during their missions. The maximum achievable value is roughly 0.95, as each USV must retain a mandatory 5% safety buffer at all times. The final KPI, η_{mission}, is a strict requirement: values below 1 mean that at least one USV task was not completed, and the scenario is classified as unsuccessful. Together, these KPIs provide a consistent framework for evaluating how each EMS strategy influences energy usage, fleet coordination, and overall operational reliability.

7.2 Scenario 1 — Local Ship-Centred EMS (Constant Tasks)

This first scenario acts as the baseline test, evaluating how the mothership performs when operating without any knowledge of USV missions. The Local EMS functions purely reactively and only responds to incoming refuelling requests. The mothership departs from port, sails to the origin point, and remains stationary throughout the mission, refuelling one USV at a time as they return from their fixed three-task schedules inside their assigned Areas of Operation.

The key setup conditions are:

- Each USV has a unique AO with three sequential tasks of 3.5 days each.
- After each task sequence, the USV returns to the mothership for refuelling.
- Only one USV can refuel at any given time.
- The mothership is stationary and has no knowledge of USV timing or fuel state.

Under these controlled and fully deterministic conditions, Scenario 1 reveals how the integrated energy system behaves without any higher-level coordination. For each fleet size, the six KPIs defined in Table 7.1 were tracked. The results are shown in Table 7.2.

Table 7.2: Scenario 1 – Local Ship-Centred EMS. KPI results for different fleet sizes.

#USV	η_{reactor}	η_{energy}	η_{coord}	η_{fuel}	$\eta_{\text{usv fuel}}$	η_{mission}
1	0.77	0.17	1.00	1.38	0.69	1.00
2	0.95	0.16	1.00	1.38	0.69	1.00
3	0.95	0.16	1.00	1.07	0.69	1.00
4	0.95	0.16	0.99	0.51	0.69	1.00
5	0.95	0.16	0.72	0.05	0.46	0.93
6	0.95	0.16	0.46	0.10	0.24	0.61

High Moderate
Low Poor

The results show that the Local EMS can support one or two USVs. In both cases, the mothership ends the mission with its maximum fuel surplus ($\eta_{\text{fuel}} = 1.38$). With three USVs, the system remains self-sustaining ($\eta_{\text{fuel}} = 1.07$) and all missions complete successfully. At three USVs the first signs of waiting behaviour do appear as η_{coord} drops below 1. This is seen in Figure 7.2

USV fuel utilisation ($\eta_{\text{usv fuel}}$) remains constant up to four USVs, since the rule-based EMS applies identical refuelling logic for each vessel and all USVs return along the same distance, leading to equal fuel use.

At four USVs the system reaches its operational limit: missions complete, but waiting time increases noticeably and mothership fuel reserves drop to $\eta_{\text{fuel}} = 0.51$. The USVs experience long delays, waiting over 12 hours for the mothership to produce sufficient fuel for a full refuelling cycle.

Beyond four USVs, performance degrades completely: coordination breaks down, fuel reserves drop to almost zero, and the mission can no longer be completed ($\eta_{\text{mission}} < 1$). These results indicate that the Local EMS can only support up to three USVs under constant-task conditions.

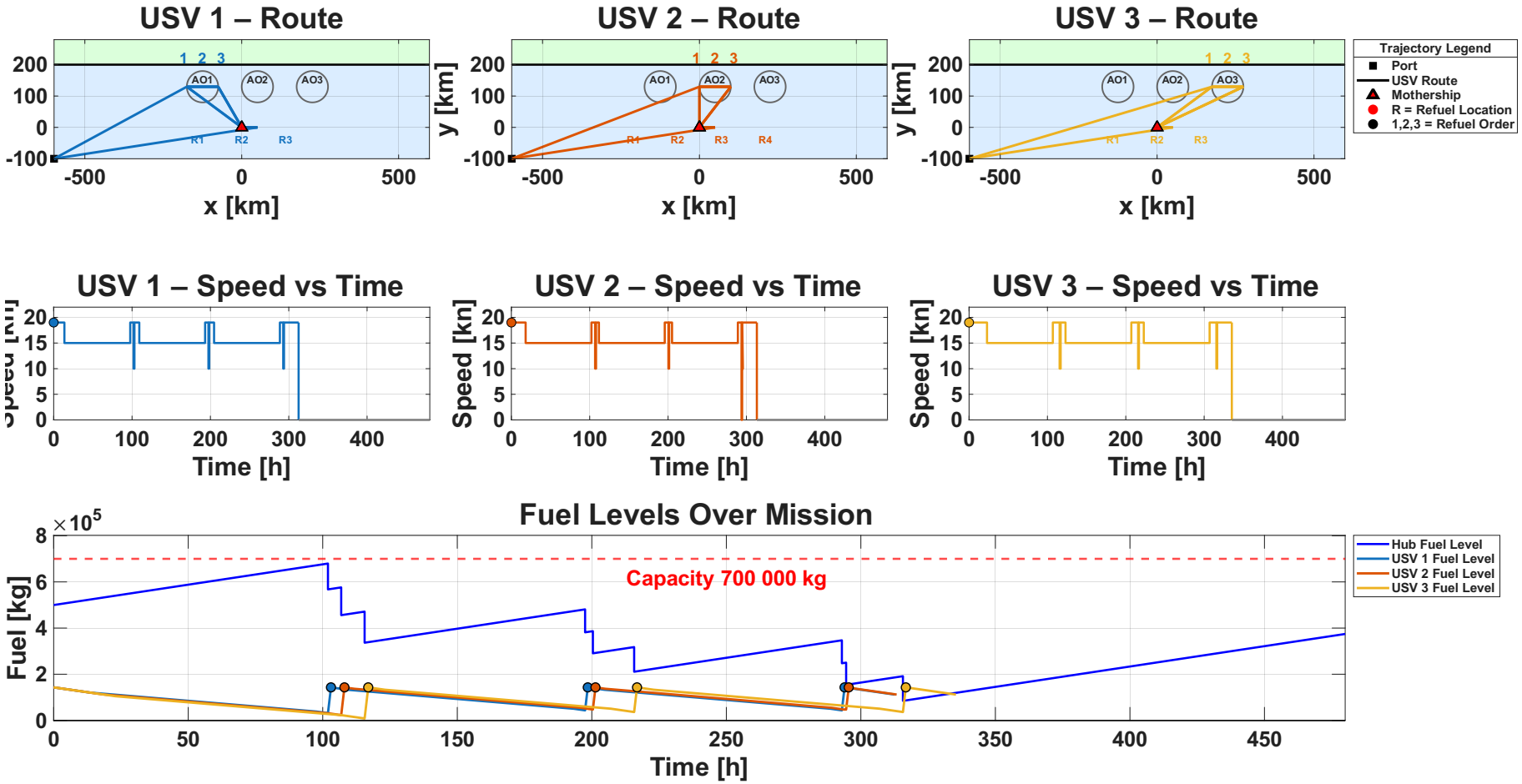

Figure 7.2: Local EMS with 4 USVs: Route, Speed and Fuel level plots

7.3 Scenario 2 — Local Mission-Aware EMS (Constant Tasks)

This second scenario extends the baseline case by giving the mothership limited mission awareness. The Local EMS still operates with rule-based logic, but the mothership now actively relocates to refuelling points closer to each USV's AO. This reduces transit distances and improves timing, while the USV missions themselves remain unchanged, with each USV still completing three fixed tasks before returning for refuelling. This scenario therefore isolates the benefit of improved mothership positioning without altering USV behaviour or adding global coordination.

The key setup conditions are:

- The mothership moves to an optimal refuelling point near each USV's AO.
- Each USV follows the fixed three-task mission structure as in Scenario 1.
- Task duration remains constant at roughly 3.5 days.
- Only one USV can refuel at a time; the Local EMS does not coordinate between USVs.

The resulting KPI values for different fleet sizes are shown in Table 7.3. These reflect how situational awareness influences refuelling efficiency and fleet behaviour when tasks remain fully deterministic.

Table 7.3: Scenario 2 – Local Mission-Aware EMS (Constant Tasks)

#USV	η_{reactor}	η_{energy}	η_{coord}	η_{fuel}	$\eta_{\text{usv fuel}}$	η_{mission}
1	0.77	0.17	1.00	1.38	0.69	1.00
2	0.96	0.17	1.00	1.38	0.71	1.00
3	0.96	0.17	0.99	1.13	0.72	1.00
4	0.96	0.17	0.99	0.64	0.72	1.00
5	0.96	0.17	0.86	0.11	0.73	1.00
6	0.95	0.17	0.52	0.07	0.31	0.66

High Moderate Low Poor

The results show a clear efficiency gain compared to the fully local scenario. By repositioning, the mothership reduces USV transit time, which improves fuel retention (η_{fuel}) and slightly increases USV fuel utilisation ($\eta_{\text{usv fuel}}$). These gains allow the system to technically support up to five USVs, as the increased proximity reduces the total refuelling load on the plant.

However, operating at this scale introduces large waiting periods. The coordination KPI (η_{coord}) declines sharply beyond three USVs, indicating significant waiting time for USVs. While η_{mission} remains equal to one for up to five USVs, this masks long periods where both the mothership and USVs lack sufficient fuel to proceed. The fuel plant struggles to recover after the first refuelling cycle, delaying multiple USVs and causing cumulative waiting periods.

Figure 7.3 illustrates these effects for the five USV case: each USV experiences prolonged zero speed intervals while waiting for the mothership to produce fuel, and the mothership's own fuel level depletes to zero after each refuelling session.

Overall, the mission-aware EMS does improves energy efficiency and reduces unnecessary transit compared to Scenario 1. However, it remains self-sustaining for only up to three USVs. At four and five USVs the system becomes fuel-limited and long waiting times appear.

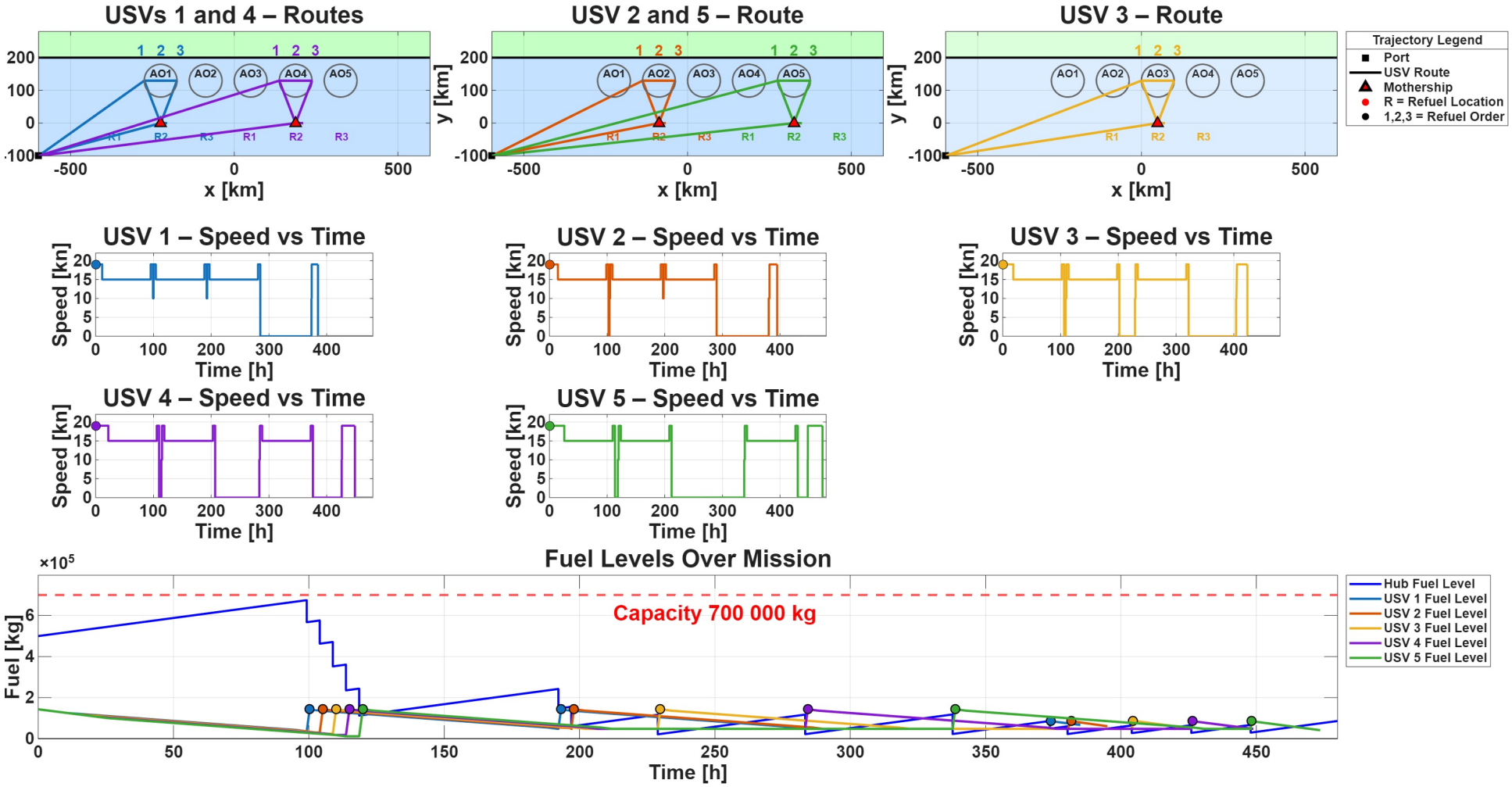

Figure 7.3: Local Mission-Aware EMS with 5 USVs and constant task times: Route, Speed and Fuel level plots

7.4 Scenario 3 — Local Mission-Aware EMS (Varying Tasks)

This third scenario builds on the mission-aware case by making the USVs mission more realistic. This is done by making the USV task durations varied. In Scenario 2 the system could technically support up to five USVs, but their refuelling requests occurred too closely together simply due to task durations all being equal. To address this, each USV now spends a different amount of time in its AO which is more realistic, an effect of this is their refuelling times become staggered. The total task time per USV remains identical across scenarios to ensure fair comparison. The resulting KPI values are shown in Table 7.4.

The key setup conditions are:

- Task durations vary between 2.5, 3.5, and 4.5 days to show more realistic USV return times. The order of the different task times was randomly mixed.
- Each USV still completes three sequential tasks in a unique AO.
- Total operational time per USV is kept constant to allow direct comparison across scenarios.
- The mothership relocates to the ideal refuelling point based on received requests.

This scenario isolates the influence of realistic staggered scheduling on system efficiency without modifying USV routes or introducing additional coordination logic.

Table 7.4: Scenario 3 – Local Mission-Aware EMS (Varying Tasks). KPI results for different fleet sizes.

#USV	η_{reactor}	η_{energy}	η_{coord}	η_{fuel}	$\eta_{\text{usv fuel}}$	η_{mission}
1	0.76	0.17	1.00	1.38	0.70	1.00
2	0.96	0.18	1.00	1.38	0.71	1.00
3	0.96	0.17	1.00	1.13	0.72	1.00
4	0.97	0.17	1.00	0.64	0.73	1.00
5	0.96	0.18	0.89	0.15	0.73	1.00
6	0.96	0.17	0.56	0.13	0.35	0.77

High Moderate
Low Poor

The results show that varying the task durations causes desynchronised refuelling events (as seen in Figure 7.4), producing measurable improvements across several KPIs. Coordination efficiency (η_{coord}) improves notably for the five-USV case, with total waiting time reduced by roughly 250 hours compared to Scenario 2. Since the mothership's fuel production rate remains unchanged, fuel retention (η_{fuel}) shows only minor variation, as expected.

For six USVs, mission success (η_{mission}) increases by approximately 11%, indicating that more tasks were completed before resource limits were reached. The USV fuel utilisation KPI ($\eta_{\text{usv fuel}}$) also increases slightly due to more evenly distributed refuelling cycles.

Figure 7.4 illustrates the task variation clearly in the speed profiles. USV 1 follows a short–medium–long sequence, while USV 2 performs a medium–long–medium pattern. Although individual task lengths differ, the total number of long and short tasks across all USVs is balanced such that the combined mission time remains equal to the baseline case, where every task lasted 3.5 days in the first two scenarios.

Comparing Figure 7.3 and Figure 7.4 shows that the refuelling locations remain identical; the performance gain comes solely from improved distribution of refuelling requests. These findings indicate that in more realistic task scheduling scenarios, the systems performance in enhanced and suggest that further optimisation of mission parameters could unlock additional efficiency gains.

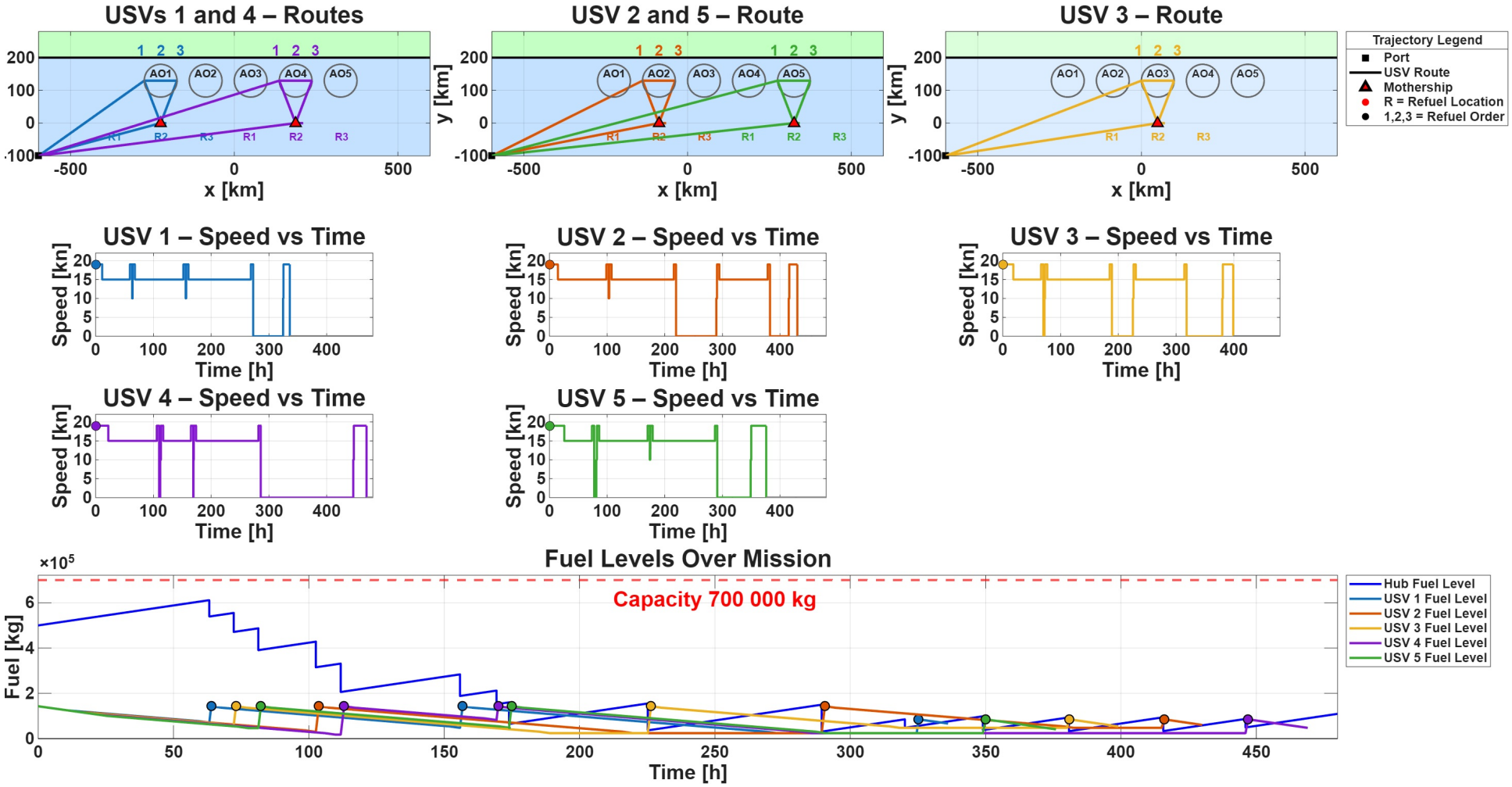

Figure 7.4: Local Mission-Aware EMS with 5 USVs and varying task times: Route, Speed and Fuel level plots

7.5 Scenario 4 — Fleet-Wide EMS (Varying Tasks with Optimisation)

This final scenario introduces the Fleet-Wide EMS described in section 5.2. Scenario 3 improved performance by varying task durations, but its decisions remained reactive and based only on local information. The Fleet-Wide EMS addresses this by optimising task order, refuelling timing, and mothership refuelling locations for all USVs. This coordinated approach prevents clustered return times and spreads refuelling demand more evenly across the mission.

The key setup conditions are:

- The optimiser selects USV routes, refuelling order, and refuelling locations to minimise total refuelling.
- Each USV performs three tasks of 2.5, 3.5, and 4.5 days, as in Scenario 3.
- Total task time matches the constant-task scenarios for fair comparison.
- The mothership relocates to optimiser-selected refuelling points to maximise fuel retention and coordination efficiency.

The resulting KPI values are presented in Table 7.5.

Table 7.5: Scenario 4 – Fleet-Wide EMS (Varying Tasks). KPI results for different fleet sizes.

#USV	η_{reactor}	η_{energy}	η_{coord}	η_{fuel}	$\eta_{\text{usv fuel}}$	η_{mission}
1	0.79	0.17	1.00	1.38	0.95	1.00
2	0.96	0.18	1.00	1.38	0.95	1.00
3	0.96	0.17	1.00	1.38	0.95	1.00
4	0.96	0.17	1.00	1.29	0.95	1.00
5	0.96	0.17	1.00	0.93	0.95	1.00
6	0.97	0.17	1.00	0.84	0.95	1.00

High Moderate
Low Poor

The results show substantial improvements across nearly all KPIs. Most notably, mission success (η_{mission}) is achieved for every fleet size, and all waiting time is eliminated ($\eta_{\text{coord}} = 1.00$). Fuel retention ($\eta_{\text{fuel}}$) remains above 1 for up to four USVs and only slightly decreases for the five and six-USV cases, remaining at 0.93 and 0.84 respectively. For five USVs, this corresponds to the mothership being capable of completing roughly twelve consecutive missions before fuel reserves are depleted.

Figure 7.5 illustrates the six-USV case, where refuelling events are evenly distributed across the mission, especially visible in the fuel-level trace. A key improvement is that each USV can skip one refuelling stop compared to previous scenarios. This is enabled by the higher USV fuel utilisation ($\eta_{\text{usv fuel}}$), which reaches its theoretical maximum of 0.95. This means each USV uses all available fuel except for the mandatory 5% emergency reserve.

The Fleet-Wide EMS also assigns USVs to different task sequences op purpose. It does so to desynchronise their return times. For example, USV 5 completes two short tasks followed by a long one, while USV 3 performs three medium-length tasks. Combined with optimised refuelling locations, this prevents clustering of refuelling events and maximises the utilisation of the mothership's fuel production capacity.

Overall, the Fleet-Wide EMS significantly enhances performance compared to all previous scenarios. It eliminates USV idle time, improves fuel utilisation, and enables sustained, long-term operation for fleets of up to five USVs. This demonstrates the advantages of global coordination over local rule-based control.

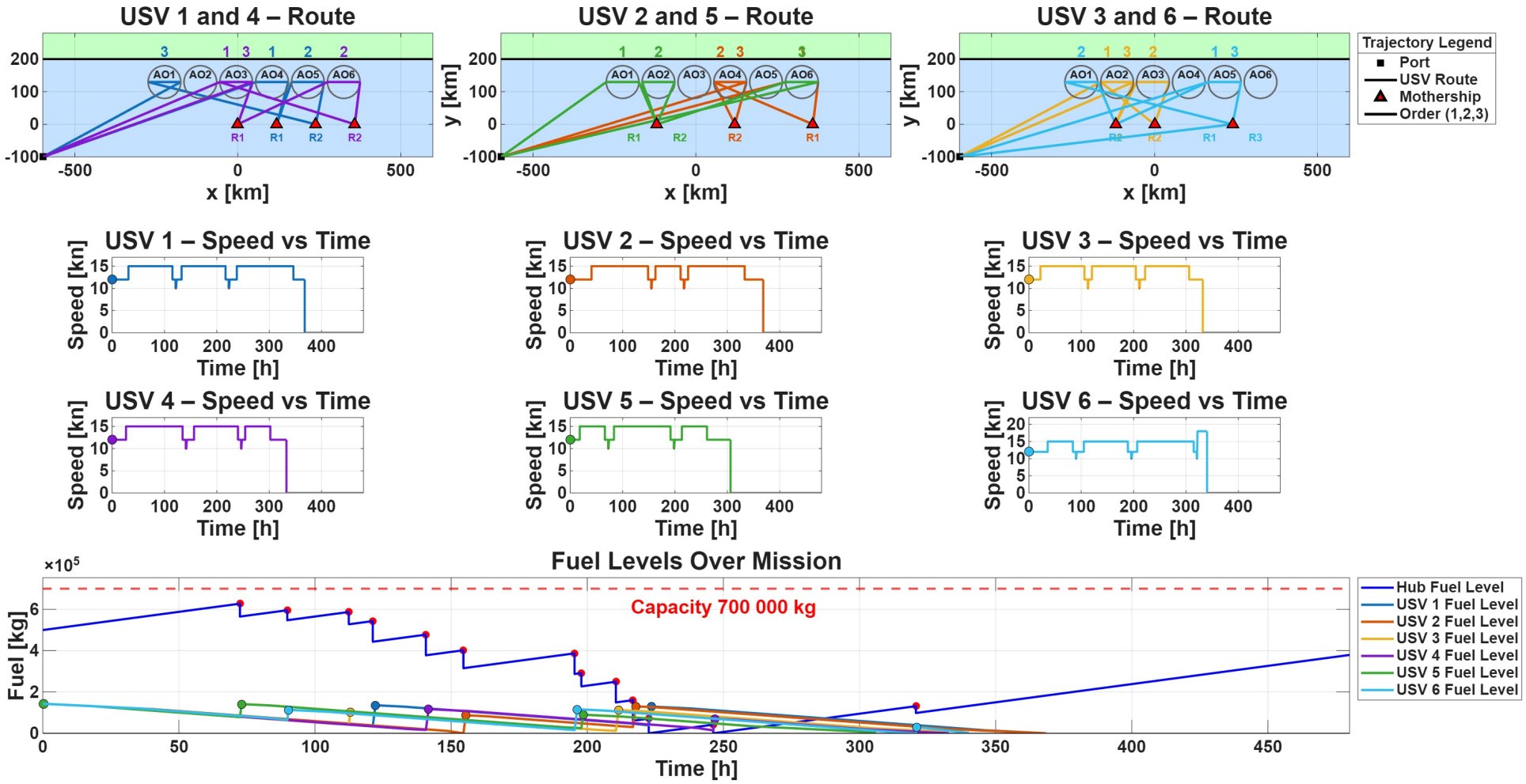

Figure 7.5: Fleet-Wide EMS with 6 USVs: Route, Speed and Fuel level plots

7.6 Results Discussion

The four scenarios together provide a comprehensive assessment of how the nuclear powered mothership performs as a refuelling hub for different USV fleet sizes. The complete KPI overview is presented in Table 7.6.

The internal KPIs, η_{reactor} and η_{energy}, show similar trends across all scenarios. For a single USV, both metrics remain relatively low because the mothership's fuel tanks frequently reach full capacity, requiring the fuel production plant to shut down and reducing overall reactor utilisation. with more USVs fuel demand increases and the reactor operates more continuously, improving both KPIs by a few percent. Since all scenarios use the same internal rule-based EMS for managing the fuel-production chain, substantial differences in these internal KPIs were neither expected nor observed. all improvements seen where due to more efficient propulsion load utilization and better refuelling scheduling.

EMS Configuration	#USV	η_{reactor}	η_{energy}	η_{coord}	η_{fuel}	$\eta_{\text{usv fuel}}$	η_{mission}
Local Ship-Centred EMS Constant Tasks	1	0.77	0.17	1.00	1.38	0.69	1.00
	2	0.95	0.16	1.00	1.38	0.69	1.00
	3	0.95	0.16	1.00	1.07	0.69	1.00
	4	0.95	0.16	0.99	0.51	0.69	1.00
	5	0.95	0.16	0.72	0.05	0.46	0.93
	6	0.95	0.16	0.46	0.10	0.24	0.61
Local Mission-Aware EMS Constant Tasks	1	0.77	0.17	1.00	1.38	0.69	1.00
	2	0.96	0.17	1.00	1.38	0.71	1.00
	3	0.96	0.17	0.99	1.13	0.72	1.00
	4	0.96	0.17	0.99	0.64	0.72	1.00
	5	0.96	0.17	0.86	0.11	0.73	1.00
	6	0.95	0.17	0.52	0.07	0.31	0.66
Local Mission-Aware EMS Varying Tasks	1	0.76	0.17	1.00	1.38	0.70	1.00
	2	0.96	0.18	1.00	1.38	0.71	1.00
	3	0.96	0.17	1.00	1.13	0.72	1.00
	4	0.97	0.17	1.00	0.64	0.73	1.00
	5	0.96	0.18	0.89	0.15	0.73	1.00
	6	0.96	0.17	0.56	0.13	0.35	0.77
Fleet-Wide EMS Varying Tasks	1	0.79	0.17	1.00	1.38	0.95	1.00
	2	0.96	0.18	1.00	1.38	0.95	1.00
	3	0.96	0.17	1.00	1.38	0.95	1.00
	4	0.96	0.17	1.00	1.29	0.95	1.00
	5	0.96	0.17	1.00	0.93	0.95	1.00
	6	0.97	0.17	1.00	0.84	0.95	1.00

High performance | Moderate performance | Low performance | Poor performance

Table 7.6: KPI comparison across all EMS configurations

The internal KPIs, η_{reactor} and η_{energy}, show similar trends across all scenarios. For a single USV, both metrics remain relatively low because the mothership's fuel tanks frequently reach full capacity, requiring the fuel production plant to shut down and reducing overall reactor utilisation. with more USVs fuel demand increases and the reactor operates more continuously, improving both KPIs by a few percent. Since all scenarios use the same internal rule-based EMS for managing the fuel-production chain, substantial differences in these internal KPIs were neither expected nor observed. all improvements seen where due to more efficient propulsion load utilization and better refuelling scheduling.

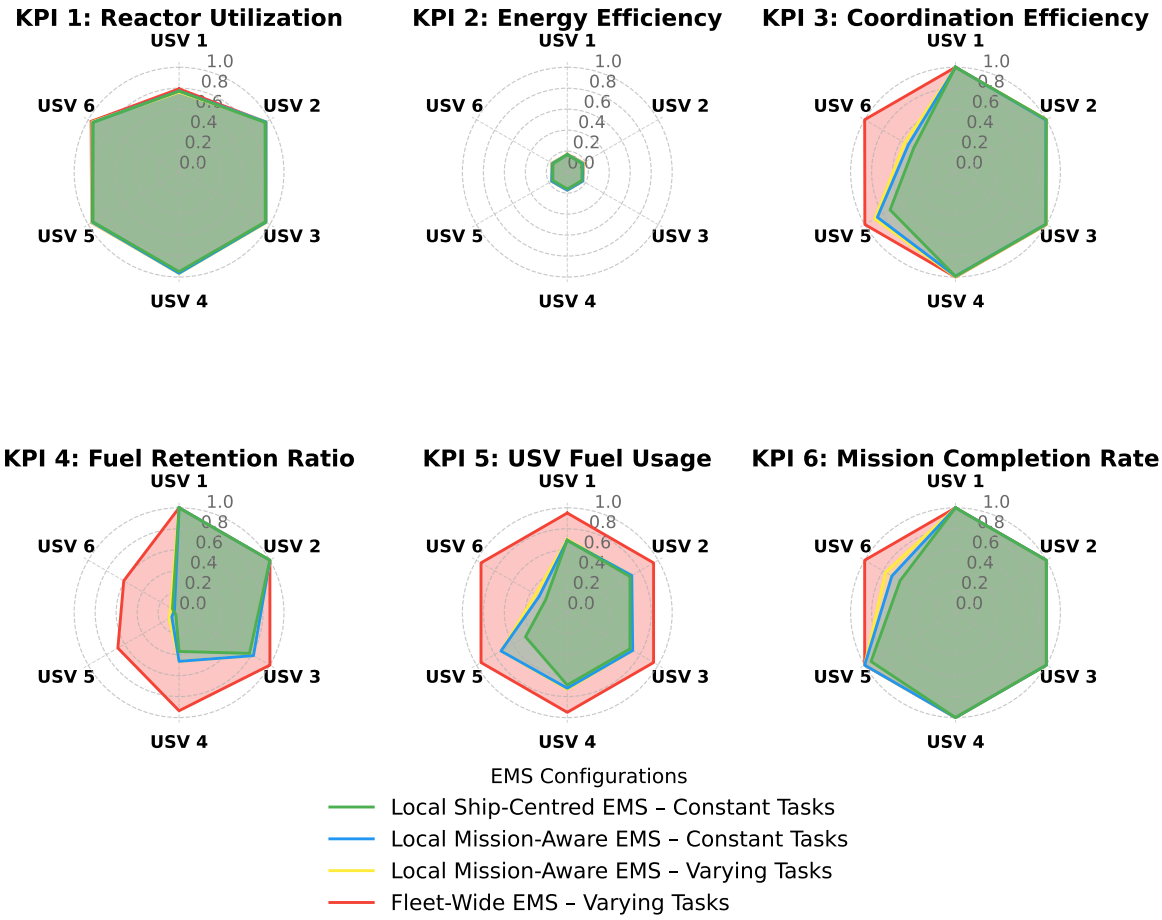

Figure 7.6: Spider plots showing KPI results per number of USVs for all four scenarios.

The most significant differences between EMS configurations appear in the mission-level KPIs: η_{coord}, η_{fuel}, $\eta_{\text{usv fuel}}$, and η_{mission}. These represent the system's ability to coordinate USV arrivals, maintain fuel reserves, and ensure mission completion. As seen in Figure 7.6, performance improves stepwise from Scenario 1 to Scenario 4.

The Local and Mission-Aware EMS configurations function effectively for small fleets but begin to exhibit increasing waiting times, reduced fuel retention, and unfinished missions as the fleet grows beyond three or four USVs. The coordination KPI, η_{coord}, declines sharply once clustered refuelling requests exceed the mothership's production recovery rate. Fuel retention, η_{fuel}, also drops significantly in these scenarios due to the rapid depletion of diesel reserves.

The USV fuel utilisation metric, $\eta_{\text{usv fuel}}$, remains nearly identical for Scenarios 1–3, since the rule-based logic was set to always refuels each USV to the same level. In contrast, the Fleet-Wide EMS optimises the schedule such that each USV finishes with only the mandatory 5% reserve left. This results in the theoretical maximum utilisation of 0.95 across all fleet sizes, reducing unnecessary refuelling cycles and improving coordination. As a consequence, the fleet-wide EMS reduces the number of refuelling stops per USV to only two, significantly lowering the strain on the mothership's fuel production system.

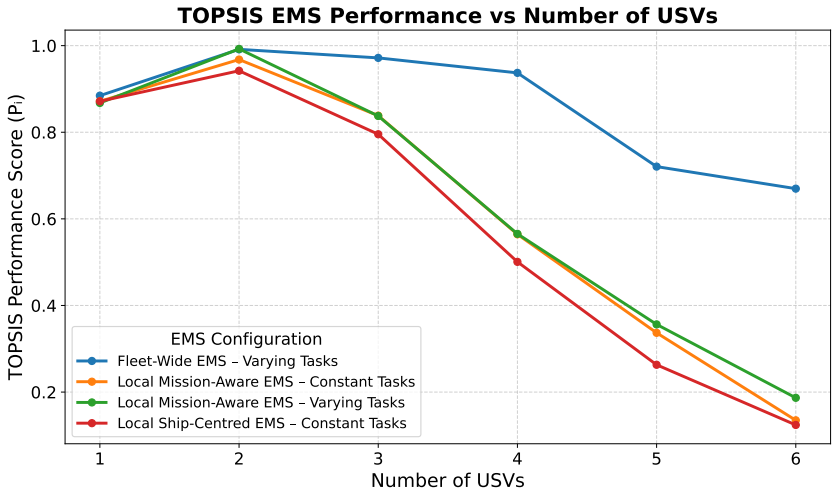

Figure 7.7: KPI TOPSIS scenario performance versus number of USVs.

To compare the EMS configurations holistically, the TOPSIS method [83] was applied. TOPSIS is a multi-criteria decision making method that ranks alternatives by measuring their closeness to an ideal case and their distance from a worst case. An equal weighting of one was applied across all KPIs so that each metric contributed uniformly to the final ranking. As shown in Figure 7.7, EMS choice has little impact for one or two USVs. Beyond this point, however, the Fleet-Wide EMS clearly outperforms the others, achieving the highest multi-KPI score up to five USVs, with only a slight decline at six USVs.

Taken together, the results show that fleets of two or fewer USVs can be supported by all EMS configurations, but such small fleets do not fully utilise the mothership's fuel production or reactor potential. At least three USVs are required to use the mothership's internal systems effectively, and doing so reliably requires a higher level of coordination. When the Fleet-Wide EMS is applied, the system can sustain operations for up to five USVs. This highlights the importance not only of designing a high-capacity synthetic fuel system, but also of implementing an intelligent EMS capable of scheduling and coordinating distributed USV operations efficiently.

8 | Conclusion

This thesis set out to determine whether a nuclear-powered naval vessel could operate as an independent energy hub capable of producing its own synthetic fuel while supporting a fleet of unmanned maritime vehicles. The study was guided by one central research question:

> *"What energy system design is needed for a nuclear-powered naval vessel to function as an independent energy hub for a fleet of unmanned maritime vehicles?"*

Using the Damen MMS concept as the reference for mothership size, a complete internal energy system architecture was developed and modelled. The vessel was equipped with a 130 MW_{th} VHTR, a 10 MWe ESS, and a full synthetic-fuel production chain comprising seawater purification, SOEC hydrogen production, DAC-based CO_2 capture, RWGS, and Fischer–Tropsch synthesis. Propulsion and hotel loads were included to represent realistic operational conditions. A rule-based EMS coordinated energy flows while respecting the reactor's ramp-rate limits. Dynamic verification confirmed that the integrated model behaved consistently with physical expectations. A physical feasibility assessment further demonstrated that the full energy system could be accommodated within the MMS reference hull.

With the energy system verified, the model was used to assess the mothership's ability to refuel and support a fleet of one to six USVs. Three EMS configurations were evaluated. The Local EMS, which keeps the mothership stationary, was able to support up to four USVs but could not maintain long-term energy balance. Introducing a Mission-Aware EMS improved performance by allowing the mothership to reposition to more optimal refuelling locations, enabling five USVs to operate but resulting in significant waiting times and very poor fuel retention. Introducing more realistic variation in task durations provided marginal efficiency gains but did not resolve underlying scheduling limitations.

The most significant improvement came from the MILP-based Fleet-Wide EMS. This optimisation layer was applied on top of the rule-based EMS and coordinated refuelling timing, task sequences, and refuelling locations for the entire fleet. It eliminated waiting time, increased USV fuel utilisation, and maintained high fuel retention. This configuration enabled six USVs to operate within mission limits and supported sustained long-term operation with five USVs. These results demonstrate that effective coordination and scheduling are essential to fully exploit the mothership's reactor and fuel production capacity.

Overall, this thesis developed the first energy system model of a nuclear powered refuelling vessel and evaluated its performance across multiple operational scenarios. The results show that, when combined with a Fleet-Wide EMS, the mothership can sustainably support up to five USVs. This demonstrates that a nuclear-powered refuelling mothership is technically feasible and highlights the critical role of advanced fleet wide energy management.

As the maritime domain moves toward longer, more independent operations, this work outlines how self-sustaining nuclear refuelling vessels could form the backbone of future at sea logistics systems, supporting fleets that no longer rely on traditional supply chains.

Recommendations and Future Work

While this thesis provides a literature-backed and verified simulation framework, it is only one step forward in a topic with many possible directions for future development. The recommended next steps to take are:

1. Detailed subsystem validation: The current dynamic model used simple input/ output block. Future work should incorporate thermodynamic flows and control models of key

subsystems. Particularly the SOEC, DAC, and Fischer–Tropsch units should be investigated to prove feasibility of such systems on a ship.

2. Hybrid EMS and real-time optimisation: The Fleet-Wide EMS proved most effective but computationally intensive. Future research should explore hybrid architectures combining deterministic rule-based layers with predictive or reinforcement-learning controllers to achieve near real-time operation and improved scalability for larger fleets.

3. Identify UXV types: The USV used in this study represented the largest class of UXV considered feasible for the mothership to support. Future work should define the full range of UXV types that could operate under the mothership's logistical envelope, as smaller units may significantly reduce the required onboard fuel production capacity.

4. Extension to multi-mothership operations: The present study focused on a single mothership supporting up to five USVs. Future work could expand the concept to coordinated multi-mothership fleets, exploring distributed refuelling strategies, inter-ship energy exchange, and coordinated EMS scheduling between hubs.

5. Alternatives to DAC: DAC remains the least mature and most space-intensive subsystem. Emerging offshore CO_2 storage reservoirs present a potential alternative source. If reservoirs become accessible for extraction, they could provide large CO_2 supply systems, thereby increasing fuel production on the Mothership.

References

[1] Jacquelyn Schneider and Julia Macdonald. 'Looking Back to Look Forward: Autonomous Systems, Military Revolutions, and the Importance of Cost'. In: *Journal of Strategic Studies* 47.2 (2024), pp. 162–184. DOI: 10.1080/01402390.2022.2164570.

[2] Ronald O'Rourke. *Navy Large Unmanned Surface and Undersea Vehicles: Background and Issues for Congress*. Tech. rep. RL32418. Congressional Research Service, 2024. URL: https://crsreports.congress.gov/product/pdf/RL/RL32418.

[3] John C. Jackson et al. *Assessment of Deployment- and Mobilization-to-Dwell Policies for Active and Reserve Component Forces: An Examination of Current Policy Using Select U.S. Joint Force Elements*. Tech. rep. RR-A670-1. Santa Monica, CA: RAND Corporation, 2023. DOI: 10.7249/RRA670-1.

[4] Robin Paul Bushore. 'Synthetic fuel generation capabilities of nuclear power plants with applications to naval ship technology.' PhD thesis. Massachusetts Institute of Technology, 1977.

[5] Robert P. Girrier and Wayne P. Hughes. *Fleet Tactics and Naval Operations*. Annapolis, MD: Naval Institute Press, 2018. ISBN: 1682474860.

[6] Isuru Munasinghe, Asanka Perera and Ravinesh C. Deo. 'A Comprehensive Review of UAV-UGV Collaboration: Advancements and Challenges'. In: *Journal of Sensor and Actuator Networks* 13.6 (2024). DOI: 10.3390/jsan13060081.

[7] David Axe. *Drone War Vietnam*. Great Britain: Pen & Sword, Military, 2021, pp. 51–52. ISBN: 9781526770264.

[8] Alexandros Dimos et al. 'A Survey on UxV Swarms and the Role of Artificial Intelligence as a Technological Enabler'. In: *Drones* 9 (Oct. 2025), p. 700. DOI: 10.3390/drones9100700.

[9] Ismar Klomp. *Energy Management System for a Maritime Nuclear Energy Hub*. Literature Study Report 2025.MME.9062. Delft University of Technology, 2025.

[10] Carlos Barrera et al. 'Trends and Challenges in Unmanned Surface Vehicles (USV): From Survey to Shipping'. In: *TransNav, the International Journal on Marine Navigation and Safety of Sea Transportation* 15 (Mar. 2021), pp. 135–142. DOI: 10.12716/1001.15.01.13.

[11] Wayne K. Talley. 'Determinants of Ship Accident Seaworthiness'. In: *International Journal of Maritime Economics* 1 (1999), pp. 1–14. DOI: 10.1057/ijme.1999.9.

[12] Damen Shipyards. *VSX 5209 Patrol Vessel*. 2024. URL: https://www.damen.com/vessels/defence-and-security/stan-patrol-vessels/vsx-5209-patrol.

[13] D. L. Zverev et al. 'Nuclear ship reactor installations: from gen 1 to 5'. In: *Atomic Energy* 129.1 (2020), pp. 1–7. DOI: 10.1007/s10512-021-00704-z.

[14] Marco Deluca and A. Köck. 'Current Perspectives for Autonomous Sensor Nodes'. In: *Proceedings* 56 (Dec. 2020), p. 7. DOI: 10.3390/proceedings2020056007.

[15] T.J. Dijkman and R.M.J. Benders. 'Comparison of renewable fuels based on their land use using energy densities'. In: *Renewable and Sustainable Energy Reviews* 14.9 (2010), pp. 3148–3155. ISSN: 1364-0321. DOI: https://doi.org/10.1016/j.rser.2010.07.029.

[16] M. K. Loganathan et al. 'Review and selection of advanced battery technologies for post 2020 era electric vehicles'. In: Dec. 2019, pp. 1–5. DOI: 10.1109/ITEC-India48457.2019.ITECINDIA2019-254.

[17] 'A review of lithium-ion battery safety concerns: The issues, strategies, and testing standards'. In: *Journal of Energy Chemistry* 59 (2021), pp. 83–99. ISSN: 2095-4956. DOI: https://doi.org/10.1016/j.jechem.2020.10.017.

[18] Ahmad Pesaran et al. *Battery Requirements for Plug-In Hybrid Electric Vehicles: Analysis and Rationale*. Tech. rep. NREL/CP-540-45809. National Renewable Energy Laboratory (NREL), 2009.

[19] Qingsong Wang et al. 'Thermal runaway caused fire and explosion of lithium-ion battery'. In: *Journal of Power Sources* 208 (2012), pp. 210–224. DOI: 10.1016/j.jpowsour.2012.02.038.

[20] Anna Tomaszewska et al. 'Lithium-ion battery fast charging: A review'. In: *eTransportation* 1 (2019), p. 100011. ISSN: 2590-1168. DOI: https://doi.org/10.1016/j.etran.2019.100011.

[21] Behdad Shadidi, Gholamhassan Najafi and Talal Yusaf. 'A Review of Hydrogen as a Fuel in Internal Combustion Engines'. In: *Energies* 14.19 (2021). DOI: 10.3390/en14196209.

[22] Mahrokh Samavati et al. 'Synthetic Diesel Production as a Form of Renewable Energy Storage'. In: *Energies* 11 (May 2018), p. 1223. DOI: 10.3390/en11051223.

[23] Jurie Steyn and Christine Render. *Hydrogen as Energy Carrier*. Online resource. 2020. URL: https://www.researchgate.net/publication/339627476_Hydrogen_as_Energy_Carrier.

[24] Marika Wieliczko and Ned Stetson. 'Hydrogen technologies for energy storage: A perspective'. In: *MRS Energy & Sustainability* 7 (2020), E41. DOI: 10.1557/mre.2020.43.

[25] Josef Rötzer. *Design and Construction of LNG Storage Tanks*. John Wiley Sons / Ernst Sohn, 2019. ISBN: 978-3-433-03277-0. DOI: 10.1002/9783433609989.

[26] Sebastian Verhelst et al. 'Methanol as a fuel for internal combustion engines'. In: *Progress in Energy and Combustion Science* 70 (2019), pp. 43–88. ISSN: 0360-1285. DOI: https://doi.org/10.1016/j.pecs.2018.10.001.

[27] John D Tosh, David S Moulton and Clifford A Moses. *Navy fuel specification standardization*. Tech. rep. NATO, 1992.

[28] Lipei Fu et al. 'Research progress on CO2 capture and utilization technology'. In: *Journal of CO2 Utilization* 66 (2022), p. 102260. ISSN: 2212-9820. DOI: https://doi.org/10.1016/j.jcou.2022.102260.

[29] R B Anderson. *Fischer-Tropsch synthesis*. 1984.

[30] Kevin Brian Terry. 'Synthetic fuels for naval applications produced using shipboard nuclear power'. PhD thesis. Massachusetts Institute of Technology, 1995.

[31] S. Locke Bogart et al. 'Production of Liquid Synthetic Fuels from Carbon, Water, and Nuclear Power on Ships and at Shore Bases for Military and Potential Commercial Application'. In: *Proceedings of the 2006 International Congress on Advanced Power Plants (ICAPP 2006), Reno, NV*. 2006.

[32] John Michael Galle-Bishop, Charles W. Forsberg and Michael J. Driscoll. 'Nuclear tanker producing liquid fuels from air and water'. In: *Transactions of the American Nuclear Society* 104.1 (2011), pp. 589–590.

[33] Liam J. F. Comidy, Mark D. Staples and Steven R. H. Barrett. 'Technical, Economic, and Environmental Assessment of Liquid Fuel Production on Aircraft Carriers'. In: *Applied Energy* 256 (2019), p. 113810. DOI: 10.1016/j.apenergy.2019.113810.

[34] N. Kapoor and R. Pawling. 'Mobile Marine Fuel Generation Based on a Micro Nuclear Reactor'. In: *Proceedings of the International Naval Engineering Conference (INEC) 2024*. Institute of Marine Engineering, Science and Technology (IMarEST), 2024. DOI: 10.24868/11200.

[35] *Small Modular Reactors: Advances in SMR Developments 2024*. Non-serial Publications. Vienna: International Atomic Energy Agency, 2024. URL: https://www.iaea.org/publications/15790/small-modular-reactors-advances-in-smr-developments-2024.

[36] William Edward Cummins and Regis Matzie. 'Design evolution of PWRs: Shippingport to generation III+'. In: *Progress in Nuclear Energy* 102 (2018). Shippingport 60th Anniversary: A Time to Take Stock of Nuclear Energy's Status, pp. 9–37. ISSN: 0149-1970. DOI: https://doi.org/10.1016/j.pnucene.2017.08.008.

[37] 'Generation IV nuclear reactors: Current status and future prospects'. In: *Energy Policy* 61 (2013), pp. 1503–1520. ISSN: 0301-4215. DOI: https://doi.org/10.1016/j.enpol.2013.06.101.

[38] Trevor M. Letcher. '4 - Current and future nuclear power reactors and plants'. In: *Managing Global Warming*. Academic Press, 2019, pp. 117–197. ISBN: 978-0-12-814104-5. DOI: https://doi.org/10.1016/B978-0-12-814104-5.00004-1.

[39] Jérôme Serp et al. 'The molten salt reactor (MSR) in generation IV: Overview and perspectives'. In: *Progress in Nuclear Energy* 77 (2014), pp. 308–319. ISSN: 0149-1970. DOI: https://doi.org/10.1016/j.pnucene.2014.02.014.

[40] Kazumi Aoto et al. 'A summary of sodium-cooled fast reactor development'. In: *Progress in Nuclear Energy* 77 (2014), pp. 247–265. DOI: https://doi.org/10.1016/j.pnucene.2014.05.008.

[41] Alessandro Alemberti et al. 'Overview of lead-cooled fast reactor activities'. In: *Progress in Nuclear Energy* 77 (2014), pp. 300–307. DOI: https://doi.org/10.1016/j.pnucene.2013.11.011.

[42] Jeffrey J. Powers and Brian D. Wirth. 'A review of TRISO fuel performance models'. In: *Journal of Nuclear Materials* 405.1 (2010), pp. 74–82. DOI: https://doi.org/10.1016/j.jnucmat.2010.07.030.

[43] Jerzy Gluch et al. 'Thermodynamic Efficiency of an Advanced 4th Generation VHTR Propulsion Engine for Large Container Ships'. In: *Polish Maritime Research* 31 (Dec. 2024), pp. 76–88. DOI: 10.2478/pomr-2024-0052.

[44] H. Franklin Harvey and W. E. Thau. 'Electric Propulsion of Ships'. In: *Transactions of the American Institute of Electrical Engineers* XLIV (1925). DOI: 10.1109/T-AIEE.1925.5061130.

[45] Aziz Nechache and Stéphane Hody. 'Alternative and innovative solid oxide electrolysis cell materials: A short review'. In: *Renewable and Sustainable Energy Reviews* 149 (2021), p. 111322. ISSN: 1364-0321. DOI: https://doi.org/10.1016/j.rser.2021.111322.

[46] Younggy Kim and Bruce E. Logan. 'Hydrogen Production from Inexhaustible Supplies of Fresh and Salt Water Using Microbial Reverse-Electrodialysis Electrolysis Cells'. In: *Proceedings of the National Academy of Sciences* 108.39 (2011), pp. 16176–16181. DOI: 10.1073/pnas.1105714108.

[47] Thomas Bacquart et al. 'Hydrogen for Maritime Application—Quality of Hydrogen Generated Onboard Ship by Electrolysis of Purified Seawater'. In: *Processes* 9.7 (2021), p. 1252. DOI: 10.3390/pr9071252.

[48] A. Houaijia et al. 'Solar Hydrogen by High-temperature Electrolysis: Flowsheeting and Experimental Analysis of a Tube-type Receiver Concept for Superheated Steam Production'. In: *Energy Procedia* 49 (2014). Proceedings of the SolarPACES 2013 International Conference, pp. 1960–1969. ISSN: 1876-6102. DOI: https://doi.org/10.1016/j.egypro.2014.03.208.

[49] Huang Zhang et al. 'Superheated steam technology: Recent developments and applications in food industries'. In: *Comprehensive Reviews in Food Science and Food Safety* 23.6 (2024), e70073. DOI: 10.1111/1541-4337.70073.

[50] Bahram Ghorbani et al. 'Thermochemical water-splitting structures for hydrogen production: Thermodynamic, economic, and environmental impacts'. In: *Energy Conversion and Management* 297 (2023), p. 117599. ISSN: 0196-8904. DOI: https://doi.org/10.1016/j.enconman.2023.117599.

[51] Kai Zeng and Dongke Zhang. 'Recent progress in alkaline water electrolysis for hydrogen production and applications'. In: *Progress in Energy and Combustion Science* 36.3 (2010), pp. 307–326. ISSN: 0360-1285. DOI: https://doi.org/10.1016/j.pecs.2009.11.002.

[52] Abed Alaswad et al. 'Technical and Commercial Challenges of Proton-Exchange Membrane (PEM) Fuel Cells'. In: *Energies* 14.1 (2021), p. 144. DOI: 10.3390/en14010144.

[53] Shuang Zong et al. 'Advances and challenges with SOEC high temperature co-electrolysis of CO2/H2O: Materials development and technological design'. In: *Carbon Capture Science Technology* 12 (2024), p. 100234. ISSN: 2772-6568. DOI: https://doi.org/10.1016/j.ccst.2024.100234.

[54] Yujun Suo et al. 'Recent advances in cobalt-based Fischer-Tropsch synthesis catalysts'. In: *Journal of Industrial and Engineering Chemistry* 115 (2022), pp. 92–119. ISSN: 1226-086X. DOI: https://doi.org/10.1016/j.jiec.2022.08.026.

[55] Szabina Tomasek et al. 'Fuel purpose hydrocracking of biomass based Fischer-Tropsch paraffin mixtures on bifunctional catalysts'. In: *Energy Conversion and Management* 213 (2020), p. 112775. ISSN: 0196-8904. DOI: https://doi.org/10.1016/j.enconman.2020.112775.

[56] Gaurav Nahar and Valerie Dupont. 'Recent Advances in Hydrogen Production Via Autothermal Reforming Process (ATR): A Review of Patents and Research Articles'. In: *Recent Patents on Chemical Engineering* 6 (Mar. 2013), pp. 8–42. DOI: 10.2174/2211334711306010003.

[57] Yolanda Daza and John Kuhn. 'CO2 conversion by reverse water gas shift catalysis: Comparison of catalysts and mechanisms and their consequences for CO2 conversion to liquid fuels'. In: *RSC Adv.* 6 (May 2016). DOI: 10.1039/C6RA05414E.

[58] Sumudu Karunarathne et al. 'Review on CO2 removal from ocean with an emphasis on direct ocean capture (DOC) technologies'. In: *Separation and Purification Technology* 353 (2025), p. 128598. ISSN: 1383-5866. DOI: https://doi.org/10.1016/j.seppur.2024.128598.

[59] Omnya Al Yafiee et al. 'Direct air capture (DAC) vs. Direct ocean capture (DOC)–A perspective on scale-up demonstrations and environmental relevance to sustain decarbonization'. In: *Chemical Engineering Journal* 497 (2024), p. 154421. ISSN: 1385-8947. DOI: https://doi.org/10.1016/j.cej.2024.154421.

[60] Damen Shipyards Group. *VSX 5209 Patrol Vessel*. https://www.damen.com/vessels/defence-and-security/stan-patrol-vessels/vsx-5209-patrol. 2024.

[61] Truong M. N. Bui et al. 'An Energy Management Strategy for DC Hybrid Electric Propulsion System of Marine Vessels'. In: *2018 5th International Conference on Control, Decision and Information Technologies (CoDIT)*. IEEE, 2018, pp. 80–85. DOI: 10.1109/CoDIT.2018.8394800.

[62] JongHak Lee and JinSeok Oh. 'A Study on Load Monitoring Algorithms for EMS of Hybrid Electric Propulsion Ship'. In: *Journal of Advanced Marine Engineering and Technology* 48 (2024), pp. 402–413.

[63] Sidum Adumene et al. 'Advances in nuclear power system design and fault-based condition monitoring towards safety of nuclear-powered ships'. In: *Ocean Engineering* 251 (2022), p. 111156. ISSN: 0029-8018. DOI: https://doi.org/10.1016/j.oceaneng.2022.111156.

[64] Md Ibrahim Adham. 'Analysis and Optimal Planning of Nuclear-Renewable Hybrid Energy Systems for Ships'. MA thesis. Ontario Tech University, 2021. URL: https://hdl.handle.net/10155/1323.

[65] Halvor Schøyen and Kenn Steger-Jensen. 'Nuclear propulsion in ocean merchant shipping: The role of historical experiments to gain insight into possible future applications'. In: *Journal of Cleaner Production* 169 (2017). Experimentation for climate change solutions, pp. 152–160. ISSN: 0959-6526. DOI: https://doi.org/10.1016/j.jclepro.2017.05.163.

[66] Byeongdoo Jeon and Mojdeh Khorsand. 'Energy Management System in Naval Submarines'. In: *2020 IEEE Transportation Electrification Conference Expo (ITEC)*. 2020, pp. 802–808. DOI: 10.1109/ITEC48692.2020.9161480.

[67] Xiuliang Zhao et al. 'Energy management strategies for fuel cell hybrid electric vehicles: Classification, comparison, and outlook'. In: *Energy Conversion and Management* 270 (2022), p. 116179. ISSN: 0196-8904. DOI: https://doi.org/10.1016/j.enconman.2022.116179.

[68] D. Mitropoulou et al. 'Multi-objective Optimisation and Energy Management: Adapt Your Ship to Every Mission'. In: *Proceedings of the International Ship Control Systems Symposium (iSCSS)*. 2020. DOI: 10.24868/issn.2631-8741.2020.015.

[69] Hermann Meissner, Rebecca Ilsen and Jan C. Aurich. 'Analysis of Control Architectures in the Context of Industry 4.0'. In: *Procedia CIRP* 62 (2017). 10th CIRP Conference on Intelligent Computation in Manufacturing Engineering - CIRP ICME '16. [Edited by: Roberto Teti, Manager Editor: Doriana M. D'Addona], pp. 165–169. ISSN: 2212-8271. DOI: https://doi.org/10.1016/j.procir.2016.06.113.

[70] S. P. Monckton and G. S. Broten. 'Command, Control, and Autonomous Swarms'. In: *Unmanned Ground Vehicle Technology VII, Proceedings of SPIE Vol. 5804*. 2005. DOI: 10.1117/12.604337.

[71] T. Wien and G. J. Meijn. 'Dynamic potential of naval nuclear power generation: modelling of a high-temperature reactor with a supercritical carbon dioxide power conversion cycle'. In: *Conference Proceedings of INEC*. 2024.

[72] Xing L. Yan. 'Chapter 3 - Very High Temperature ReactorThis book has a companion website hosting complementary materials.' In: *Handbook of Generation IV Nuclear Reactors (Second Edition)*. Second Edition. Woodhead Publishing Series in Energy. Woodhead Publishing, 2023, pp. 133–165. ISBN: 978-0-12-820588-4. DOI: https://doi.org/10.1016/B978-0-12-820588-4.00009-8.

[73] C. Wu and R. L. Kiang. 'Power Performance of a Nonisentropic Brayton Cycle'. In: *Journal of Engineering for Gas Turbines and Power* 113.4 (1991), pp. 501–504. DOI: 10.1115/1.2906268.

[74] S. S. Gupta, P. Kumar and P. C. Gopi. 'Inventory Management and Control Options for Transient Operation of sCO2 Brayton Cycles'. In: *Proceedings of the ASME Turbo Expo 2025: Turbomachinery Technical Conference and Exposition*. Memphis, Tennessee, USA: ASME, 2025, V009T28A018. DOI: 10.1115/GT2025-153599.

[75] A. Hauch et al. 'Recent advances in solid oxide cell technology for electrolysis'. In: *Science* 370.6513 (2020), eaba6118. DOI: 10.1126/science.aba6118.

[76] Asfaw Yohannes and Ian Gates. 'A century of evolution: Progress and milestones in fischer-tropsch synthesis'. In: *Coordination Chemistry Reviews* 547 (2026), p. 217096. ISSN: 0010-8545. DOI: https://doi.org/10.1016/j.ccr.2025.217096.

[77] Michael L. Luyben, Bjorn D. Tyreus and William L. Luyben. 'Plantwide control design procedure'. In: *AIChE Journal* 43.12 (1997), pp. 3161–3174. DOI: https://doi.org/10.1002/aic.690431205.

[78] Mincho Hadjiski, Nencho Deliiski and Natalia Tumbarkova. 'Mathematical Description of the Latent Heat of Water Vaporization in Capillary Porous Materials'. In: 2019 (May 2020), pp. 1–9. DOI: 10.7546/itc-2019-0001.

[79] Government of Canada, Department of National Defence. *Protecteur Class — Royal Canadian Navy*. 2025. URL: https://www.canada.ca/en/navy/corporate/fleet-units/surface/protecteur-class.html.

[80] T. M. Williams, R. P. Gittins and D. M. Burke. 'Replenishment at Sea'. In: *Journal of the Operational Research Society* 40.10 (1989), pp. 881–887. DOI: 10.1057/jors.1989.156.

[81] Minhui Song et al. 'Design and Study of a Series Active Filter for the 10MW-Level High Power and High Stability DC Power Supply'. In: *IEEE Transactions on Applied Superconductivity* 32.6 (2022), pp. 1–5. DOI: 10.1109/TASC.2022.3172651.

[82] Christodoulos A. Floudas and Xiaoxia Lin. 'Mixed Integer Linear Programming in Process Scheduling: Modeling, Algorithms, and Applications'. In: *Annals of Operations Research* 139 (2005), pp. 131–162. DOI: 10.1007/s10479-005-3446-x.

[83] Majid Behzadian et al. 'A state-of the-art survey of TOPSIS applications'. In: *Expert Systems with Applications* 39.17 (2012), pp. 13051–13069. ISSN: 0957-4174. DOI: https://doi.org/10.1016/j.eswa.2012.05.056.

[84] Boeing. *ScanEagle Unmanned Aerial System*. 2024. URL: https://www.boeing.com/defense/autonomous-systems/scaneagle.

[85] AeroVironment. *JUMP 20 Unmanned Aerial System*. 2024. URL: https://www.avinc.com/uas/jump-20.

[86] Schiebel Group. *CAMCOPTER S-100 Unmanned Air System*. 2024. URL: https://schiebel.net/products/camcopter-s-100/.

[87] André Breitinger, Esteban Clua and Leandro A. F. Fernandes. 'An Augmented Reality Periscope for Submarines with Extended Visual Classification'. In: *Sensors* 21.22 (2021). DOI: 10.3390/s21227624.

[88] Teledyne Marine. *Gavia Offshore Surveyor AUV*. 2024. URL: https://www.teledynemarine.com/gavia-auv.

[89] L3Harris Technologies. *Iver4 900 Autonomous Underwater Vehicle*. 2024. URL: https://www.l3harris.com/all-capabilities/iver4-900-auv.

[90] Saab Group. *Sabertooth Hybrid AUV/ROV*. 2024. URL: https://www.saab.com/products/sabertooth.

[91] Boeing. *Orca Extra-Large Unmanned Undersea Vehicle (XLUUV)*. 2024. URL: https://www.boeing.com/defense/xluuv.

[92] Malcolm Palmer. *HMS Chiddingfold (M37) Departing HM Naval Base, Portsmouth*. https://www.flickr.com/photos/145219007@N05/50201224958/. 2020.

[93] *ESVAGT SERVER - Offshore Tug/Supply Ship*. 2025. URL: https://www.vesselfinder.com/vessels/details/9592977.

[94] U.S. Navy. *Navy Increases Unmanned Capabilities with Newly Established Unmanned Surface Division*. 2022. URL: https://www.navy.mil/Press-Office/News-Stories/Article/3031832/navy-increases-unmanned-capabilities-with-newly-established-unmanned-surface-di/.

[95] Fincantieri S.p.A. *Saettia MK2 - Diciotti Class Patrol Vessel*. 2024. URL: https://www.fincantieri.com/it/prodotti-servizi/navi-militari/pattugliatori-costieri/saettia-mk2-diciotti/.

[96] Abu Dhabi Ship Building (ADSB). *510 OPV Product Brochure*. 2023. URL: https://products-webfiles.edgegroup.ae/s3fs-public/2023-10/adsb-510-opv-product-brochure.pdf.

[97] Textron Systems. *Common Unmanned Surface Vehicle (CUSV)*. 2024. URL: https://www.textronsystems.com/products/cusv.

[98] Maritime Tactical Systems (MARTAC). *MANTAS T38 Unmanned Surface Vessel*. 2024. URL: https://martacsystems.com/mantas-t38/.

[99] Swiftships. *23 Meter Patrol Boat*. 2024. URL: https://swiftships.com/vessels/23-meter-patrol-boat/.

[100] 'Ragone plots revisited: A review of methodology and application across energy storage technologies'. In: *Journal of Energy Storage* 73 (2023), p. 109097. ISSN: 2352-152X. DOI: https://doi.org/10.1016/j.est.2023.109097.

9 | Appendix A — Modelling and Simulation Framework

9.1 Simulink System Overview

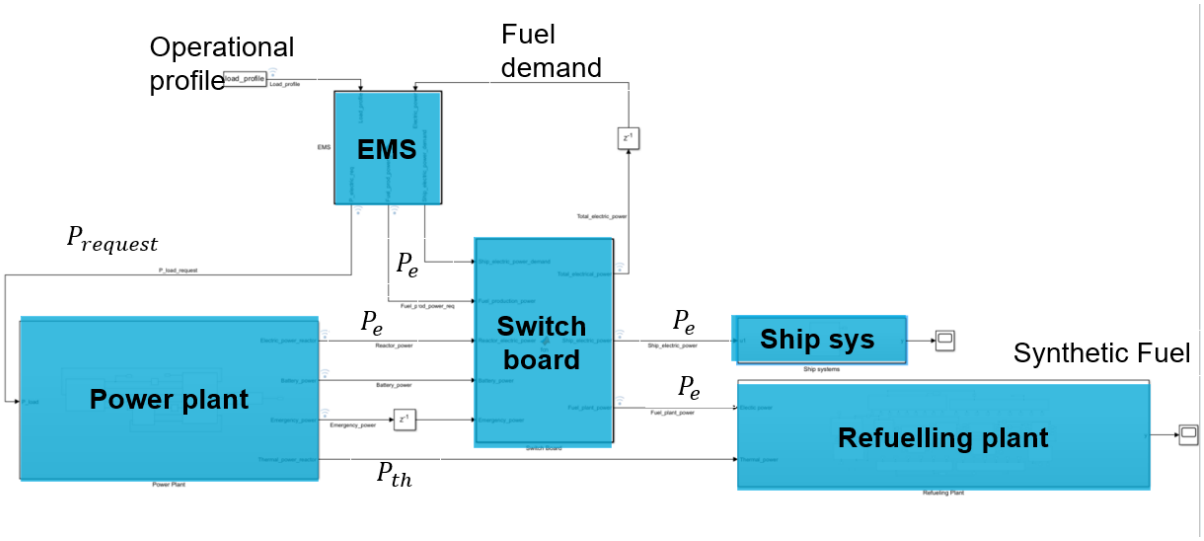

Figure 9.1: Overview of Simulink Energy Model

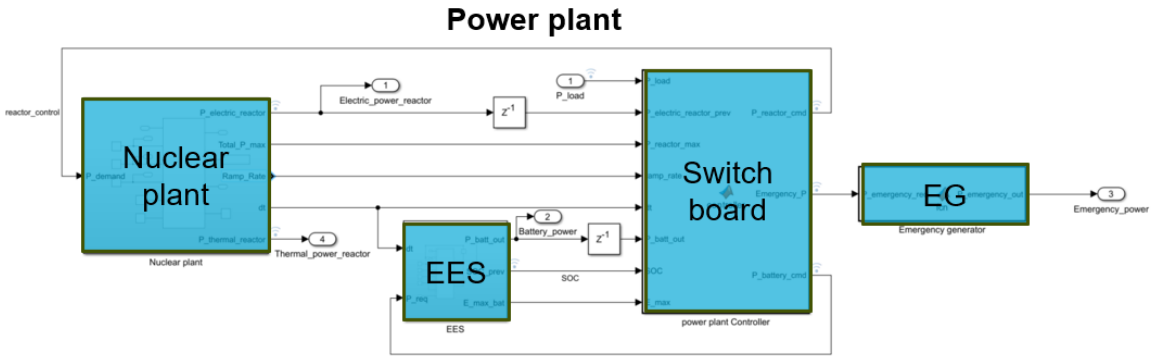

Figure 9.2: Simulink Power Plant Subsystem Design

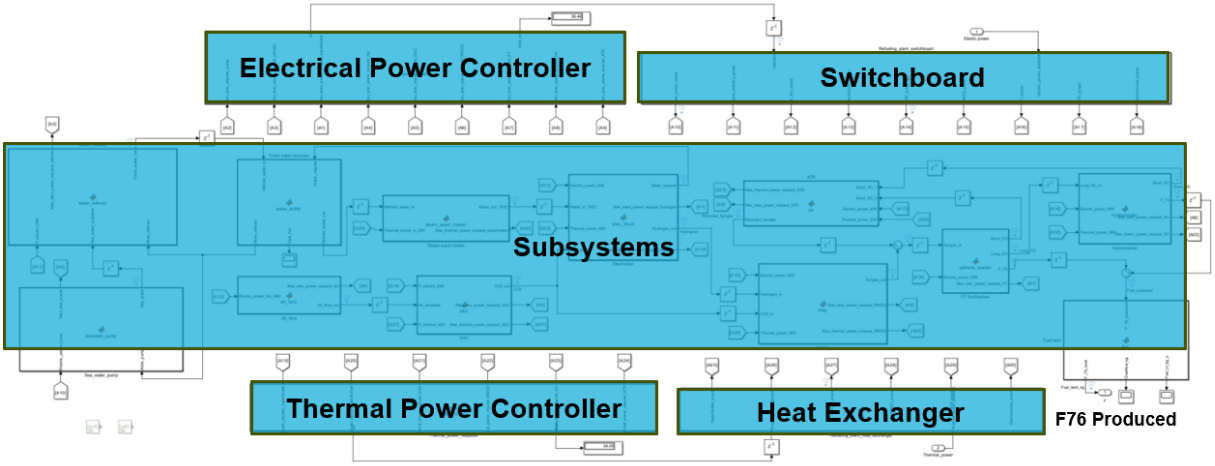

Figure 9.3: Simulink Fuel Production Plant Design

Table 9.1: Symbols used in chapter 4

Symbol	Description
Reactor and ESS	
$P_{\text{th,max}}$, $P_{\text{e,max}}$	Max thermal and electrical power available after accounting for process heat.
$P_{\text{e,target}}$, $P_{\text{e,prev}}$	Requested and previous electrical output used for ramp-rate control.
η_{curr}, η_{prev}, η_{max}	Current, previous, and maximum reactor conversion efficiencies.
r	Reactor ramp-rate limit (fraction per minute).
SOC, E_{max}	Battery state of charge and total capacity.
$P_{\text{max}}^{\text{dis}}$, $P_{\text{max}}^{\text{ch}}$	Max battery discharge and charge power.
η_{dis}, η_{ch}	Battery discharge and charge efficiency.
Ship Systems	
v_{knots}, $v_{\text{km/s}}$	Ship speed in knots and km/s.
$\mathbf{x}_k$, $\mathbf{x}_{\text{tgt}}$	Current ship position and target waypoint.
d_k, $\hat{\mathbf{d}}_k$	Distance to waypoint and its direction unit vector.
d_{tol}	Arrival tolerance radius (100 m).
Water Production (Pump + Purification)	
$\dot{m}_{\text{sw}}$, $\dot{m}_{\text{fw}}$	Seawater inflow and freshwater output mass flow.
$\dot{m}_{\text{sw,target}}$, $\dot{m}_{\text{fw,target}}$	Target flow based on pump power and purification availability.
r_{sw}, r_{fw}	Ramp-rate constants (pump and purification).
E_{spec}	Specific energy for purification (0.5 kWh kg^{-1}).
Superheater + SOEC	
T_{in}, T_{boil}, T_{target}	Inlet, boiling, and 700°C steam temperature.
$E_{\text{per,kg}}$	Total heat required per kg to reach 700°C.
$\dot{m}_{700^\circ\text{C}}$	Superheated steam flow.
r_{sh}	Superheater ramp-rate limit.
E_{elec}, E_{thermal}	Electrical and thermal specific energy for hydrogen production.
$\dot{m}_{\text{H}_2}$	Hydrogen mass-flow produced by SOEC.
Air Fan + Direct Air Capture	
$\dot{m}_{\text{air}}$	Airflow supplied to DAC.
$E_{\text{per flow}}$	Specific fan energy per airflow unit (40 W s kg^{-1}).
r_{fan}	Air-fan ramp-rate limit.
$\dot{m}_{\text{CO}_2}$	CO_2 capture rate.
$R_{\text{air}/\text{CO}_2}$	Air–to–CO_2 mass ratio.
RWGS	
$\dot{m}_{\text{CO}}$, $\dot{m}_{\text{H}_2,\text{left}}$	CO produced and hydrogen remaining after RWGS reaction.
$\dot{m}_{\text{syngas}}$	Total syngas output (CO + H_2).
$\dot{m}_{\text{max}}$	RWGS maximum syngas capacity.
Fischer–Tropsch Synthesis	
$\dot{m}_{\text{HC}}$	Total hydrocarbon output from FT reactor.
η_{conv}	Syngas conversion efficiency (0.92).
$\dot{m}_{\text{short}}$, $\dot{m}_{\text{F-76}}$, $\dot{m}_{\text{long}}$	Short, diesel-range, and long hydrocarbon fractions.
E_{FT}	Specific energy requirement for FT synthesis.
Autothermal Reformer	
$\dot{m}_{\text{short,tot}}$	Total short hydrocarbons sent to ATR.
$\dot{m}_{\text{ATR}}$	ATR syngas output.
Hydrocracker	
$\dot{m}_{\text{feed}}$	Long-chain hydrocarbon feed.
$\dot{m}_{\text{conv}}$	Converted fraction (90%).

9.2 Subsystem Block Diagrams

Table 9.2: Summary of Reactor Block Function

Component Aspect	Description
Operational Logic	The reactor output is governed by its ramp rate, efficiency scaling, and operational limits. At each timestep ($\Delta t = 1$ s), only the rate-limited fraction of the remaining difference to the target power is applied. Minimum and maximum operating bounds are enforced; if the demand falls below 30% of the reactor's rated thermal capacity, the output is clamped to this limit to maintain stable operation. These mechanisms ensure smooth ramping, stable load tracking, and protection against subcritical operation.
Inputs and Outputs	**Inputs:** – Demanded power vector: $P_{\text{demand}} = [P_{\text{elec}}, P_{\text{therm}}]$ **Outputs:** – Electrical generation: P_{electric} [MW] – Direct thermal output: $P_{\text{thermal,direct}}$ [MW] – Reactor utilisation signal
Fixed Parameters	**Rated capacity:** $P_{\text{max}} = 130$ MW. **Ramp rate:** 10% per minute. **Operational range:** 30–100% of rated thermal power. **Efficiency definition:** Six discrete slots define electrical conversion efficiency η across fractional load, ranging from 25% to 45% [71].
Delays and Memory	A persistent state variable stores the previous electrical output $P_{e,k-1}$ to ensure smooth temporal transitions and realistic ramp dynamics between timesteps.
Energy Conversion Logic	The active efficiency slot determines both the ramp scaling and the thermal–electric conversion ratio. Thermal and electrical outputs are related through $$P_{\text{electric}} = \eta\big(P_{\text{thermal,total}} - P_{\text{thermal,direct}}\big).$$

Table 9.3: Summary of Energy Storage System (ESS) Block Function

Component Aspect	Description
Operational Logic	The battery adjusts its output according to the requested power P_{req}, while respecting charge and discharge limits. Charging is restricted by the remaining capacity ($E_{\max} - SOC_{\text{prev}}$), and discharging by the stored energy (SOC_{prev}). At each timestep ($\Delta t = 1$ s), the energy change is computed as $E = P\Delta t/3600$, updating the state of charge smoothly and preventing over- or under-charging.
Inputs and Outputs	**Inputs:** – Requested power: P_{req} (positive = discharge, negative = charge) – Previous state of charge: SOC_{prev} **Outputs:** – Delivered or absorbed power: $P_{\text{batt,out}}$ – Updated state of charge: SOC_{new}
Fixed Parameters	**Capacity:** $E_{\max} = 10$ MWh. **Charge/discharge limits:** 10 MW / 15 MW. **Efficiency:** $\eta_{\text{ch}} = \eta_{\text{dis}} = 0.95$. **Timestep:** $\Delta t = 1$ s.
Delays and Memory	Each updated SOC_{new} becomes the input for the next timestep, maintaining consistent energy tracking and avoiding discontinuities.
Energy Conversion Logic	During discharge, the internal energy drawn equals $E_{\text{out}}/\eta_{\text{dis}}$, and during charging, $\eta_{\text{ch}}E_{\text{in}}$ is stored. The corresponding power exchange is $$P_{\text{batt,out}} = \pm\frac{E \cdot 3600}{\Delta t}.$$

Table 9.4: Summary of Power Plant Controller Block Function

Component Aspect	Description
Operational Logic	At each timestep ($\Delta t = 1$ s), the controller updates the reactor command subject to a 10%/min ramp rate. Battery requests are generated to offset any mismatch between reactor output and system demand, smoothed through asymmetric slew-rate limits (90 MW/min for discharge, 40 MW/min for charge). If demand exceeds the available reactor output, the battery discharges up to 15 MW; when surplus power exists, it charges up to 10 MW. If total supply remains insufficient, fuel plant demand is temporarily reduced. A 0.25 MW deadband prevents power oscillations and switching chatter.
Inputs and Outputs	**Inputs:** – EMS power request: P_{load} (ship + fuel plant) – Previous reactor output: $P_{\text{electric,prev}}$ – Reactor capacity: $P_{\text{reactor,max}}$ – Total demand: $P_{\text{demanded,total}}$ – Battery output: $P_{\text{batt,out}}$ – State of charge ratio: SOC/E_{max} **Outputs:** – Reactor command: P_{reactor} – Battery power request: $P_{\text{batt,req}}$ – Wasted power: P_{wasted}
Fixed Parameters	**Ramp rate:** Reactor limited to 10%/min. **Deadband:** 0.25 MW to prevent chatter. **Battery limits:** 15 MW discharge, 10 MW charge. **Reserve:** Minimum $SOC_{\text{min}} = 0.5$ MWh.
Delays and Memory	Previous outputs are stored as internal states to ensure smooth transitions and prevent abrupt power steps between iterations.
Energy Balance and Waste Handling	Excess reactor power is first directed to the battery if capacity allows. Any remaining unused power is classified as waste: $$P_{\text{wasted}} = P_{\text{reactor,out}} - (P_{\text{demanded,total}} + P_{\text{batt,charge}}).$$

Table 9.5: Summary of Seawater Pump Block Function

Component Aspect	Description
System Response	When activated, the pump ramps up gradually until flow matches the level permitted by available electrical power. If water storage up stream is full the control signal turns off the pump. Ramp-down occurs instantly when the pump is turned off.
Inputs and Outputs	**Inputs:** – Electrical power input: $P_{\text{pump,elec}}$ – Control signal: $\text{Allow}_{\text{pump}}$ (1 = ON, 0 = OFF) **Outputs:** – Rated electrical demand: $P_{\text{elec,max}}$ – Seawater flow rate: $\dot{m}_{\text{sea}}$
Fixed Parameters	**Rated demand:** $P_{\text{elec,max}} = 0.1$ MW. **Flow capacity:** $\dot{m}_{\max} = 8$ kg/s. **Ramp rate:** 0.05 kg/s^2, timestep $\Delta t = 1$ s. **Conversion coefficient:** 8000 W$\cdot$(kg/s)$^{-1}$.
Delays and Memory	Previous $\dot{m}_{k-1}$ is stored to ensure smooth ramp-up transitions.
Energy Conversion Logic	Electrical power input is converted to flow by $$\dot{m}_{\text{sea}} = \frac{P_{\text{pump,elec}} \times 10^6}{\text{pump}_{\text{coeff}}},$$ bounded by $\dot{m}_{\max} = 8$ kg/s. The rated demand $P_{\text{elec,max}}$ is full-capacity operation. $\dot{m}_{\text{sea}}$ is set to zero when $\text{Allow}_{\text{pump}} = 0$.

Table 9.6: Summary of Water Refinery Block Function

Component Aspect	Description
Operational Logic	The refinery converts seawater to freshwater based on available electrical power and seawater feed. Flow ramps smoothly toward the achievable target, limited by the defined ramp rate. If $\text{Allow}_{\text{refinery}} = 0$, production halts due to a full freshwater storage. Otherwise, output is governed by the lower of the available power or seawater inflow.
Inputs and Outputs	**Inputs:** – Electrical power input: P_{electric} [MW] – Seawater inflow: $\dot{m}_{\text{sea}}$ [kg/s] – Control signal: $\text{Allow}_{\text{refinery}}$ (1 = ON, 0 = buffer full) **Outputs:** – Rated electrical demand: $P_{\text{elec,max}}$ [MW] – Purified water flow: $\dot{m}_{\text{fresh}}$ [kg/s]
Fixed Parameters	**Rated power:** $P_{\text{elec,max}} = 0.0025$ MW. **Specific energy:** $E_{\text{per kg}} = 0.5$ kWh/kg. **Flow ratio:** Seawater to freshwater = 1.3. **Ramp rate:** 0.05 kg/s^2. **Timestep:** $\Delta t = 1$ s.
Delays and Memory	A persistent variable stores the previous freshwater output $\dot{m}_{\text{fresh},k-1}$ to ensure smooth ramp-up and ramp-down transitions.
Energy Conversion Logic	The energy required to produce freshwater is $$E_{\text{per kg}} = 0.5 \text{ kWh/kg}.$$ The corresponding electrical power demand for a given flow is $$P_{\text{electric}} = \dot{m}_{\text{fresh}} \times \frac{E_{\text{per kg}}}{3600}.$$

Table 9.7: Summary of Steam Superheater Block Function

Component Aspect	Description
Operational Logic	The superheater determines the achievable water flow based on available thermal power and feedwater supply. Flow ramps smoothly within defined rate limits, accounting for boiling delay, transport delay, and thermal inertia. If insufficient heat is available, the output decreases automatically while maintaining stable operation.
Inputs and Outputs	**Inputs:** – Refined water inflow: $\dot{m}_{\text{refined}}$ [kg/s] – Supplied thermal power: $P_{\text{thermal,in}}$ [MW] **Outputs:** – Superheated water flow: $\dot{m}_{700^\circ\text{C}}$ [kg/s] – Rated thermal demand: $P_{\text{thermal,max}}$ [MW]
Fixed Parameters	**Thermal demand:** $P_{\text{thermal,max}} = 15.9$ MW. **Temperature stages:** $T_{\text{in}} = 25^\circ$C, $T_{\text{boil}} = 100^\circ$C, $T_{\text{target}} = 700^\circ$C. **Specific heats:** $c_{p,\text{liq}} = 0.00116$, $c_{p,\text{steam}} = 0.00208$ kWh/(kg·K). **Latent heat:** $h_{\text{vap}} = 0.627$ kWh/kg. **Ramp rate:** 0.167 kg/s^2. **Timestep:** $\Delta t = 1$ s.
Delays and Memory	Boiling delay (10 s) and transport delay (5 s) are modelled using a memory buffer. A thermal lag $\tau = 15$ s smooths transients, and the previous output $\dot{m}_{k-1}$ ensures continuity.
Energy Conversion Logic	The total energy to heat water to 700°C is $$E_{\text{per kg}} = c_{p,\text{liq}}(T_{\text{boil}} - T_{\text{in}}) + h_{\text{vap}} + c_{p,\text{steam}}(T_{\text{target}} - T_{\text{boil}}).$$ The corresponding thermal–mass flow relation is $$\dot{m}_{700^\circ\text{C}} = \frac{P_{\text{thermal,in}}}{E_{\text{per kg}}},$$ bounded by ramp and delay dynamics.

Table 9.8: Summary of Solid Oxide Electrolyzer Cell (SOEC) Block Function

Component Aspect	Description
Operational Logic	The SOEC converts superheated steam into hydrogen using both electrical and thermal energy. Hydrogen output ramps smoothly toward the achievable limit, constrained by power, heat, and water availability. If any input is insufficient, production decreases while maintaining stable operation. A time delay anticipates a 15 s combined delay from the superheater and intermediate systems. Although the SOEC itself does not process CO_2, it continuously monitors the incoming CO_2 feed to the RWGS to determine the appropriate hydrogen production rate. This predictive coupling keeps the H_2:CO_2 ratio consistent for the synthesis step, preventing hydrogen overproduction and ensuring coordinated operation between subsystems.
Inputs and Outputs	**Inputs:** – Electrical power: $P_{\text{elec,in}}$ [MW] – Thermal power: $P_{\text{thermal,in}}$ [MW] – Superheated water inflow: $\dot{m}_{\text{H2O,700°C}}$ [kg/s] – CO_2 reference signal (from RWGS): $\dot{m}_{\text{CO2,ref}}$ [kg/s] **Outputs:** – Hydrogen production: $\dot{m}_{\text{H2,out}}$ [kg/s] – Water request: $\dot{m}_{\text{H2O,req}}$ [kg/s] – Rated electrical and thermal demands: $P_{\text{elec,max}}$, $P_{\text{thermal,max}}$ [MW]
Fixed Parameters	**Rated demands:** $P_{\text{elec,max}} = 25$ MW, $P_{\text{thermal,max}} = 10.4$ MW. **Energy requirements:** $E_{\text{elec}} = 24$ kWh/kg H_2, $E_{\text{thermal}} = 10$ kWh/kg H_2. **Water consumption:** 9 kg H_2O per kg H_2. **Reference ratio:** $H_{2/\text{CO}} = 0.3929$ kg H_2 per kg CO_2 (used to align production rates). **Ramp rate:** 0.0006 kg/s^2. **Timestep:** $\Delta t = 1$ s.
Delays and Memory	A memory variable stores the previous hydrogen output $\dot{m}_{\text{H2},k-1}$ to ensure continuity. Predictive scheduling accounts for a 15 s system delay between steam and electrolysis stages.
Energy Conversion Logic	Energy demand per unit hydrogen is $$E_{\text{H2}} = E_{\text{elec}} + E_{\text{thermal}}.$$ The achievable hydrogen production rate follows $$\dot{m}_{\text{H2}} = \min\left(\frac{P_{\text{elec,in}}}{3.6E_{\text{elec}}}, \frac{P_{\text{thermal,in}}}{3.6E_{\text{thermal}}}, 2\,\dot{m}_{\text{CO2,ref}}\,H_{2/\text{CO}}\right),$$ and the corresponding water requirement is $$\dot{m}_{\text{H2O,req}} = 9\,\dot{m}_{\text{H2}}.$$ The water request is predicted ahead based on reachable production within the anticipation horizon.

Table 9.9: Summary of Air Fan Block Function

Component Aspect	Description
Operational Logic	The fan converts electrical power into airflow for the DAC system. Airflow ramps up smoothly under a 20 kg/s^2 limit and decreases instantly when power drops. The output is linearly related to electrical input and capped at rated capacity, ensuring mechanical stability during acceleration and deceleration.
Inputs and Outputs	**Inputs:** – Electrical power input: $P_{\text{elec,fan}}$ [MW] **Outputs:** – Airflow to DAC: $\dot{m}_{\text{air}}$ [kg/s] – Rated electrical demand: $P_{\text{elec,max}}$ [MW]
Fixed Parameters	**Rated power:** $P_{\text{elec,max}} = 0.18$ MW. **Maximum flow:** $\dot{m}_{\text{air,max}} = 3000$ kg/s. **Power coefficient:** 40 W·(kg/s)$^{-1}$. **Ramp rate:** 20 kg/s^2. **Timestep:** $\Delta t = 1$ s.
Delays and Memory	A persistent variable stores the previous airflow $\dot{m}_{k-1}$ to provide a ramped and continuous response to power changes.
Energy Conversion Logic	Airflow is determined by $$\dot{m}_{\text{air}} = \frac{P_{\text{elec,fan}} \times 10^6}{\text{power}_{\text{per flow}}},$$ where $\text{power}_{\text{per flow}} = 40$ W·(kg/s)$^{-1}$. The flow is limited to $\dot{m}_{\text{air,max}} = 3000$ kg/s under rated conditions.

Table 9.10: Summary of Direct Air Capture (DAC) Block Function

Component Aspect	Description
Operational Logic	The DAC unit captures CO_2 from air using electrical and thermal power. Its output ramps smoothly according to available energy and airflow, operating in three speed modes: *slow* below 30% capacity, *medium* between 30% and 60%, and *fast* above 60%. These modes ensure stable start-up, controlled load transitions, and safe dynamic behaviour, with capture rate limited by the lowest of the three inputs.
Inputs and Outputs	**Inputs:** Electrical power input: $P_{\text{elec,in}}$ [MW] Thermal power input: $P_{\text{thermal,in}}$ [MW] Airflow input: $\dot{m}_{\text{air}}$ [kg/s] **Outputs:** Captured CO_2 flow: $\dot{m}_{\text{CO2,out}}$ [kg/s] Rated power demands: $P_{\text{elec,max}}$, $P_{\text{thermal,max}}$ [MW]
Fixed Parameters	**Rated power:** $P_{\text{elec,max}} = 0.8$ MW, $P_{\text{thermal,max}} = 4.2$ MW. **Energy intensities:** 6.8×10^{-6} MW·(kg CO_2)$^{-1}$ (electric), 4.04×10^{-5} MW·(kg CO_2)$^{-1}$ (thermal). **Air intake ratio:** 1667 kg air per kg CO_2. **Ramp rate limits:** 0.000333 (slow), 0.001 (medium), 0.002 (fast) [fraction of capacity per second]. **Timestep:** $\Delta t = 1$ s.
Delays and Memory	A persistent memory variable stores the previous CO_2 output $\dot{m}_{\text{CO2},k-1}$, ensuring continuous ramping behaviour across time steps and preventing unrealistic step changes.
Energy Conversion Logic	The CO_2 capture rates are determined by $$\dot{m}_{\text{CO2,elec}} = \frac{P_{\text{elec,in}}}{6.8 \times 10^{-6}}, \qquad \dot{m}_{\text{CO2,thermal}} = \frac{P_{\text{thermal,in}}}{4.04 \times 10^{-5}}.$$ The achievable CO_2 capture rate is then $$\dot{m}_{\text{CO2,out}} = \min\left(\dot{m}_{\text{CO2,elec}}, \dot{m}_{\text{CO2,thermal}}, \frac{\dot{m}_{\text{air}}}{1667}\right).$$ This ensures that CO_2 capture performance scales realistically with power, heat, and air availability while respecting dynamic ramping limits.

Table 9.11: Summary of Reverse Water Gas Shift (RWGS) Block Function

Component Aspect	Description
Operational Logic	The RWGS unit converts CO_2 and H_2 into CO and H_2O, forming a syngas mixture. Production depends on the available electrical, thermal, and reactant inputs, with smooth ramp up during operation and immediate response to supply loss. The target syngas composition uses a hydrogen to carbon monoxide ratio of 2 to 1 on a molar basis, with any excess hydrogen remaining in the outlet stream.
Inputs and Outputs	**Inputs:** Electrical power: $P_{\text{elec,in}}$ [MW] Thermal power: $P_{\text{thermal,in}}$ [MW] Hydrogen inflow: $\dot{m}_{\text{H2,in}}$ [kg s^{-1}] Carbon dioxide inflow: $\dot{m}_{\text{CO2,in}}$ [kg s^{-1}] **Outputs:** Syngas flow: $\dot{m}_{\text{syngas,out}}$ [kg s^{-1}] Rated power demands: $P_{\text{elec,max}}$, $P_{\text{thermal,max}}$
Fixed Parameters	**Rated demands:** $P_{\text{elec,max}} = 1$ MW, $P_{\text{thermal,max}} = 2.5$ MW. **Molar masses for conversion:** $M_{H_2} = 2.016$ g mol^{-1}, $M_{CO_2} = 44.01$ g mol^{-1}, $M_{CO} = 28.01$ g mol^{-1}, $M_{H_2O} = 18.015$ g mol^{-1}. **Stoichiometry and target:** $CO_2 + H_2 \rightarrow CO + H_2O$, with outlet $H_2 : CO = 2:1$ on a molar basis. **Energy intensity:** 1.4×10^{-5} MW per kg syngas (electrical), 3.57×10^{-5} MW per kg syngas (thermal). **Ramp constant:** 300 s to full capacity (50 kg s^{-1}). **Timestep:** $\Delta t = 1$ s.
Delays and Memory	A persistent state variable stores the previous syngas output $\dot{m}_{\text{syngas},k-1}$ to ensure continuous ramping and stable transitions.
Energy Conversion and Reaction Logic	Main reaction in moles $$CO_2 + H_2 \rightarrow CO + H_2O.$$ Inlet mass flows are first converted to molar flows using the molar masses $M_{H_2} = 2.016$ g mol^{-1}, $M_{CO_2} = 44.01$ g mol^{-1}, $M_{CO} = 28.01$ g mol^{-1}, and $M_{H_2O} = 18.015$ g mol^{-1}. The reaction maintains an outlet ratio of $H_2 : CO = 2:1$ on a molar basis, which corresponds to approximately 1 : 7 by mass. For complete CO_2 conversion, a feed ratio of $H_2 : CO_2 = 3:1$ (mol) is used. The resulting syngas mass flow is the sum of produced CO and remaining H_2, limited by the available electrical and thermal power as $$\dot{m}_{\text{syngas,out}} \leq \min\left(\frac{P_{\text{elec,in}}}{1.4 \times 10^{-5}}, \frac{P_{\text{thermal,in}}}{3.57 \times 10^{-5}}\right).$$

Table 9.12: Summary of Fischer–Tropsch (FT) Synthesis Reactor Block Function

Component Aspect	Description
Operational Logic	The FT reactor converts syngas into hydrocarbons through catalytic polymerisation. Output ramps gradually toward the feasible production target, limited by available syngas, electrical power, and design capacity. The Anderson–Schulz–Flory (ASF) model defines the distribution across short (C_1–C_{10}), diesel (C_{12}–C_{20}), and long (C_{21}^+) chains, where only the diesel range ($\dot{m}_{\text{F-76}}$) is extracted as fuel and the rest is recycled.
Inputs and Outputs	**Inputs:** – Electrical power: $P_{\text{elec,in}}$ [MW] – Syngas inflow: $\dot{m}_{\text{syngas,in}}$ [kg/s] **Outputs:** – Diesel fraction: $\dot{m}_{\text{F-76}}$ [kg/s] – Short hydrocarbons: $\dot{m}_{\text{short}}$ (recycled gas) – Long hydrocarbons: $\dot{m}_{\text{long}}$ (recycled waxes) – Rated electrical demand: $P_{\text{elec,max}}$ [MW]
Fixed Parameters	**Rated power:** $P_{\text{elec,max}} = 8.28$ MW. **Conversion efficiency:** $\eta_{\text{conv}} = 0.92$. **Production limit:** 4 kg/s, ramp rate 0.5 kg/s^2. **Chain growth probability:** $\alpha = 0.9$ (ASF model). **Energy intensity:** 1.443×10^{-4} MW·(kg HC)$^{-1}$ ($\approx$0.3 kWh/kg). **Timestep:** $\Delta t = 1$ s.
Delays and Memory	A persistent variable stores the previous total hydrocarbon output $\dot{m}_{\text{HC},k-1}$ to ensure smooth ramp transitions between time steps.
Energy Conversion Logic	Electrical input defines the maximum producible hydrocarbon mass flow: $$\dot{m}_{\text{HC,max}} = \frac{P_{\text{elec,in}}}{1.443 \times 10^{-4}}.$$ Total output is $$\dot{m}_{\text{HC,out}} = \min(\dot{m}_{\text{HC,max}},\, \eta_{\text{conv}}\dot{m}_{\text{syngas,in}},\, 4)\,,$$ distributed as $$\dot{m}_{\text{short}} + \dot{m}_{\text{F-76}} + \dot{m}_{\text{long}} = \dot{m}_{\text{HC,out}}.$$

Table 9.13: Summary of Autothermal Reformer (ATR) Block Function

Component Aspect	Description
Operational Logic	The ATR converts short-chain hydrocarbons into syngas using both electrical and thermal power. Output ramps smoothly under ramp-rate constraints and halts instantly if any input becomes unavailable. Syngas production is governed by the lowest of the feed, electrical, thermal, and capacity limits, ensuring stable autothermal operation.
Inputs and Outputs	**Inputs:** – Short-chain hydrocarbon streams: $\dot{m}_{\text{short},1}$, $\dot{m}_{\text{short},2}$ [kg/s] – Electrical power: $P_{\text{elec,in}}$ [MW] – Thermal power: $P_{\text{thermal,in}}$ [MW] **Outputs:** – Recycled syngas flow: $\dot{m}_{\text{syngas,recycled}}$ [kg/s] – Rated power demands: ($P_{\text{elec,max}}$, $P_{\text{thermal,max}}$)
Fixed Parameters	**Rated demands:** $P_{\text{elec,max}} = 0.2$ MW, $P_{\text{thermal,max}} = 0.65$ MW. **Conversion efficiency:** $\eta_{\text{conv}} = 0.85$. **Capacity limit:** 2.8 kg/s; ramp rate 0.00167 kg/s^2. **Energy intensity:** 2.3×10^{-5} MW·(kg syngas)$^{-1}$ (electrical), 1.04×10^{-5} MW·(kg syngas)$^{-1}$ (thermal). **Timestep:** $\Delta t = 1$ s.
Delays and Memory	A persistent variable stores the previous syngas output $\dot{m}_{\text{syngas},k-1}$, ensuring smooth ramp-up and realistic thermal startup behaviour.
Energy Conversion Logic	The achievable syngas mass flow is determined by $\dot{m}_{\text{syngas}} = \min\Big(\frac{P_{\text{elec,in}}}{2.3\times10^{-5}}, \frac{P_{\text{thermal,in}}}{1.04\times10^{-5}}, 0.85\,(\dot{m}_{\text{short},1}+\dot{m}_{\text{short},2}), 2.8\Big)$. The reactor output $\dot{m}_{\text{syngas,recycled}}$ is ramp-limited to represent gradual heating and reaction initiation under autothermal operation.

Table 9.14: Summary of Hydrocracker Block Function

Component Aspect	Description
Operational Logic	The hydrocracker upgrades long-chain hydrocarbons into shorter, more valuable products through catalytic cracking and hydrogenation. Output ramps gradually under rate limits, while reductions in feed or power trigger immediate ramp-down. Production is limited by feed availability, power input, and design capacity, with mass split into 70% diesel and 30% short-chain hydrocarbons.
Inputs and Outputs	**Inputs:** – Long-chain hydrocarbon inflow: $\dot{m}_{\text{long,in}}$ [kg/s] – Electrical power: $P_{\text{elec,in}}$ [MW] – Thermal power: $P_{\text{thermal,in}}$ [MW] **Outputs:** – Diesel fraction: $\dot{m}_{\text{F-76}}$ [kg/s] – Recycled short-chain hydrocarbons: $\dot{m}_{\text{short}}$ [kg/s] – Rated electrical and thermal demands: ($P_{\text{elec,max}}$, $P_{\text{thermal,max}}$)
Fixed Parameters	**Rated demands:** $P_{\text{elec,max}} = 0.9$ MW, $P_{\text{thermal,max}} = 0.4$ MW. **Conversion efficiency:** $\eta_{\text{conv}} = 0.9$. **Product yield:** 70% diesel, 30% short hydrocarbons. **Capacity limits:** Max feed 1 kg/s, ramp rate 0.000201 kg/s^2. **Energy requirements:** 1.03×10^{-5} MW·kg^{-1} (elec), 3.4×10^{-5} MW·kg^{-1} (thermal). **Timestep:** $\Delta t = 1$ s.
Delays and Memory	Persistent memory variables store the previous diesel and short-chain outputs ($\dot{m}_{\text{F-76},k-1}, \dot{m}_{\text{short},k-1}$) to ensure smooth ramping and transitions.
Energy Conversion Logic	The feasible feed rate is given by: $$\dot{m}_{\text{feed}} = \min\left(\dot{m}_{\text{long,in}},\ \frac{P_{\text{elec,in}}}{1.03 \times 10^{-5}},\ \frac{P_{\text{thermal,in}}}{3.4 \times 10^{-5}},\ 1\right).$$ The converted mass flow: $$\dot{m}_{\text{conv}} = 0.9\,\dot{m}_{\text{feed}}.$$ Product split: $$\dot{m}_{\text{F-76}} = 0.7\,\dot{m}_{\text{conv}}, \qquad \dot{m}_{\text{short}} = 0.3\,\dot{m}_{\text{conv}}.$$

Table 9.15: Summary of Fuel Storage Block Function

Component Aspect	Description
Operational Logic	Stores produced F-76 diesel and coordinates refuelling according to predefined requests. Fuel inflow increases tank level based on production rate, while outflow occurs only when refuelling conditions of time and position are satisfied. If the stored fuel is insufficient for the next request, the system enters a waiting state until production replenishes the tank. A position latch ensures refuelling starts only when the mothership is within 0.1 km of the refuelling point.
Inputs and Outputs	**Inputs:** Fuel inflow from production: $\dot{m}_{\text{fuel,in}}$ [kg/s] Refuelling requests: time, quantity, and position [s, kg, km] Ship position: (x, y) [km] **Outputs:** Remaining fuel in storage: $\dot{m}_{\text{fuel,out}}$ [kg] Active request index: i_{req} (waiting, active, or complete) Refuelling start event flag
Fixed Parameters	**Initial fuel level:** 500,000 kg **Maximum capacity:** 700,000 kg. **Maximum flow rate:** 100,000 kg/h (27.8 kg/s). **Distance tolerance:** 0.1 km for refuelling latch. **Timestep:** $\Delta t = 1$ s.
Control and Memory	Persistent state variables track stored fuel, current and next requests, and refuelling progress. A one-shot event flag is triggered when refuelling begins for each request, allowing synchronised control between the EMS and the ship's motion plan.
Fuel Balance Relation	The tank storage level evolves over time according to the net mass flow balance $$m_{\text{fuel}}(t + \Delta t) = m_{\text{fuel}}(t) + \dot{m}_{\text{fuel,in}}\,\Delta t - \dot{m}_{\text{fuel,refuel}}\,\Delta t,$$ where inflow originates from the onboard fuel production plant and outflow represents the controlled transfer to USVs during refuelling operations.

Table 9.16: Summary of Ship Systems Block Function

Component Aspect	Description
Operational Logic	Divides total incoming power between propulsion and hotel services. The constant hotel load of 3 MW is subtracted first, and the remaining power is used for propulsion. Ship speed is interpolated from a predefined speed–power curve and converted to displacement per second to update position. When the target position is reached within 0.1 km, propulsion power is reduced to zero and the ship stops.
Inputs and Outputs	**Inputs:** Total available power: $P_{\text{total,in}}$ [MW] Target position: $(x_{\text{target}}, y_{\text{target}})$ [km] Current position: $(x_{\text{ship}}, y_{\text{ship}})$ [km] Time: t [s] **Outputs:** Ship speed: v_{ship} [kn] Propulsion power: $P_{\text{propulsion}}$ [MW] Hotel power: P_{hotel} [MW] Updated ship position: (x, y) [km] Distance to target: d_{target} [km]
Fixed Parameters	**Hotel load:** $P_{\text{hotel}} = 3$ MW. **Speed–power curve:** 0–22 kn corresponding to 3.6–21.1 MW. **Distance tolerance:** 0.1 km. **Conversion:** 1 kn = 1.852 km/h. **Timestep:** $\Delta t = 1$ s.
Control and Memory	Persistent memory stores the previous position and time to ensure continuous motion and accurate integration of travelled distance. If no power is available, the ship remains stationary until propulsion power is restored.
Power and Motion Relation	Ship speed is computed as a function of available propulsion power according to $v_{\text{ship}} = f(P_{\text{propulsion}}), \quad \text{where} \quad P_{\text{propulsion}} = \max(P_{\text{total,in}} - P_{\text{hotel}}, 0).$ Position is updated each timestep using $\vec{x}(t + \Delta t) = \vec{x}(t) + \vec{u}\, v_{\text{ship}} \dfrac{1.852}{3600} \Delta t,$ with $\vec{u}$ as the unit vector from the ship to the target position.

Table 9.17: Summary of Energy Management System (EMS) Block Function

Component Aspect	Description
Operational Logic	The EMS block coordinates propulsion, refuelling, and fuel production based on mission state and available energy. It follows a finite-state navigation scheme with distinct operational stages: *to_ origin*, *to_ refuel*, *refuel_ and_ drift*, *hold_ at_ refuel*, *hold_ after_ drift*, and *to_ port*. The system dynamically selects targets, manages transitions between states, and adjusts ship speed and power demand accordingly. Power distribution prioritises propulsion and hotel loads, while surplus power is directed to the fuel production plant under battery-dependent policies.
Inputs and Outputs	**Inputs:** Electric power available: P_{electric} [MW] Reactor maximum power: $P_{\text{reactor,max}}$ [MW] Refuelling requests matrix: RefuelRequests [–] Current position: $\mathbf{x}_{\text{ship}}$ [km] Active request index: active_req_idx [–] Fuel storage level: $m_{\text{fuel,stored}}$ [kg] Battery state of charge: SOC [–] Simulation time: t_{now} [s] **Outputs:** Reactor electric power request: $P_{\text{electric,req}}$ [MW] Fuel production power: P_{fuel} [MW] Ship electric power demand: P_{ship} [MW] Target position: $\mathbf{x}_{\text{target}}$ [km] Total demanded power: $P_{\text{total,req}}$ [MW]
Fixed Parameters	**Fuel storage capacity:** 700 t. **Hotel load:** 3 MW. **Battery full threshold:** 9 MWh (of 10 MWh nominal). **Speed–power curve:** Defined between 0–22 kn for realistic propulsion scaling. **Ramp limits:** Propulsion ramp = 30 MW min^{-1}, reactor ramp = 0.08 P_{max} min^{-1}. **Tolerances:** 0.1 km for arrival detection. **Low-pass filter constants:** $\tau_{\text{fuel}} = 5$ s, $\tau_{\text{preq}} = 5$ s.
Delays and Memory	Persistent memory variables store the last reactor request, fuel production history, and previous time step, ensuring smooth ramping and consistent state transitions between time steps. These include: Fuel_hist, P_req1_prev, stage_state, and hold_point.
Control and Power Management Logic	Ship navigation and power control are governed by a state machine. Each stage assigns a target position and sailing speed: • *to_ origin, to_ refuel, to_ port*: 17 kn; • *refuel_ and_ drift*: 10 kn; • *hold_ at_ refuel, hold_ after_ drift*: 0 kn. The propulsion and hotel loads determine the ship's electric power demand, which is ramp-limited and combined with fuel production power to form the total demand. The EMS prioritises essential loads, limits fuel production when the fuel tanks are near full, and modulates reactor requests based on available electric power and battery SOC to ensure stable operation across all mission phases.

9.3 Fleet-Wide EMS: Mathematical Model

The following mathematical formulation represents the optimization model implemented in Python. The objective is to minimize total refuelled fuel mass across all USVs while satisfying timing, fuel, and berth constraints. All parameters correspond to the reference case used in the numerical implementation.

Sets and Indices

Table 9.18: Notation — Sets and Indices

Symbol	Description	Index set
U	Set of USVs	$u \in U = \{1, 2, \ldots, \lvert U\rvert - 1\}$
P	Mission slots per USV	$p \in P = \{1, 2, 3\}$
I	Set of tasks	$i \in I$
A	Operational areas	$a \in A = \{1, \ldots, \lvert A\rvert - 1\}$
S	Discrete sailing speeds	$s \in S = \{12, 15, 18, 21, 24\}$
X	Discrete hub positions	$x \in X = \{1, \ldots, N_x\}$
$\mathcal{R}$	Set of refuel events (u, p)	$r \in \mathcal{R}$

Parameters

Table 9.19: Notation — Parameters

Parameter	Description	Units / Value
$T^{\max}$	Mission horizon	480 h
$\tau^{\mathrm{AO}}_{a,p}$	AO dwell time	[60,84,108] h
ρ^{ref}	Fuel transfer rate	1.0×10^5 kg h^{-1}
$F^{\min}$	Minimum refuel amount	3.3×10^4 kg
F^{cap}	USV fuel capacity	1.43×10^5 kg
F^{minUSV}	Minimum safe USV fuel	7.15×10^3 kg
S_0	Initial hub fuel store	5.0×10^5 kg
η^{prod}	Fuel production rate	1.76×10^3 kg h^{-1}
$V^{\max}_{\mathrm{hub}}$	Max hub movement speed	31.5 km h^{-1}
M	Big-M constant	10^5
d^{PAI}_a	Port→AO(in) distance	[km]
d^{HAI}_a	Hub→AO(in) distance	[km]
$d^{\mathrm{AOH}}_{a,x}$	AO(out)→Hub(pos x)	[km]
$d^{\mathrm{AA}}_{a,a'}$	AO→AO direct distance	[km]
d^{HP}	Hub→Port distance	[km]
d^{AP}_a	AO→Port distance	[km]
$v(s)$	Sailing speed	[km h^{-1}]
$\phi(s)$	Speed fuel burn rate	[kg h^{-1}]
ϕ^{AO}	Dwell fuel rate	450 kg h^{-1}

Decision Variables

Table 9.20: Notation — Decision Variables

Variable	Description	Domain
$a_{u,p,i}$	Task i assigned to USV u slot p	binary
$x_{u,i}$	Task performed by USV u	binary
$w_{u,p,i',i}$	AO→AO link indicator	binary
$r_{u,p}$	Refuel after slot p	binary
$y^P_{u,p,s}, y^H_{u,p,s}, y^R_{u,p,s}, y^B_{u,s}$	One speed choices	binary
$t^{\text{start}}_{u,p}, t^{\text{in}}_{u,p}, t^{\text{out}}_{u,p}$	Timing variables	[h]
$t^H_{u,p}, t^R_{u,p}, t^{\text{end}}_{u,p}$	Hub/refuel/end times	[h]
$f^{\text{dep}}_{u,p}, f^{\text{bef}}_{u,p}, f^{\text{aft}}_{u,p}$	Fuel states	[kg]
f^{depP}_u	Fuel before port return	[kg]
$X_{u,p}$	Hub location during refuel	[km]
$z_{u,p,x}$	Hub-location selector	binary
$b_{r,s}$	Refuel order indicator	binary
$g_{r,s}$	Fuel precedence variable	[kg]

Objective

$$\min \; J = \sum_{u\in U}\sum_{p\in P}\left(f^{\text{aft}}_{u,p} - f^{\text{bef}}_{u,p}\right) + \varepsilon \sum_{u\in U} t^{\text{end}}_{u,|P|-1}. \tag{9.1}$$

The objective minimizes total fuel delivered to USVs, with a small penalty encouraging shorter mission durations.

Constraints

Task assignment and slot filling

$$\sum_{u\in U}\sum_{p\in P} a_{u,p,i} = 1 \qquad \forall i \in I \tag{9.2}$$

$$\sum_{i\in I} a_{u,p,i} = 1 \qquad \forall u, p \tag{9.3}$$

$$x_{u,i} = \sum_{p} a_{u,p,i} \qquad \forall u, i \tag{9.4}$$

Each task is assigned exactly once, each slot is filled, and $x_{u,i}$ activates if USV u performs task i.

Consecutive slot linking

$$w_{u,p,i',i} \le a_{u,p-1,i'}, \qquad w_{u,p,i',i} \le a_{u,p,i}, \tag{9.5}$$

$$\sum_{i'} w_{u,p,i',i} = a_{u,p,i}, \qquad \sum_{i} w_{u,p,i',i} = a_{u,p-1,i'} \tag{9.6}$$

Binary variables w identify the ordered AO pairs in consecutive mission slots.

Speed selection per leg

$$\sum_{s} y^{P}_{u,p,s} = \mathbf{1}\{p = 0\}, \tag{9.7}$$

$$\sum_{s} y^{H}_{u,p,s} = \mathbf{1}\{p \geq 1\}, \tag{9.8}$$

$$\sum_{s} y^{R}_{u,p,s} = 1, \qquad \sum_{s} y^{B}_{u,s} = 1 \tag{9.9}$$

Exactly one sailing speed is chosen for each type of leg.

Inbound AO arrival

$$t^{\text{in}}_{u,0} = t^{\text{start}}_{u,0} + \sum_{i,s} a_{u,0,i} y^{P}_{u,0,s} \tfrac{d^{\text{PAI}}_{a(i)}}{v(s)}, \tag{9.10}$$

$$t^{\text{in}}_{u,p} - t^{\text{start}}_{u,p} - \sum_{i,s} a_{u,p,i} y^{H}_{u,p,s} \tfrac{d^{\text{HAI}}_{a(i)}}{v(s)} \leq M(1 - r_{u,p-1}), \tag{9.11}$$

$$t^{\text{in}}_{u,p} - t^{\text{start}}_{u,p} - \sum_{i',i,s} w_{u,p,i',i} y^{H}_{u,p,s} \tfrac{d^{\text{AA}}_{a(i'),a(i)}}{v(s)} \leq M r_{u,p-1} \tag{9.12}$$

Big-M switches between hub→AO or AO→AO routing depending on whether a refuel occurred previously.

AO dwell and outbound travel

$$t^{\text{out}}_{u,p} = t^{\text{in}}_{u,p} + \sum_{i} a_{u,p,i} \tau^{\text{AO}}_{a(i),p}, \tag{9.13}$$

$$t^{H}_{u,p} - \Big(t^{\text{out}}_{u,p} + \sum_{i,s,x} a_{u,p,i} y^{R}_{u,p,s} z_{u,p,x} \tfrac{d^{\text{AOH}}_{a(i),x}}{v(s)} \Big) \leq M(1 - r_{u,p}) \tag{9.14}$$

AO dwell time is enforced, and hub travel time depends on chosen hub position.

Refueling timing

$$t^{R}_{u,p} \geq t^{H}_{u,p} - M(1 - r_{u,p}), \tag{9.15}$$

$$t^{\text{end}}_{u,p} - t^{R}_{u,p} = \frac{f^{\text{aft}}_{u,p} - f^{\text{bef}}_{u,p}}{\rho^{\text{ref}}} + 1 \tag{9.16}$$

Refueling begins after hub arrival and lasts proportional to the transferred mass plus one hour of setup time.

Fuel limits and requirements

$$f^{\text{bef}}_{u,p} \geq F^{\text{minUSV}}, \tag{9.17}$$

$$f^{\text{aft}}_{u,p} \leq F^{\text{cap}}, \tag{9.18}$$

$$f^{\text{aft}}_{u,p} - f^{\text{bef}}_{u,p} \geq F^{\text{min}} r_{u,p} \tag{9.19}$$

USV fuel never drops below the emergency limit, never exceeds tank capacity, and each refuel event meets the minimum transfer requirement.

Fuel continuity (Big-M)

$$f_{u,0}^{\text{dep}} = F^{\text{cap}}, \tag{9.20}$$
$$f_{u,p}^{\text{dep}} \le f_{u,p-1}^{\text{aft}} + M(1 - r_{u,p-1}), \tag{9.21}$$
$$f_{u,p}^{\text{dep}} \ge f_{u,p-1}^{\text{bef}} - M(1 - r_{u,p-1}) \tag{9.22}$$

Fuel continuity switches between "after refuel" and "before refuel" depending on whether a refuel occurred previously.

Single-berth non-overlap

$$t_s^R \ge t_r^{\text{end}} - M(1 - b_{r,s}), \tag{9.23}$$
$$t_r^R \ge t_s^{\text{end}} - M b_{r,s} \tag{9.24}$$

Only one USV may refuel at a time; refuel events cannot overlap.

Hub mobility

$$|X_s - X_r| \le V_{\text{hub}}^{\max}(t_s^R - t_r^{\text{end}}) + M(1 - b_{r,s}) \tag{9.25}$$

The mothership cannot move faster than its physical mobility limit between consecutive refuels.

Hub fuel store feasibility

$$f_{u,p}^{\text{aft}} - f_{u,p}^{\text{bef}} \le S_0 + \eta^{\text{prod}} t_{u,p}^R - \sum_{q<r} g_{q,r} \tag{9.26}$$

Refuelled mass cannot exceed the mothership's fuel in storage plus onboard production minus previous allocations.

Return-to-port feasibility

$$t_u^{P1} - \left(t_u^{P0} + \tfrac{d^{\text{HP}}}{v(s)}\right) \le M(1 - r_{u,2}), \tag{9.27}$$
$$t_u^{P1} - \left(t_u^{P0} + \tfrac{d_{a(i)}^{\text{AP}}}{v(s)}\right) \le M r_{u,2}, \tag{9.28}$$
$$t_u^{P1} \le T^{\max} \tag{9.29}$$

Final port return uses AO→Port or Hub→Port distance depending on the last refuel event.

Equations governing Big-M logic form the key framework for route switching, fuel continuity, and single-berth coordination across all USVs.

10 | Appendix B — Reference Figures and Literature Data

10.1 Unmanned Systems Overview

This section explains the UXV types explored in the literture review. As seen the UAVs and the UUVs were placed to the appendix.

10.1.1 UAVs

In addition to USVs, UAVs are considered essential for mission support. Although the mothership is not intended to serve as an aircraft carrier, it is assumed to have a helicopter pad. Therefore, selected UAVs must be capable of vertical takeoff or be launched from a rail setup [84, 85, 86].

These UAVs are typically lightweight, with relatively low energy demands and limited endurance. As a result, they are not capable of carrying any of the heavy weapon systems that may be required by the mothership. However, their ability to cover large distances in short periods makes them well-suited for surveillance missions. This role remains a critical component of the mothership's overall operational capability and should be factored into the design. Table 10.1 lists the UAVs considered for this application.

UAV Name	Specifications	Energy Systems	Image
ScanEagle [84]	Wingspan: 3.1m Weight: 18kg Length: 1.5m	Fuel: Gasoline (2-stroke) Power: 500 W cruise Energy: 12 kWh Endurance: 24 hr	
JUMP 20 [85]	Wingspan: 5.5m Weight: 97kg Length: 2.9m	Fuel: Hybrid (Gasoline + Electric VTOL) Power: 4 kW Energy: 60 kWh Endurance: 14+ hr	
S-100 Camcopter [86]	Rotor Diameter: 3.4m Weight: 200kg Length: 3.1m	Fuel: Jet A-1 / Heavy Fuels Power: 25 kW cruise Energy: 170 kWh Endurance: 6 hr	

Table 10.1: Overview of Small UAVs for Shipboard Launch and Operation

As seen in Table 10.1, the types of UAVs considered range in mass from 18 kg to 200 kg, which is a considerable spread. However, this variation is minor when compared to the range of USVs shown in Table 10.3. Also insignificant is the energy demands of UAVs compared to the USVS, meaning these can be charged using the battery of the mothership with out having notable impact on the ships energy system. This topic will be further analyzed in section 2.1. For now, the specific choice of UAV remains open, as its impact on the overall system is limited. Ultimately, the actual operational use case will determine which UAV is selected, and that decision falls outside the scope of this literature study.

10.1.2 UUVs

UUVs are typically deployed for surveillance or for their weapons. Unlike UAVs, they benefit from buoyancy, which reduces weight constraints and makes them an interesting option to accompany the mothership. Torpedo systems and sonar equipment are examples of valuable payloads they can carry. However, one key limitation is their restricted ability to communicate. Submarines cannot easily receive signals from above the water and must rise to periscope depth to transmit or receive data [87]. This compromises one of their main advantages - stealth. While this issue can be mitigated by allowing UUVs to operate independently, it introduces additional complexity. In such a setup, the UUVs would need to receive mission parameters in advance and carry out their tasks autonomously, without real-time guidance or communication.

Another challenge is maintaining operational range with the mothership. Most existing UUVs are relatively small and lack the endurance to travel alongside a larger surface vessel for extended periods. As a result, they would need to be stored on the mothership and deployed when needed. This approach limits responsiveness and would take up space on the mother ship.

An overview of selected UUVs, ranging from small to large, is provided in Table 10.2 to give an idea of the types currently available.

UUV Name	Specifications	Energy Systems	Image
Gavia Offshore Surveyor [88]	Length: 2.7m Diameter: 20cm Weight: 100kg	Batteries: Lithium-ion Power: 800 W Energy: 11 kWh Endurance: 12 hr	
Iver4 900 [89]	Length: 4.6m Diameter: 23cm Weight: 200kg	Batteries: Lithium-ion Power: 1.5 kW Energy: 30 kWh Endurance: 20+ hr	
Saab Sabertooth [90]	Length: 3.0m Diameter: 0.5m Weight: 3 tons	Batteries: Lithium-ion Power: 2 kW Energy: 20 kWh Endurance: 20 hr	
Orca XLUUV [91]	Length: 15.5m Diameter: 2.6m Weight: 80 tons	Diesel-electric hybrid Power: 40 kW Energy: 8000 kWh Endurance: Several weeks	

Table 10.2: Overview of Selected UUVs for Shipboard and Autonomous Operations

As seen in Table 10.2, the first three UUVs have an endurance of only 20 hours, yet they still occupy substantial space if needed to be stored on the mothership. This limits the number that can be carried and deployed by the mothership. This makes them less practical for large-scale operations. Additionally, their small size prevents them from carrying any significant weapon systems.

This leaves the Orca XLUUV. As the name suggests, it is already classified as an "extra-large" UUV and is currently the largest of its kind available. The Orca is capable of long-duration missions, able to operate independently for weeks without refueling. For these reasons, this UUV is selected as the representative type for the purposes of this literature study.

USV-Size	Specifications	Ships	Ship Information	Image
Large USV-LUSV	Length: 60–140m Displacement: >500t	HMS Chiddingfold [92]	Length: 60m Gross Tonnage: 750t Fuel: F-76 NATO standard Energy: 450 MWh — 3.6 MW for 125 hr	
		ESVAGT Server [93]	Length: 72.0m Gross Tonnage: 2,568t Fuel: F-76 NATO standard Energy: 5170 MWh — 8.0 MW for 645 hr	
Medium USV-MUSV	Length: 25–60m Displacement: <500t	VSX 5209 [60]	Length: 53.2m Gross Tonnage: 454t Fuel: F-76 NATO standard Energy: 1690 MWh — 13.1 MW for 129 hr	
		Sea Hunter [94]	Length: 40m Gross Tonnage: 145t Fuel: F-76 NATO standard Energy: 526 MWh — 632 kW for 833 hr	
		Lightning Mk2 [95]	Length: 52.8m Gross Tonnage: 427t Fuel: F-76 NATO standard Energy: 950 MWh — 10.2 MW for 93 hr	
		510 OPV [96]	Length: 51m Displacement: 600t Fuel: F-76 NATO standard Energy: 650 MWh — 1.5 MW for 433 hr	

Table 10.3: Overview of Large and Medium USVs, Part 1

USV-Size	Specifications	Ships	Ship Information	Image
Small USV-SUSV	Length: <25m Displacement: <100t	CUSV [97]	Length: 11m Displacement: 8t Fuel: F-76 NATO standard Energy: 10.2 MWh — 425 kW for 24 hr	
		MANTAS T38 [98]	Length: 11.6m Displacement: 2.95t Fuel: F-76 NATO standard Energy: 10 MWh — 500 kW for 20 hr	
		Swiftships 23m [99]	Length: 23m Displacement: 50t Fuel: F-76 NATO standard Energy: 75.7 MWh — 4.1 MW for 18.5 hr	

Table 10.4: Overview of Small USVs, Part 2

10.1.3 Energy Requirements of All UXVs

To evaluate the feasibility of the mothership as an energy hub, the energy demands of all UXV types must be compared. The MUSV has been considered the most relevant UXV type and to visualize this comparison, all UXV examples listed in Tables 10.3, 10.4, 10.1, and 10.2 are plotted in a Ragone graph [100], shown in Figure 10.1. The Ragone graph compares the power and energy requirements of the different UXVs, with diagonal lines indicating endurance. All axes are plotted on a logarithmic scale.

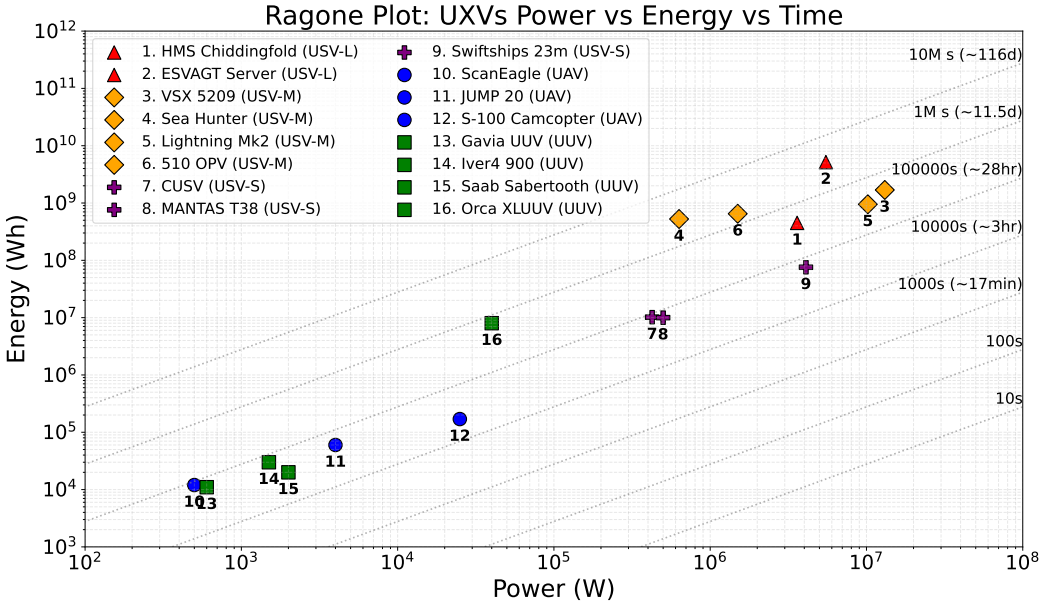

Figure 10.1: Ragone-style plot illustrating the relationship between installed power and energy capacity, indicating expected refueling intervals for various UXVs.

The Ragone plot in Figure 10.1 shows that USVs, particularly MUSVs, have by far the highest energy and power demands among the UXV types. This makes them the critical design driver for the mothership's energy system. In contrast, UAVs and UUVs require only a fraction of the energy—approximately 0.001% and 1% of a MUSV's demand, respectively. While appropriate refueling solutions for these smaller vehicles will be discussed, their impact on the sizing of the energy production system is negligible. As seen in Table 10.1 and Table 10.2, these vehicles use the same fuel type as the USVs or use electricity which can both be provided by the mothership, leaving no extra fuel producing system to be needed especially for them.

As established in section 2.1, the MUSV is the most energy demanding support unit and will be used as the baseline for selecting a suitable fuel type and defining the mothership's daily energy production capacity.

10.1.4 Very High Temperature Reactor

The VHTR, also referred to as the High Temperature Gas Reactor (HTGR), offers a strong combination of technological maturity, high thermal efficiency, and compatibility with synthetic fuel production. A typical VHTR design is illustrated in Figure 10.2.

VHTRs operate at core outlet temperatures between 700°C and 800°C, significantly higher than those of conventional reactors. This enables highly efficient heat conversion and makes them particularly suited for thermochemical processes such as hydrogen production and Fischer–Tropsch

synthesis. Helium, a chemically inert gas, is used as the coolant. Its lack of chemical reactivity minimizes corrosion issues and enhances reactor safety.

These reactors often employ modular pebble-bed or prismatic block designs, which can be scaled or adapted for marine applications [72]. Additionally, VHTRs use TRISO (TRi-structural ISOtropic) fuel particles, which encapsulate fissile material in multiple containment layers. This structure retains fission products even in high-temperature accident scenarios, offering exceptional passive safety [42].

However, VHTRs still face a number of practical challenges when considered for maritime deployment. While helium cooling eliminates corrosion concerns, it complicates heat exchange and containment due to its low density and high diffusivity. Furthermore, limited marine-specific adaptations exist.

Overal, while VHTRs technology is not yet matrure in the maritime setting, it represents one of the most promising reactor types for high-efficiency energy conversion on naval vessels.

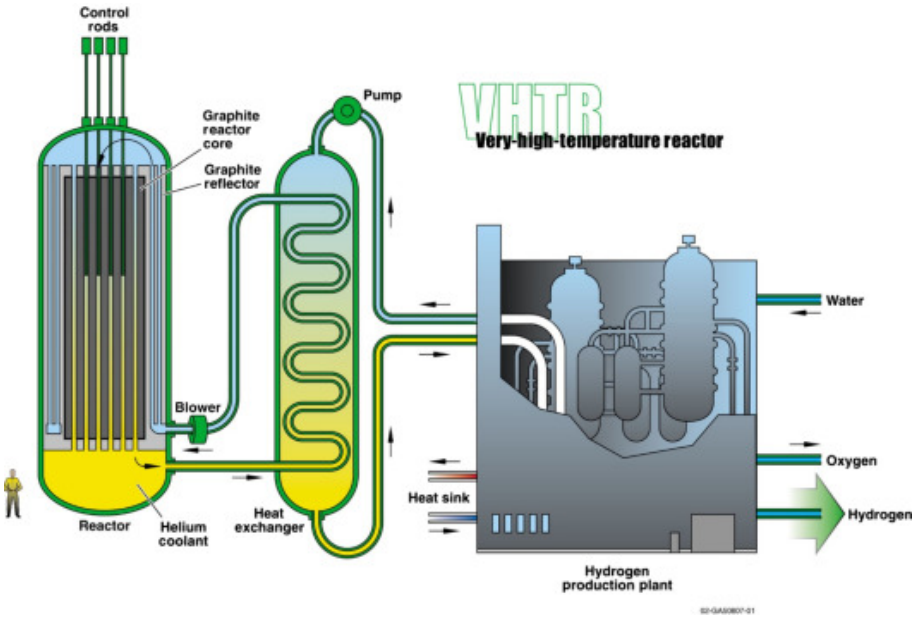

Figure 10.2: Typical Very High Temperature Reactor [38]

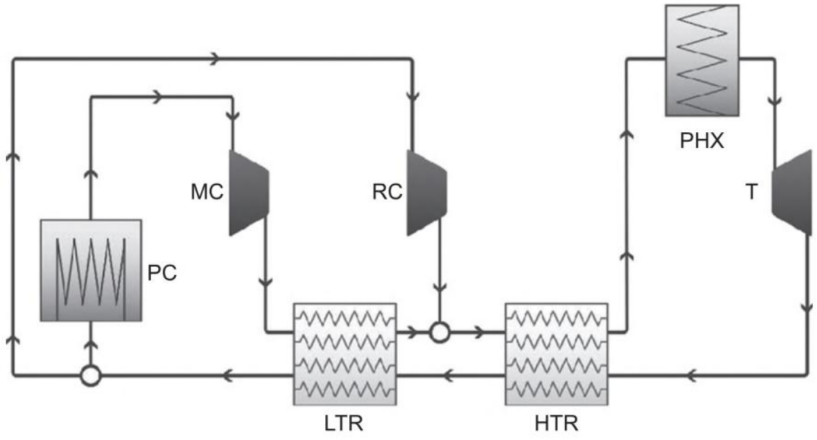

Figure 10.3: Brayton Recompression Cycle

10.2 Mothership energy system resizing

After having created the model of the energy system, each component was resized to see what tuning the modelled power and mass flows had as an effect on the overal system.

Table 10.5: Estimated Volume and Mass of Onboard Subsystems based on created simulink model

Subsystem	**Volume (m^3)**	**Mass (tonnes)**	**Description / Primary Weight Contribution**
Reactor Block 1	320	120	Nuclear reactor module including containment and shielding
Reactor Block 2	320	120	Nuclear reactor module including containment and shielding
Steam Superheater	280	112	High-temperature piping, heat exchangers, and thermal insulation
Deionizer	15	3	Water purification system and storage housing
SOEC Electrolyzer	800	358	Stack modules and electrical plant equipment
RWGS Reactor	20	24	Pressure vessel and catalytic reactor shell
Fischer–Tropsch Reactor	30	39	Reactor casing, piping network, and thermal management hardware
Hydrocracker	10	16	Reactor casing and internal catalyst beds
ATR Unit	15	17	Reformer chamber and process piping
DAC Towers	4 800	1 920	Main structural chemical plant; roughly 60% of the weight is due to air-handling fans
ESS	100	60	Battery modules, casings, and cooling system mass
Fuel Tank	700	560	F-76 fuel storage and tank reinforcement structure
Control Room	400	160	Steel-framed bridge
Crew Quarters	3 600	720	Accommodation spaces
Superstructure	9 600	1 920	Full top deckhouse forming the primary topside mass
Total Estimated	**20 118**	**6 147**	Majority of total mass located in DAC system, fuel tank, and superstructure

11 | Appendix C – Thesis Paper

Page intentionally left blank

Energy System Design for a Nuclear-Powered Refuelling Vessel Supporting Unmanned Maritime Vehicles

Submitted by

Ismar Klomp

Thesis Paper

In fulfilment of the requirements for the degree of
Master of Science
in Mechanical Engineering

at the Department Maritime and Transport Technology of Faculty Mechanical, Maritime and Materials Engineering of Delft University of Technology.

Student number:	4817761	
MSc track:	Multi-Machine Engineering	
Report number:	2025.MME.9132	
Supervisors:	Dr. Ir. Henk Polinder	TU Delft Supervisor
	Ir. Gert Jan Meijn	Damen Naval Supervisor
	Ir. Sankarshan Durgaprasad	TU Delft Daily Supervisor
Date:	28th November 2025	

Abstract:

This paper presents the design and modelling of a next-generation nuclear-powered mothership capable of serving as a self-sustaining refuelling hub for unmanned maritime vehicles. A 140 m vessel equipped with a 130 MW_{th} Very High Temperature Reactor was modelled as an integrated energy system that converts nuclear heat into synthetic diesel (F-76), through high-temperature electrolysis, direct air capture, and Fischer–Tropsch synthesis. An Energy Management System (EMS) was developed to coordinate power balance onboard. The EMS was extended with a mixed-integer linear programming layer, allowing fleet-wide optimisation of refuelling and mission timing for up to six unmanned surface vehicles. Mission scenario simulation results show that a nuclear mothership can maintain long-term autonomous operations with minimal external fuel dependence, providing a carbon-neutral alternative to conventional refuelling ships.

TU Delft

DAMEN NAVAL

1 Introduction

Modern warfare is being redefined before our eyes, the battlefield is no longer defined solely by size or tonnage. The war in Ukraine demonstrates how low-cost aerial drones and unmanned systems have disrupted traditional army structures and forced a reassessment of how military power is applied.[1]. Large surface ships are increasingly vulnerable, leading to new operational strategies that distribute combat and surveillance roles across multiple smaller units [1]. The U.S. Navy classifies these systems collectively as Unmanned "X" Vehicles (UXVs) [2]. For this paper, the focus is placed on the largest class of UXVs, the Unmanned Surface Vehicle (USV).

While this distributed approach increases resilience, it also introduces endurance and refuelling challenges, as small vessels cannot remain deployed for long durations without external energy supply. The U.S. Navy requires such fleets to operate for up to eight months [3], creating a clear demand for a reliable and continuous power source for these USVs.

To meet the continuous demand for fuel, this paper proposes a self-sustaining nuclear-powered refuelling ship capable of producing synthetic fuel at sea. Nuclear energy provides an exceptionally high energy density, as illustrated in Figure 1. This energy density enables continuous onboard fuel production, allowing the fleet to operate independently of the logistically complex and vulnerable refuelling supply chains used today [2, 4].

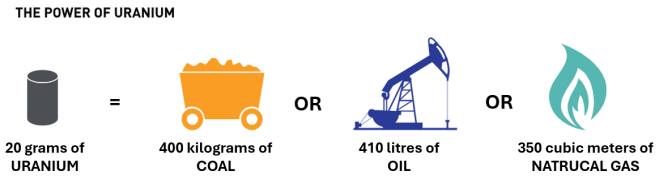

Figure 1: Energy density comparison between uranium and conventional fuels[2]

This paper focuses on the feasibility and operational scope of a nuclear-powered refuelling vessel capable of functioning as a self-sustaining energy hub. To assess this concept, the internal energy system of the mothership is modelled and scaled to determine its onboard fuel production capacity. Using this model, a series of mission scenarios are then developed to evaluate how effectively the vessel can refuel a fleet of USVs.

Modelling such an energy system requires not only an understanding of the thermodynamic and power demands of each subsystem but also of how energy is managed across the full system. This paper therefore extends to examining suitable energy management strategies in depth. A rule-based control structure is developed for internal energy distribution, and an additional fleet-wide scheduling optimisation layer is implemented to demonstrate the overall coordination capabilities of the system.

Based on the literature review in section 2, two key research gaps have been identified in the field of nuclear-powered ships and refuelling systems for autonomous fleets:

Gap 1: The integrated modelling of a nuclear-powered ship energy system that supports onboard fuel production has not been systematically investigated.

Gap 2: Energy Management Systems have been studied in isolated ship contexts, but their coordinated operation across reactor control, onboard energy distribution, and fleet-level refuelling scenarios remains largely unexplored.

These gaps leads to the central research question of this thesis:

Research Question: "What energy system design is needed for a nuclear-powered naval vessel to function as an independent energy hub for a fleet of unmanned maritime vehicles?"

2 Literature review

The concept of employing nuclear-powered ships as refuelling platforms for other vessels has been explored in research since as early as 1977 [5]. In parallel, the use of unmanned vehicles for surveillance, reconnaissance, and other naval operations has developed rapidly [6], establishing them as key components of future maritime defence systems.

The VSX 5209 [3] was selected as the reference USV for this study. This ship is a Medium USV as categories by the U.S. Navy [2]. This offshore patrol vessel of 60 meters is designed with a versatile deck layout that allows adaptation to a wide range of operational roles. It features powerful thrusters capable of 0-24 kn. Based the operational profile seen in subsection 8.2, the endurance of this ship is expected to be 5 to 6 days, giving them the capability of independently completing mission tasks but needing a refuelling ship to remain in the proximity to refuel. Its size and endurance also make it a good benchmark for evaluating the mothership's fuel production capability. The idea is that, if the mothership can meet the energy needs of a fleet of VSX 5209 vessels, it should also be capable of supporting a larger number of smaller units.

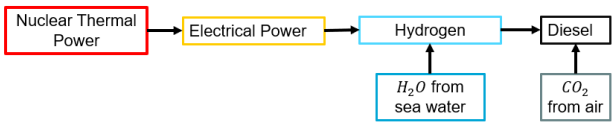

Figure 2: Selection of energy storage choices for nuclear power, including the required external inputs for conversion.

The nuclear mothership can store reactor power in several forms, as shown in Figure 2. Nuclear energy is released as heat [7] and converted to electricity through a thermodynamic cycle [8], but storing this electricity directly in batteries is infeasible for the USV because the required energy would result in excessive mass and volume [9], as illustrated in Figure 4.

[1] https://euro-sd.com/2025/03/articles/43406/naval-operations-lessons-from-recent-conflicts

[2] https://cna.ca/reactors-and-smrs/nuclear-fuel/

[3] Damen Naval VSX 5209

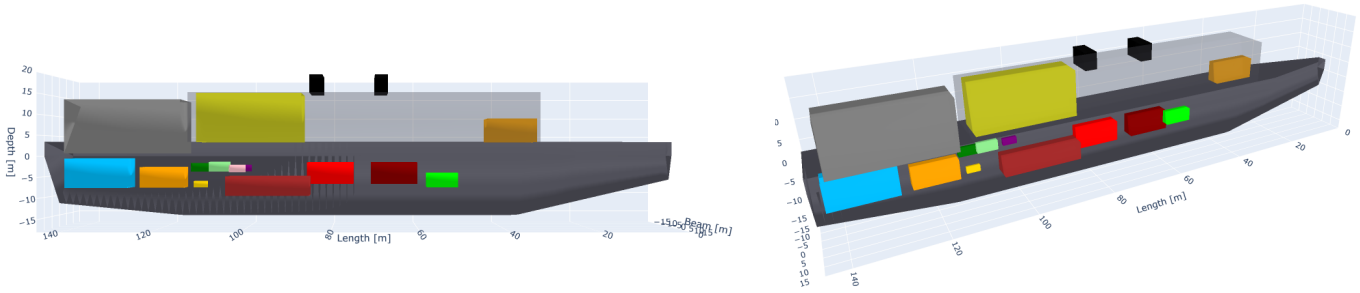

(a) Side view — hull and deck structure

(b) Rear view — propulsion and DAC modules

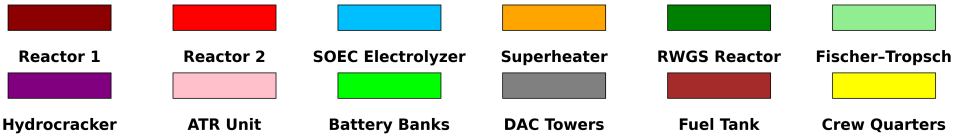

(c) Subsystem legend

Figure 3: 3D spatial feasibility model showing the side and rear views of the mothership, with subsystem legend.

Converting electrical power into hydrogen via electrolysis [10] is a second option. Using seawater purification systems that are already standard on naval vessels [11], modern Solid Oxide Electrolyser Cell (SOEC) systems can produce upwards of 50 tonnes of hydrogen per hour, as proven by the convergion of 37.5 $\mathrm{kWh\,kg_{H_2}^{-1}}$. However, hydrogen's low volumetric energy density, even when liquefied or compressed [12](Figure 4), cause large storage and safety concerns. These limitations motivate synthesising hydrogen into diesel, which offers high energy density, stable storage, and engine compatibility [13]; the required CO_2 can be obtained through onboard Direct Air Capture (DAC), identified as the most practical maritime solution [14, 15].

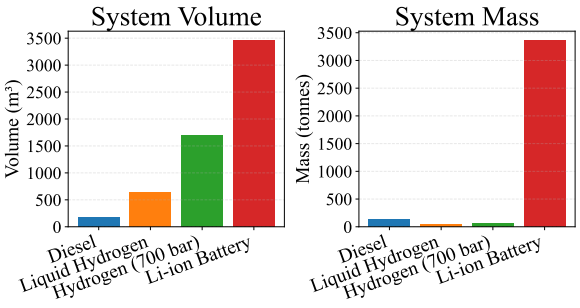

Figure 4: Mass and volume for equivalent energy storage by different sources. Data from [9, 16, 13]

Previous studies have explored the production of synthetic fuels aboard nuclear-powered ships [5, 17, 15, 18, 19, 20]. Among these, Bogart (2006)[15] provided the first modern and realistic component-level design, although the DAC system proposed at the time was not yet technically feasible. Subsequent work by Galla (2011)[18] still identified the DAC installation as considerably oversized, while Comidy (2019)[19] expanded the component modelling depth and concluded that such a system could be feasible with current technology. Kapoor (2024)[20] contributed the most recent sizing assessment. Despite these advances, none of the studies attempt to model the fuel-production chain as an integrated system, and real-world implementation and control are only briefly discussed. Notably, no work to date includes an EMS for coordinating the onboard energy flows.

EMS principles are well established in internal ship-level control, with recent developments introducing artificial intelligence and advanced control methods [21, 22]. The renewed interest in nuclear propulsion has increased research activity into nuclear-vessel-specific EMS, yet most work remains focused on safety and regulation [23, 24]. For fleet-wide EMS, broader reviews [25, 26] analyse EMS approaches for multi-energy systems combining diesel engines, fuel cells, and batteries. None, however, address the dynamic coupling of a nuclear reactor, fuel-synthesis plant, and shipboard loads. As a result, no verified EMS framework currently exists for a nuclear-powered refuelling ship.

To assess whether the proposed onboard energy architecture could physically fit within a ship, a feasibility study was performed by estimating subsystem volumes and arranging all major components inside a 145 m × 20 m × 15 m hull, a detailed account of the component sizing can be found in the accompanying report [27]. A 3D spatial model was then constructed and is shown in Figure 3. The DAC units is the largest componet occupying the aft section of the upper deck, while the reactor, fuel-production plant, ESS, and fuel tanks are all with in the hull of the vessel. This confirms that the full energy architecture fits within a realistic hull envelope, demonstrating the physical plausibility of the proposed design.

This literature review identifies the two research gaps as stated in section 1.

[3] `https://www.bloomenergy.com/bloomelectrolyzer/`

3 Energy System Modelling

The energy system model was designed based on original scaling experiments done in [27], refer to this previous work to obtain detailed reasoning behind values. Each major subsystem is implemented as an individual Simulink component, as shown in Figure 5. The overall model design consists of four core components:

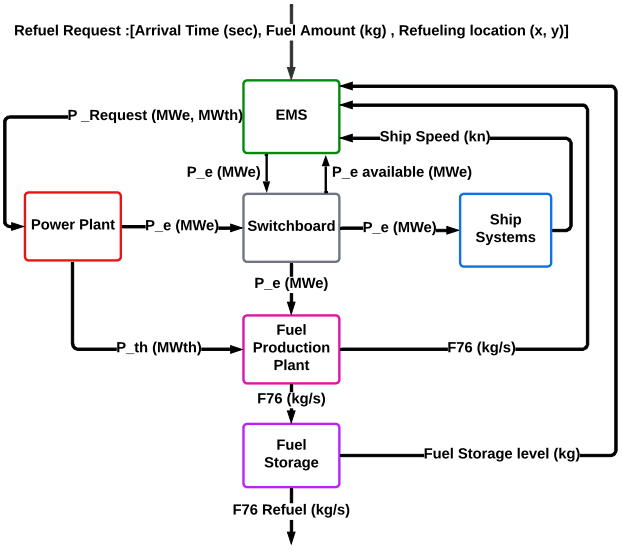

Figure 5: Ship Energy System Flow Chart

1. **Power Plant**: This subsystem represents the power generation. It includes the nuclear plant as the primary source and the Energy Storage System (ESS), which provides immediate short-term power support during rapid load changes.
2. **Ship Systems** This subsystem includes all onboard consumers that are not part of the fuel production plant, such as propulsion, hotel load, and auxiliary systems.
3. **Fuel Production Plant** This subsystem models the complete synthetic fuel production chain, from hydrogen generation through to final F-76 production.
4. **Energy Management System (EMS)** Acting as the supervisory control layer, the EMS governs power allocation, operational logic, and the interactions between all subsystems. The EMS design is discussed in detail in section 4.

This modular structure ensures that each subsystem can be validated independently. The full system is simulated on a second-by-second timescale, providing the high resolution required for the multi-week representative mission scenarios.

3.1 Power Plant: Nuclear plant

The nuclear reactor must be based a Small Modular Reactor (SMR) [28].

For the mothership, the primary reactor requirements are:

- Electrical output above 60 MW(e) to support continuous fuel production,
- Outlet temperature above 700°C for thermochemical integration,
- High efficiency over a wide operational range (30–90%),
- Ramp rates of 10–15% per minute for naval manoeuvrability,
- Compliance with naval safety and reliability standards.

The VHTR was selected as the most suitable option. VHTRs provide high outlet temperatures (700–850°C) using super critical CO_2, and incorporate strong passive safety features [29]. Their high conversion efficiency, reaching up to 45% [30], makes them well suited for powering a thermochemical fuel plant at sea.

The plant configuration follows established VHTR–Brayton cycle designs [31, 32, 29]. Reactor power is controlled using control rods [29]. Because the fuel production plant maintains a near continuous electrical load, Brayton cycle inventory or bypass control [33] is assumed not to be required. A cold dump is available for emergencies if too much heat is produced in the reactor and not used in the Brayton cycle.

Based on control-rod ramping limits [31], a ten-percent-per-minute ramp limit was applied to ensure realistic reactor behaviour. The maximum available thermal power for electricity generation $P_{\mathrm{e\_th,max}}$ is obtained by subtracting the direct thermal draw $P_{\mathrm{th,dir}}$ from the reactor limit $P_{\max}$:

$$P_{\mathrm{th,max}} = \max(P_{\max} - P_{\mathrm{th,dir}}, 0). \tag{1}$$

This thermal margin is converted to a maximum electrical limit $P_{\mathrm{e,max}}$ using the peak efficiency $\eta_{\max}$:

$$P_{\mathrm{e,max}} = \eta_{\max} P_{\mathrm{th,max}}. \tag{2}$$

The allowable change in electrical power $\Delta P_{\mathrm{e,ramp}}$ follows from the ramp rate r, previous efficiency η_{prev}, and timestep Δt:

$$\Delta P_{\mathrm{e,ramp}} = r \, \frac{\eta_{\mathrm{prev}}}{\eta_{\max}} P_{\mathrm{e,max}} \frac{\Delta t}{60}. \tag{3}$$

A lower ramp bound is applied to determine if the target electrical power $P_{\mathrm{e,target}}$ was less then maximum possible compared to the previous output $P_{\mathrm{e,prev}}$:

$$P_{\mathrm{e,target,lim}} = \max(P_{\mathrm{e,prev}} - \Delta P_{\mathrm{e,ramp}}, P_{\mathrm{e,target}}). \tag{4}$$

The updated electrical output P_{e} is then capped so it cannot rise faster than $\Delta P_{\mathrm{e,ramp}}$:

$$P_{\mathrm{e}} = \min(P_{\mathrm{e,prev}} + \Delta P_{\mathrm{e,ramp}}, P_{\mathrm{e,target,lim}}). \tag{5}$$

The resulting thermal nuclear power requirement P_{th} follows from the current efficiency η_{curr} and the direct thermal draw $P_{\mathrm{th,dir}}$:

$$P_{\mathrm{th}} = \frac{P_{\mathrm{e}}}{\eta_{\mathrm{curr}}} + P_{\mathrm{th,dir}}. \tag{6}$$

Power Plant: ESS

The reactor's ramp rate of ten percent per minute can lead to short periods where the power demand rises faster than the reactor can respond. Therefore, an ESS system is included to buffer these fluctuations.

The ESS is not intended for large-scale energy storage, as the fuel production plant itself already functions as the energy buffer. Instead, the ESS is included to sharpen the system's transient power response. The selected ESS provides 10 MWh of capacity with discharge and charge limits of 15 MW and 10 MW.

The battery model follows power-limited and capacity-limited behaviour. For a power request P_{req} (positive for discharge and negative for charge), the energy exchanged in a timestep Δt is

$$E = |P_{\text{actual}}| \, \frac{\Delta t}{3600}, \tag{7}$$

where P_{actual} is the power actually delivered after limiting. The discharge and charge powers are constrained by the maximum discharge and charge limits $P_{\text{max}}^{\text{dis}}$ and $P_{\text{max}}^{\text{ch}}$:

$$P_{\text{actual}}^{\text{dis}} = \min\big(P_{\text{req}},\, P_{\text{max}}^{\text{dis}}\big), \tag{8}$$
$$P_{\text{actual}}^{\text{ch}} = -\min\big(|P_{\text{req}}|,\, P_{\text{max}}^{\text{ch}}\big). \tag{9}$$

The state of energy (SOE) is updated using the discharge efficiency η_{dis} and charge efficiency η_{ch}:

$$\text{Discharge:} \qquad \text{SOE}_{k+1} = \text{SOE}_k - \frac{E}{\eta_{\text{dis}}}, \tag{10}$$
$$\text{Charge:} \qquad \text{SOE}_{k+1} = \text{SOE}_k + E\,\eta_{\text{ch}}, \tag{11}$$

subject to the capacity bound E_{max}:

$$0 \le \text{SOE}_{k+1} \le E_{\text{max}}. \tag{12}$$

3.2 Fuel Production Plant Model

A schematic overview of the fuel production system is shown in Figure 6. Electrical and thermal power serve as inputs to the plant, which converts the supplied energy into synthetic diesel.

3.2.1 Water Purification System

The fuel-production chain begins with seawater extraction and purification, as shown in Figure 6. Seawater is drawn through a low-inertia centrifugal pump [11]. Because the pump reacts almost instantaneously to shutdown commands but ramps up over several seconds, its behaviour is represented by a ramp-limited r_{sw} update of the seawater mass flow rate $\dot{m}_{\text{sw}}$:

$$\dot{m}_{\text{sw},k+1} = \dot{m}_{\text{sw},k} + \min\big(\Delta\dot{m}_{\text{sw}},\, r_{\text{sw}}\Delta t\big) \tag{13}$$

$$\Delta\dot{m}_{\text{sw}} = \dot{m}_{\text{sw,target}} - \dot{m}_{\text{sw},k}, \tag{14}$$

where $\dot{m}_{\text{sw,target}}$ is the power-limited target flow.

A small freshwater buffer tank governs the activation of the purification unit: the system switches on when the tank level falls below five percent and shuts down upon the water system when full, implementing a simple on–off control that avoids inefficient part-load operation.

The electrical demand of the purification block is tied to the freshwater mass-flow rate $\dot{m}_{\text{fw}}$. Using a specific energy requirement $E_{\text{spec}} = 0.5\ \text{kWh}\,\text{kg}^{-1}$, the electrical power draw becomes:

$$P_{\text{elec}} = \dot{m}_{\text{fw}}\,\frac{E_{\text{spec}}}{3600}, \tag{15}$$

Freshwater production is both power-limited and ramp-limited. The update of $\dot{m}_{\text{fw}}$ is

$$\dot{m}_{\text{fw},k+1} = \dot{m}_{\text{fw},k} + \max(-r_{\text{fw}}\Delta t,\ X)\,, \tag{16}$$
$$X = \min(\Delta\dot{m}_{\text{fw}},\ r_{\text{fw}}\Delta t)\,, \tag{17}$$

$$\Delta\dot{m}_{\text{fw}} = \dot{m}_{\text{fw,target}} - \dot{m}_{\text{fw},k}, \tag{18}$$

with the target flow $\dot{m}_{\text{fw,target}}$ determined by both available electrical power and seawater inflow.

3.2.2 Hydrogen Production System

The hydrogen subsystem consists of a steam superheater and a SOEC, operating sequentially as shown in Figure 6.

Superheater

Water is heated from ambient conditions to 700°C. The process consists of three stages [34]: sensible heating from $T_{\text{in}} = 25°\text{C}$ to $T_{\text{boil}} = 100°\text{C}$, the latent heat of vaporisation h_{vap}, and superheating of steam to the target temperature $T_{\text{target}} = 700°\text{C}$. The total thermal energy required per kilogram is

$$E_{\text{per,kg}} = c_{p,\text{liq}}\,(T_{\text{boil}} - T_{\text{in}}) + h_{\text{vap}} + Z, \tag{19}$$
$$Z = c_{p,\text{steam}}\,(T_{\text{target}} - T_{\text{boil}}), \tag{20}$$

where $c_{p,\text{liq}}$ and $c_{p,\text{steam}}$ are the specific heat capacities of liquid water and steam.

The maximum achievable mass-flow rate at 700°C follows directly from the available thermal power P_{thermal}:

$$\dot{m}_{700°\text{C}} = \frac{P_{\text{thermal}}}{E_{\text{per,kg}}}. \tag{21}$$

In the dynamic model, this target flow $\dot{m}_{\text{target}}$ is ramp-limited using a first-order constraint with ramp rate r_{sh}:

$$\dot{m}_{k+1} = \dot{m}_k + \max\Big(-r_{\text{sh}}\Delta t,\ \min\big(\Delta\dot{m},\ r_{\text{sh}}\Delta t\big)\Big), \tag{22}$$
$$\Delta\dot{m} = \dot{m}_{\text{target}} - \dot{m}_k. \tag{23}$$

This ramp model captures the heat-up delay, transport delay, and thermal inertia of the physical superheater system.

Solid Oxide Electrolyser

The SOEC performs high-temperature electrolysis, using both electrical power P_{elec} and thermal power P_{thermal} from the reactor. The specific energy required per kilogram of hydrogen consists of an electrical component E_{elec} and a thermal component E_{thermal}:

$$E_{\text{H}_2} = E_{\text{elec}} + E_{\text{thermal}}, \tag{24}$$

The maximum hydrogen production rate $\dot{m}_{\text{H}_2}$ is constrained by available electrical power P_{elec}, thermal power P_{thermal}, and superheated water supply $\dot{m}_{700°\text{C}}$:

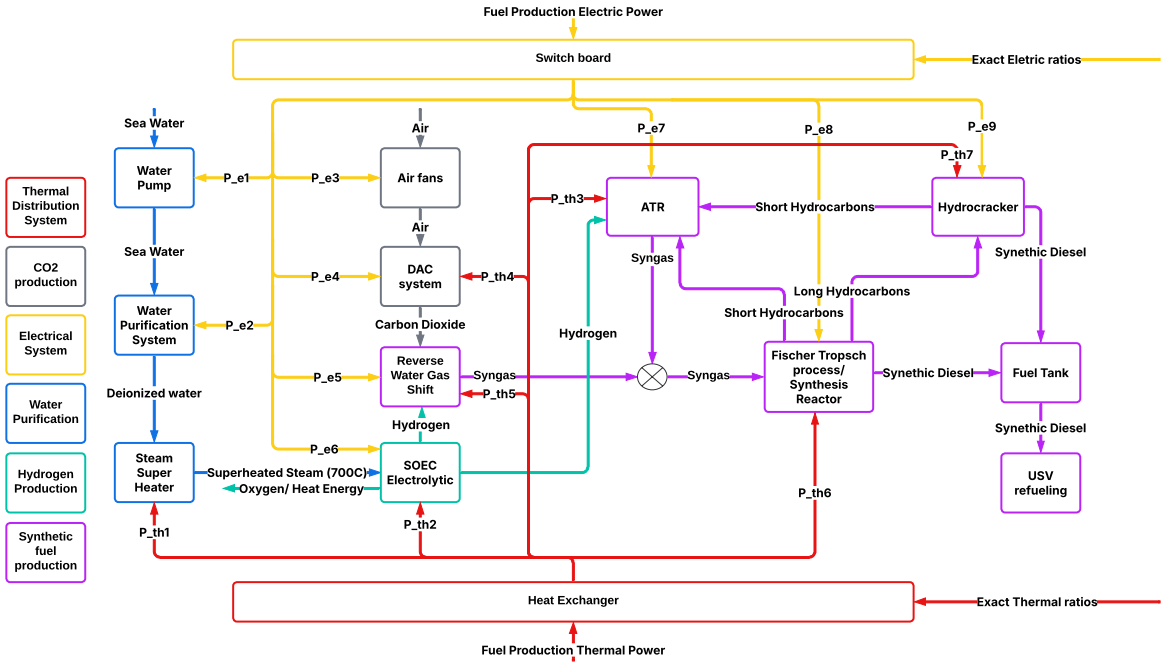

Figure 6: Schematic overview of the fuel production plant model.

$$\dot{m}_{\mathrm{H_2}} = \min\left(\frac{P_{\mathrm{elec}}}{E_{\mathrm{elec}}}, \frac{P_{\mathrm{thermal}}}{E_{\mathrm{thermal}}}, \frac{\dot{m}_{700^\circ\mathrm{C}}}{9}\right), \tag{25}$$

where 9 kg of water are required per kilogram of hydrogen produced.

A controller links the SOEC hydrogen flow $\dot{m}_{\mathrm{H_2}}$ to the CO_2 feed of the RWGS reactor, ensuring the stoichiometric ratio is maintained. This keeps the SOEC–RWGS pair within its optimal conversion range and stabilises the entire fuel-production chain.

3.2.3 CO_2 Production System

The CO_2 subsystem consists of an air fan and a DAC unit operating in sequence, as shown in Figure 6. Because atmospheric CO_2 concentration is only about 0.065%, very large airflows are required, making DAC the slowest and most energy intensive subsystem in the fuel production chain [35, 15, 20].

Air Fan System

The air fan converts electrical power P_{fan} into airflow $\dot{m}_{\mathrm{air}}$ through a linear power–flow relation using the specific energy $E_{\mathrm{per\,flow}} = 40\ \mathrm{W\,s\,kg^{-1}}$:

$$\dot{m}_{\mathrm{air}} = \frac{P_{\mathrm{fan}}}{E_{\mathrm{per\,flow}}}, \tag{26}$$

with a maximum airflow capacity of 3000 $\mathrm{kg\,s^{-1}}$.

To capture fan inertia, the dynamic airflow response is ramp-limited using the fan ramp rate r_{fan}:

$$\dot{m}_{k+1} = \dot{m}_k + \max\Big(-r_{\mathrm{fan}}\Delta t,\ \min\big(\Delta\dot{m},\ r_{\mathrm{fan}}\Delta t\big)\Big), \tag{27}$$

$$\Delta\dot{m} = \dot{m}_{\mathrm{air,target}} - \dot{m}_k, \tag{28}$$

where $\dot{m}_{\mathrm{air,target}}$ is the power-limited target airflow. This ensures realistic transient behaviour consistent with mechanical acceleration limits.

Direct Air Capture

The DAC unit receives electrical power P_{elec}, thermal power P_{thermal}, and airflow $\dot{m}_{\mathrm{air}}$, and outputs a CO_2 mass flow rate $\dot{m}_{\mathrm{CO_2}}$. Its maximum capture rate is limited by the most restrictive input:

$$\dot{m}_{\mathrm{CO_2}} = \min\left(\frac{P_{\mathrm{elec}}}{E_{\mathrm{elec}}}, \frac{P_{\mathrm{thermal}}}{E_{\mathrm{thermal}}}, \frac{\dot{m}_{\mathrm{air}}}{R_{\mathrm{air/CO_2}}}\right), \tag{29}$$

where the specific energy requirements are

$$E_{\mathrm{elec}} = 6.8 \times 10^{-6}\ \mathrm{MW\,kg^{-1}}, \tag{30}$$

$$E_{\mathrm{thermal}} = 4.04 \times 10^{-5}\ \mathrm{MW\,kg^{-1}}, \tag{31}$$

and the air–CO_2 mass ratio is $R_{\mathrm{air/CO_2}} = 1667$.

To reproduce the slow transient behaviour of DAC systems [36], the CO_2 production rate is updated through a capacity-dependent ramp model:

$$\dot{m}_{\mathrm{CO_2},k+1} = \dot{m}_{\mathrm{CO_2},k} + \Delta\dot{m}_{\mathrm{CO_2}}, \tag{32}$$

$$\Delta\dot{m}_{\mathrm{CO_2}} = \max\big(-r_{\mathrm{down}},\ \min\big(\dot{m}^{\max}_{\mathrm{CO_2}} - \dot{m}_{\mathrm{CO_2},k},\ r_{\mathrm{up}}\big)\big), \tag{33}$$

where the up- and down-ramp rates r_{up} and r_{down} are selected according to the current utilisation level. The DAC model uses three ramp regions, capturing the experimentally observed slow acceleration at low utilisation and faster response near nominal operation [36].

3.2.4 Synthetic Fuel Production System

The residual subsystems convert the hydrogen and CO_2 feeds into synthetic diesel, as shown in Figure 6. The process chain consists of four units operating in sequence: a RWGS reactor, a Fischer–Tropsch FT synthesis reactor, an ATR, and a hydrocracker. Together they form a closed recycling loop that maximises carbon utilisation and produces F–76 diesel as the final product.

Reverse Water Gas Shift Reactor

The RWGS unit converts CO_2 and H_2 into CO and H_2O, producing a syngas mixture with a target H_2/CO ratio of approximately 2:1. To achieve this, a feed molar ratio of 3:1 ($H_2 : CO_2$) is used, corresponding to a mass ratio of roughly $1 : 7.5$ [19]. The unit is constrained by electrical power P_{elec}, thermal power P_{thermal}, and available CO_2 inflow $\dot{m}_{\text{CO}_2}$. The overall reaction is

$$\text{CO}_2 + \text{H}_2 \rightarrow \text{CO} + \text{H}_2\text{O}. \tag{34}$$

Once CO_2 is converted to CO, the achievable syngas mass flow $\dot{m}_{\text{syngas}}$ is limited by CO production $\dot{m}_{\text{CO}}$, leftover hydrogen $\dot{m}_{\text{H}_2,\text{left}}$, and electrical power:

$$\dot{m}_{\text{syngas}} = \min\left(\dot{m}_{\text{CO}} + \dot{m}_{\text{H}_2,\text{left}},\ \frac{P_{\text{elec}}}{E_{\text{elec}}}\right), \tag{35}$$

Thermal power and the unit's intrinsic maximum capacity $\dot{m}_{\max}$ impose the final limits:

$$\dot{m}_{\text{syngas}} = \min\left(\dot{m}_{\text{syngas}},\ \frac{P_{\text{thermal}}}{E_{\text{thermal}}},\ \dot{m}_{\max}\right), \tag{36}$$

with specific energy requirements

$$E_{\text{elec}} = 1.4 \times 10^{-5}\ \text{MW}\,(\text{kg/s})^{-1}, \tag{37}$$

$$E_{\text{thermal}} = 3.57 \times 10^{-5}\ \text{MW}\,(\text{kg/s})^{-1}. \tag{38}$$

To capture RWGS thermal inertia and mixing delays, a ramp constraint is applied to the syngas flow using the ramp rate r_{rwgs}:

$$\dot{m}_{k+1} = \dot{m}_k + \max\Big(-r_{\text{rwgs}}\Delta t,\ \min(\Delta\dot{m},\ r_{\text{rwgs}}\Delta t)\Big), \tag{39}$$

where $\Delta\dot{m} = \dot{m}_{\text{target}} - \dot{m}_k$.

Fischer–Tropsch Reactor

Synthetic diesel is produced in the Fischer–Tropsch (FT) reactor, which converts syngas into long and short chain hydrocarbons. The overall reaction for producing an n-carbon alkane is

$$(2n+1)\,\text{H}_2 + n\,\text{CO} \rightarrow \text{C}_n\text{H}_{2n+2} + n\,\text{H}_2\text{O}. \tag{40}$$

The FT process generates a wide distribution of hydrocarbon chain lengths. As discussed in section 8, the combined action of the ATR and hydrocracker increases the usable diesel fraction from 40% to 60%, with all remaining material recycled back into syngas [37].

The achievable hydrocarbon production rate $\dot{m}_{\text{HC}}$ is limited by electrical power P_{elec}, syngas inflow $\dot{m}_{\text{syngas}}$, and reactor capacity $\dot{m}_{\max}$:

$$\dot{m}_{\text{HC}} = \min\Big(\frac{P_{\text{elec}}}{E_{\text{FT}}},\ \eta_{\text{conv}}\,\dot{m}_{\text{syngas}},\ \dot{m}_{\max}\Big), \tag{41}$$

where the specific electrical energy requirement and conversion efficiency are

$$E_{\text{FT}} = 1.443 \times 10^{-4}\ \text{MW}\,(\text{kg/s})^{-1}, \qquad \eta_{\text{conv}} = 0.92. \tag{42}$$

The hydrocarbon output is separated into short-chain, diesel-range (F-76), and long-chain fractions:

$$\dot{m}_{\text{short}} + \dot{m}_{\text{F-76}} + \dot{m}_{\text{long}} = \dot{m}_{\text{HC}}. \tag{43}$$

Autothermal Reformer

The ATR converts short-chain hydrocarbons into additional syngas. The achievable reforming rate $\dot{m}_{\text{ATR}}$ is limited by the available short-chain feed $\dot{m}_{\text{short,tot}}$, electrical and thermal power ($P_{\text{elec}}, P_{\text{thermal}}$), and the reactor capacity $\dot{m}_{\max}$:

$$\dot{m}_{\text{ATR}} = \min\Big(0.85\,\dot{m}_{\text{short,tot}},\ \frac{P_{\text{elec}}}{E_{\text{elec}}},\ \frac{P_{\text{thermal}}}{E_{\text{thermal}}},\ \dot{m}_{\max}\Big), \tag{44}$$

with specific energy requirements

$$E_{\text{elec}} = 2.3 \times 10^{-5}\ \text{MW}\,(\text{kg/s})^{-1}, \tag{45}$$

$$E_{\text{thermal}} = 1.04 \times 10^{-5}\ \text{MW}\,(\text{kg/s})^{-1}. \tag{46}$$

A ramp constraint is applied to $\dot{m}_{\text{ATR}}$ to capture thermal inertia and mixing delays.

Hydrocracker

The hydrocracker converts long-chain hydrocarbons $\dot{m}_{\text{long}}$ into shorter species. The intake flow is limited by electrical and thermal power and by the reactor capacity:

$$\dot{m}_{\text{feed}} = \min\left(\dot{m}_{\text{long}},\ \frac{P_{\text{elec}}}{E_{\text{elec}}},\ \frac{P_{\text{thermal}}}{E_{\text{thermal}}},\ \dot{m}_{\max}\right). \tag{47}$$

With hydrocracking efficiency $\eta = 0.9$, the converted mass flow is

$$\dot{m}_{\text{conv}} = \eta\,\dot{m}_{\text{feed}}. \tag{48}$$

The product split is

$$\dot{m}_{\text{F-76}} = 0.7\,\dot{m}_{\text{conv}}, \tag{49}$$

$$\dot{m}_{\text{short}} = 0.3\,\dot{m}_{\text{conv}}, \tag{50}$$

where the diesel fraction $\dot{m}_{\text{F-76}}$ exits the synthesis loop, and the short-chain fraction $\dot{m}_{\text{short}}$ is recycled to the ATR.

3.3 Fuel Storage

The mothership's internal F–76 tank receives inflow from the fuel-production chain and outputs fuel during scheduled refuelling. The maximum fuel capacity is 700 000 kg, with an initial level of 500 000 kg. This will allow fuel production to begin immediately at the start of each mission preventing inefficient use of nuclear reactor. The storage volume is deliberately smaller than that of conventional replenishment vessels [38], meaning the ship must relay on synthetic-fuel production to remain operational.

Each time step, the tank inventory is updated according to

$$M_{k+1} = M_k + (\dot{m}_{\text{in}} - \dot{m}_{\text{out}})\,\Delta t. \tag{51}$$

with $\dot{m}_{\text{in}}$ coming from the fuel production plant and $\dot{m}_{\text{out}}$ determined by ongoing refuelling operations.

3.4 Ship Systems Model

The ship systems block represents the non–fuel-production energy consumers on board, including propulsion and a fixed hotel load of $P_{\text{hotel}} = 3$ MW. The propulsion power is obtained from the remaining electrical power,

$$P_{\text{prop}} = \max\big(P_{\text{avail}} - P_{\text{hotel}},\ 0\big), \tag{52}$$

Using the current position $\mathbf{x}_k$ and target waypoint $\mathbf{x}_{\text{tgt}}$, the distance and direction vector are

$$d_k = \| \mathbf{x}_{\text{tgt}} - \mathbf{x}_k \|, \tag{53}$$

$$\hat{\mathbf{d}}_k = \begin{cases} \dfrac{\mathbf{x}_{\text{tgt}} - \mathbf{x}_k}{d_k}, & d_k > d_{\text{tol}}, \\ \mathbf{0}, & d_k \le d_{\text{tol}}, \end{cases} \tag{54}$$

with a tolerance radius $d_{\text{tol}} = 0.1$ km to avoid oscillatory behaviour near the waypoint.

The ship position is then updated using the propulsion speed $v_{\text{km s}^{-1}}$:

$$\mathbf{x}_{k+1} = \mathbf{x}_k + v_{\text{km s}^{-1}}\, \Delta t\, \hat{\mathbf{d}}_k, \tag{55}$$

while enforcing a no–overshoot condition:

$$\text{if } v_{\text{km s}^{-1}} \Delta t \ge d_k \quad \Rightarrow \quad \mathbf{x}_{k+1} = \mathbf{x}_{\text{tgt}}. \tag{56}$$

4 Energy Management System Design

At the heart of the mothership energy-system model lies the Local EMS, which governs all onboard energy flows on a second-by-second basis. It forms the stabilising layer of the model by regulating power flows, maintaining near-steady reactor operation, and ensuring realistic propulsion behaviour. While the Local EMS ensures consistent ship dynamics, it does not take advantage of the predictable operational structure of the USV mission. A optimisation layer was added to coordinate refuelling logistics across USVs. This Fleet-Wide EMS generates time–location refuelling requests for the the Local EMS to execute.

4.1 Local Energy Management System

The Local EMS uses a rule-based strategy because it provides transparent and verifiable behaviour in the absence of empirical data [25]. Its primary function is to distribute the available electrical power between ship operations and synthetic-fuel production:

$$P_{\text{total}} = P_{\text{ship}} + P_{\text{fuel}}. \tag{57}$$

Any surplus is routed to battery charging, while deficits are supplied through battery discharge. When the battery becomes depleted, the EMS automatically ramps down fuel-production power to prioritise propulsion and essential ship loads.

Ship motion is governed by a finite set of operational states (transit, refuel, drift, hold, return-to-port). Each state selects a target waypoint $\mathbf{x}_{\text{tgt}}$ and a desired sailing speed v_{cmd}, from which the EMS computes propulsion demand. Propulsion power follows the interpolated speed–power curve, the same as used by the ship systems in section 3. To ensure physical behaviour, propulsion power is ramp-limited:

$$\Delta P_{\text{ship}} = \max\big(-r_{\text{prop}},\, \min(P_{\text{ship}} - P_{\text{ship},k},\, r_{\text{prop}})\big), \tag{58}$$

where $r_{\text{prop}} = 30$ MW min^{-1} is used to make it seem instantaneous but to prevent oscillatory behaviour in the Power Plant.

Once propulsion and hotel loads are known, the EMS determines the power that can be directed to fuel production. The nominal available power is

$$P_{\text{fuel,nom}} = \max(P_{\text{target}} - P_{\text{ship}},\, 0)\,, \tag{59}$$

with the reactor operated at a fixed target level $P_{\text{target}} = 0.95\, P_{\max}$. Fuel-production power is smoothed using a moving-average/low-pass filter, where α is the filter coefficient:

$$P_{\text{fuel},k+1} = (1-\alpha)\, P_{\text{fuel},k} + \alpha\, P_{\text{fuel,raw}}, \tag{60}$$

$$\alpha = \frac{\Delta t}{\tau + \Delta t}, \qquad \tau = 5 \text{ s}, \tag{61}$$

which prevents rapid fluctuations from propagating into the thermochemical subsystems [39].

The electrical power demanded from the reactor is then

$$P_{\text{req}} = P_{\text{ship}} + P_{\text{fuel},k+1}, \tag{62}$$

and is ramp-limited using the reactor ramp rate r_{rxr}:

$$\Delta P_{\text{req}} = \max\big(-r_{\text{rxr}},\, \min(P_{\text{req}} - P_{\text{req},k},\, r_{\text{rxr}})\big), \tag{63}$$

with $r_{\text{rxr}} = 0.1\, P_{\max}$ per minute, consistent with the VHTR control model.

4.2 Fleet Wide EMS

The Fleet-Wide EMS is formulated as a Mixed-Integer Linear Program (MILP)[40] and implemented in Python using Gurobi. The optimisation jointly determines the ordering, timing, and location of refuelling events, the speed profile of each USV, the selection of operational areas (AOs), and the movement of the mothership.

Objective Function

$$\min J = \sum_{u\in U}\sum_{p\in P}\big(f^{\text{aft}}_{u,p} - f^{\text{bef}}_{u,p}\big) \;+\; \varepsilon \sum_{u\in U} t^{\text{end}}_{u,2}, \qquad \varepsilon \ll 1. \tag{64}$$

The optimisation minimises the total fuel refuelled $\big(f^{\text{aft}}_{u,p} - f^{\text{bef}}_{u,p}\big)$ across all USVs $u \in U$ and path segments $p \in P$, while adding a small penalty on total mission duration $t^{\text{end}}_{u,2}$

Constraint Structure The MILP enforces the following families of constraints.

1. *Task assignment:* Each task $i \in I$ must be assigned once, and every USV $u \in U$ must fill all three mission slots $p \in P$. The binary variable $a_{u,p,i}$ indicates whether USV u performs task i in slot p:

$$\sum_{u\in U}\sum_{p\in P} a_{u,p,i} = 1 \qquad \forall i \in I, \tag{65}$$

$$\sum_{i\in I} a_{u,p,i} = 1 \qquad \forall u \in U,\ p \in P. \tag{66}$$

2. *Travel geometry:* Travel times depend on sailing speed $v(s)$ for speed index $s \in S$. The binary $y_{u,p,s}$ selects the speed, and d denotes the travel distance:

$$t^{\text{in}}_{u,p} = t^{\text{start}}_{u,p} + \sum_{i,s} a_{u,p,i}\, y_{u,p,s}\, \frac{d}{v(s)}. \tag{67}$$

3. *AO dwell:* Each operational area $a \in A$ imposes a dwell time $\tau^{\text{AO}}_{a(i),p}$ for task i:

$$t^{\text{out}}_{u,p} = t^{\text{in}}_{u,p} + \sum_{i} a_{u,p,i}\, \tau^{\text{AO}}_{a(i),p}. \tag{68}$$

4. *Refuelling:* Only one USV may refuel at a time. Binary $b_{r,s}$ indicates whether refuel event r occurs before s; M is a big-M constant:

$$t^{R}_{s} \ge t^{\text{end}}_{r} - M(1 - b_{r,s}), \tag{69}$$

$$t^{R}_{r} \ge t^{\text{end}}_{s} - M b_{r,s}. \tag{70}$$

5. *Mothership mobility:* Mothership position during refuelling r is X_r. The Mothership speed limit is $V_{\text{hub}}^{\max}$:

$$|X_s - X_r| \le V_{\text{hub}}^{\max}\,(t_s^R - t_r^{\text{end}}) + M(1 - b_{r,s}). \quad (71)$$

6. *Mothership fuel stock:* Fuel transferred $f_{u,p}^{\text{aft}} - f_{u,p}^{\text{bef}}$ must not exceed the initial store S_0, produced fuel $\eta^{\text{prod}} t_{u,p}^R$, and remaining stock after earlier refuels $g_{q,r}$: $f_{u,p}^{\text{aft}} - f_{u,p}^{\text{bef}} \le S_0 + \eta^{\text{prod}}\, t_{u,p}^R - \sum_{q<r} g_{q,r}.$ (72)

7. *USV fuel feasibility:* Fuel before task p for USV u is $f_{u,p}^{\text{bef}}$, derived from departure fuel $f_{u,p}^{\text{dep}}$ minus: (i) travel burn, (ii) AO dwell burn, (iii) waiting burn. It must stay above the minimum safe fuel F^{minUSV}:

$$f_{u,p}^{\text{bef}} = f_{u,p}^{\text{dep}} - (\text{travel} + \text{dwell} + \text{wait}), \quad (73)$$

$$f_{u,p}^{\text{bef}} \ge F^{\text{minUSV}}. \quad (74)$$

8. *Return-to-port:* USV must return to port before the mission horizon $T^{\max}$. The time t_u^{P1} must account for either Mothership→port distance d^{HP} or AO→port distance $d_{a(i)}^{\text{AP}}$:

$$t_u^{P1} \le t_u^{P0} + \frac{d^{\text{HP}}}{v(s)}, \quad (75)$$

$$t_u^{P1} \le t_u^{P0} + \frac{d_{a(i)}^{\text{AP}}}{v(s)}, \quad (76)$$

$$t_u^{P1} \le T^{\max}. \quad (77)$$

The Fleet-Wide EMS optimisation aims to demonstrate that a feasible refuelling plan exists, so the MILP was solved with a relaxed optimality criterion. A MIPGap = 10% was used to limit computation time, meaning the solver stops once a solution within ten percent of the optimum is found.

5 Model Verification

This section verifies that the created model. Because no equivalent model of a nuclear powered fuel production vessel exists in the literature, external validation is not possible. Internal verification is therefore performed. Multiple simple tests where preformed in accompanying work[27], confirming correct steady-state behaviour and showing realistic ramp-up and ramp-down transitions. Based on this baseline, a mission-level refuelling test was executed in which the mothership transitions from stationary waiting to sailing at 10 kn while supplying fuel to a USV, before returning to the refuelling point at 17 kn, as shown in Figure 7.

Plot 1 in Figure 7 shows the vessel remaining stationary until approximately 0.8 h, after which it begins to accelerate. Plot 2 illustrates propulsion power rising from the 3 MWe hotel load to about 11 MWe, corresponding to a steady 10 kn sailing speed. During this acceleration, the ESS compensates for the reactor's ramp-limited behaviour, ensuring that fuel-production power remains undisturbed. Later, when propulsion demand reaches its peak, the ESS again supplies the shortfall, maintaining stable operation of the fuel plant.

Once the ship returns to the refuelling location, propulsion demand drops, but the EMS maintains reactor output at a level approximately 5 MWe above the ship load. This deliberate strategy recharges the ESS in preparation for the next manoeuvre.

A small deviation is observed during this phase: the direct thermal power briefly decreases. This occurs because the EMS correctly anticipates that the ESS will absorb electric fluctuations, but does not apply the same logic to thermal demand. As a result, the total thermal draw is lowered, which is not physically accurate. However, this has negligible impact on system behaviour because the fuel plant contains sufficient thermal buffering and the subsystems are not heat-limited. Plot 4 shows no noticeable effect, as the DAC and downstream units exhibit high thermal inertia. This behaviour should be refined in future work for improved realistic response.

6 Scenario Tests and Results

The energy model and EMS framework are evaluated across four mission scenarios: (i) Local, ship-centred EMS with constant USV task durations; (ii) Mission-aware EMS where the mothership intercepts USVs to reduce transit time; (iii) Same EMS as (ii) but with varying task durations to test adaptability; (iv) Fully coordinated Fleet-Wide EMS using MILP-based scheduling. The mission structure, developed with Damen Naval, is shown in Figure 8.

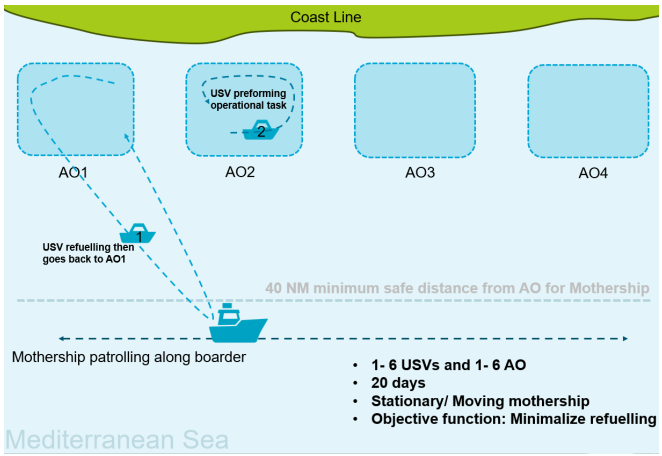

Figure 8: Overall mission structure used for the scenario tests.

To compare EMS strategies consistently, six KPIs were defined as in Table 1.

Table 1: Key Performance Indicators (KPIs) for EMS evaluation.

Name	Symbol	Description	Interpretation
Reactor Utilization	η_{reactor}	Avg. reactor P_{th} output vs max reactor P_{th} output.	Higher = Higher reactor efficiency.
Energy Efficiency	η_{energy}	P_{th} reactor converted into useful power (hotel load, propulsion or synthetic diesel).	Higher = Less energy losses.
Coordination Efficiency	η_{coord}	Inverse of total USV waiting time.	Higher = better synchronisation.
Fuel Retention	η_{fuel}	Final vs initial mothership fuel level.	Above 1 = indefinite fleet refuelling.
USV Fuel Utilization	$\eta_{\text{usv fuel}}$	Total fuel utilized by all USVs.	Higher = more USV fuel utilized.
Mission Success	η_{mission}	Fraction of completed USV missions.	Must be ≥ 1 for mission success.

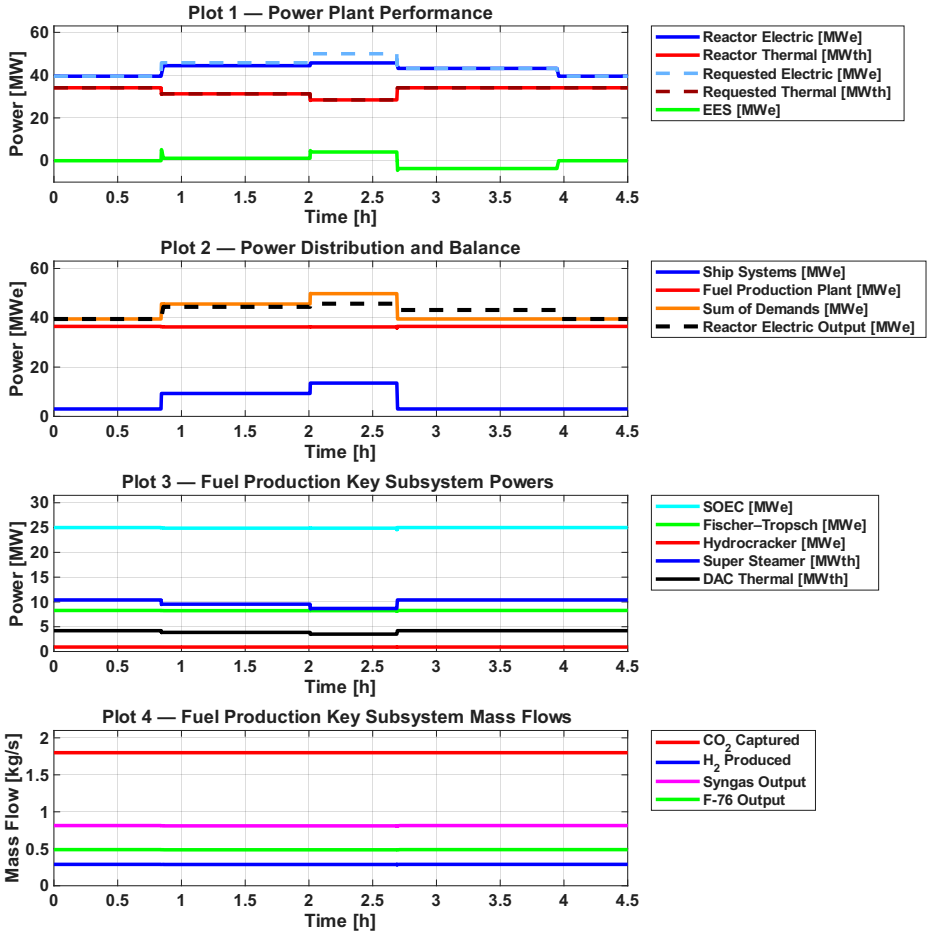

Figure 7: Mission-profile verification test showing propulsion power, reactor response, ESS compensation, and fuel-plant behaviour.

6.1 Scenario 1: Local Ship-Centred EMS

This first scenario serves as the baseline case, in which the mothership operates purely reactively: it has no knowledge of USV schedules and only responds to incoming refuelling requests. Each USV performs three fixed tasks in its assigned Area of Operation (AO) and in between each returns for refuelling. The mothership remaining stationary when arriving refuelling location. The resulting KPI values for different fleet sizes are shown in Table 2.

#USV	η_{reactor}	η_{energy}	η_{coord}	η_{fuel}	$\eta_{\text{usv fuel}}$	η_{mission}
1	0.77	0.17	1.00	1.38	0.69	1.00
2	0.95	0.16	1.00	1.38	0.69	1.00
3	0.95	0.16	1.00	1.07	0.69	1.00
4	0.95	0.16	0.99	0.51	0.69	1.00
5	0.95	0.16	0.72	0.05	0.46	0.93
6	0.95	0.16	0.46	0.10	0.24	0.61

High Moderate Low Poor

Table 2: Scenario 1: Local Ship-Centred EMS. KPI results for different fleet sizes.

The results indicate that the Local EMS operates effectively for one or two USVs, with performance declining slightly with three USVs. With four USVs the mission completes but is not self sustaining any more, as fuel shortages (η_{fuel}) and rising idle time (η_{coord}) show that the system is nearing its operational limit. Beyond this point missions fail entirely, as reflected by η_{mission}. The USV fuel utilisation metric $\eta_{\text{usv fuel}}$ remains constant up to four USVs because the rule-based EMS refuels every USV to the same level every time. Overall, the Local EMS can support only three USVs under constant-task conditions.

6.2 Scenario 2: Local Mission-Aware EMS (Constant Tasks)

The second scenario extends the baseline case by giving the mothership limited mission awareness. The mothership now relocates to refuelling points closer to each USV's AO, reducing transit distances and improving timing. The USV missions themselves remain unchanged, with each vessel completing three fixed tasks with refuelling stops in-between. The resulting KPI values are shown in Table 3.

#USV	η_{reactor}	η_{energy}	η_{coord}	η_{fuel}	$\eta_{\text{usv fuel}}$	η_{mission}
1	0.77	0.17	1.00	1.38	0.69	1.00
2	0.96	0.17	1.00	1.38	0.71	1.00
3	0.96	0.17	0.99	1.13	0.72	1.00
4	0.96	0.17	0.99	0.64	0.72	1.00
5	0.96	0.17	0.86	0.11	0.73	1.00
6	0.95	0.17	0.52	0.07	0.31	0.66

High Moderate Low Poor

Table 3: Scenario 2: Local Mission-Aware EMS (Constant Tasks). KPI results for different fleet sizes.

Allowing the mothership to reposition improves fuel retention (η_{fuel}) and reduces USV travel distance ($\eta_{\text{usv fuel}}$), enabling the system to technically support up to five USVs. However, operating at this scale introduces significant waiting times η_{coord}. For missions with more than three USVs, the fuel plant struggles to recover after early refuelling cycles, resulting in long idle periods for multiple USVs, This is clearly visible in Figure 9. Overall, the mission-aware EMS improves efficiency compared to scenario 1, but it remains self-sustaining only up to three USVs, with performance degrading rapidly beyond this level.

6.3 Scenario 3: Local Mission-Aware EMS (Varying Tasks)

This third scenario extends scenario 2 by introducing variation in USV task durations to create a more realistic and evenly distributed refuelling pattern. Important to note is that the total USV task duration remains identical across scenarios. The resulting KPI values are shown in Table 4.

#USV	η_{reactor}	η_{energy}	η_{coord}	η_{fuel}	$\eta_{\text{usv fuel}}$	η_{mission}
1	0.76	0.17	1.00	1.38	0.70	1.00
2	0.96	0.18	1.00	1.38	0.71	1.00
3	0.96	0.17	1.00	1.13	0.72	1.00
4	0.97	0.17	1.00	0.64	0.73	1.00
5	0.96	0.18	0.89	0.15	0.73	1.00
6	0.96	0.17	0.56	0.13	0.35	0.77

High Moderate
Low Poor

Table 4: Scenario 3: Local Mission-Aware EMS (Varying Tasks). KPI results for different fleet sizes.

The results show that a cause of varying task durations was reduced clustering of refuelling events, improving several KPIs, particularly in the five USV case. While fuel retention (η_{fuel}) remains largely unchanged due to the fixed production rate, coordination performance (η_{coord}) improves significantly, with roughly 250 hours less waiting time compared to scenario 2. For six USVs, the overall mission metric (η_{mission}) also increases, indicating more tasks were completed before failure. These findings show that even simple, varied task durations cause improved performance. This suggests that the mothership could use the varied task time to its advantage if it would structurally optimes the USVs schedules.

6.4 Scenario 4: Fleet-Wide EMS

This final scenario introduces the fleet-wide EMS, which adds a scheduling optimiser ontop of the local rule-based control as discussed in subsection 4.2. The optimiser determins the USV refuelling order, task sequence, and finding the optimal refuelling locations for the mothership. The resulting KPI values are shown in Table 5.

The results in Table 5 show substantial improvements in system performance. All missions are successfully completed (η_{mission}), waiting time is eliminated (η_{coord}), and fuel retention remains strong (η_{fuel}), staying above 1 up to four USVs and reaching 0.93 for five USVs. This is equivalently to the mothership still completing twelve consecutive missions before depleting its reserves.

#USV	η_{reactor}	η_{energy}	η_{coord}	η_{fuel}	$\eta_{\text{usv fuel}}$	η_{mission}
1	0.79	0.17	1.00	1.38	0.95	1.00
2	0.96	0.18	1.00	1.38	0.95	1.00
3	0.96	0.17	1.00	1.38	0.95	1.00
4	0.96	0.17	1.00	1.29	0.95	1.00
5	0.96	0.17	1.00	0.93	0.95	1.00
6	0.97	0.17	1.00	0.84	0.95	1.00

High Moderate
Low Poor

Table 5: Scenario 4: Fleet-Wide EMS (Varying Tasks). KPI results for different fleet sizes.

Figure 10 illustrates the six-USV case, where refuelling events are evenly distributed across the mission. A key improvement over the local EMS is that each USV can skip one refuelling stop, made possible by the high USV fuel-utilisation metric ($\eta_{\text{usv fuel}} = 0.95$), meaning each USV uses all fuel except its 5% emergency reserve. The optimiser also desynchronises task cycles by assigning USVs to AOs with different task durations (e.g., USV 5 performs two short tasks then a long one, while USV 3 completes three medium tasks). Overall, the Fleet-Wide EMS enables long-term operation with up to five USVs.

6.5 Results Discussion

The four scenarios together assess the refuelling limits of the nuclear-powered mothership, with KPI trends across all fleet sizes shown in Figure 11. Reactor utilisation η_{reactor} remains low for a single USV due to frequent shutdowns of the fuel-plant once the mothership's tanks are full, but increases as more USVs raise fuel demand. A similar pattern is observed in the energy-efficiency metric η_{energy}, which improves by three to five percent across scenarios because of more continuous propulsion loading. Since all scenarios use the same rule-based internal EMS, η_{energy} remains nearly identical across configurations, confirming expected behaviour for the internal KPIs.

The largest differences between EMS configurations appear in the coordination metric η_{coord}, fuel retention η_{fuel}, and mission completion η_{mission}. As seen in Figure 11, performance improves stepwise from Scenario 1 to Scenario 4, with the Fleet-Wide EMS maintaining strong values even at higher fleet sizes. The Local and Mission-Aware EMS types show growing waiting times, declining fuel retention, and eventual mission failures as more USVs are added. The USV fuel-utilisation metric $\eta_{\text{usv fuel}}$ also highlights this distinction: in the first three scenarios it remains nearly constant because the rule-based EMS always refuels each USV to the same level, whereas the Fleet-Wide EMS allows USVs to finish with only their required reserve, yielding more efficient use of onboard fuel.

To evaluate the EMS configurations holistically, the TOPSIS weighting method [41] was applied. All weights where kept equally at one. As shown in Figure 12, EMS choice has little influence for one or two USVs, but beyond this point the Fleet-Wide EMS clearly outperforms the others, achieving the highest multi-KPI score up to

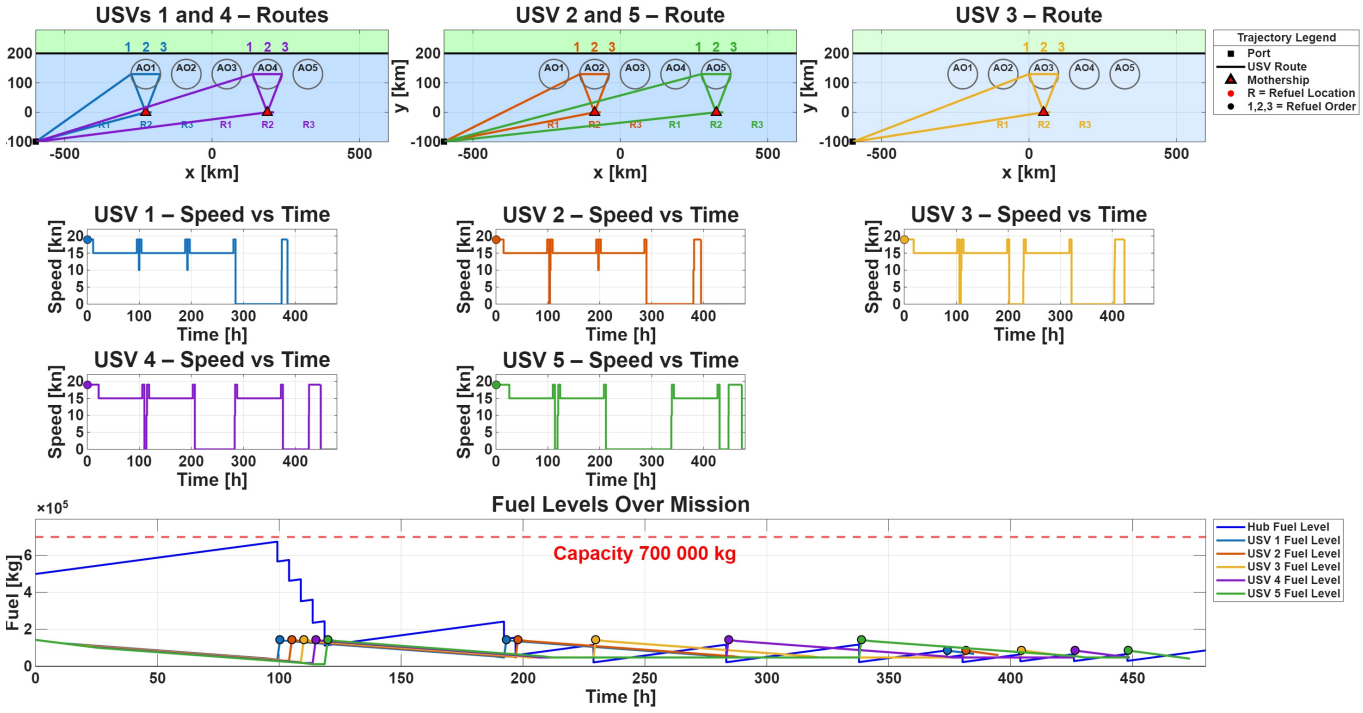

Figure 9: Local Mission-Aware EMS with 5 USVs and constant task times: route, speed, and fuel level plots.

five USVs with only a slight decline at six.

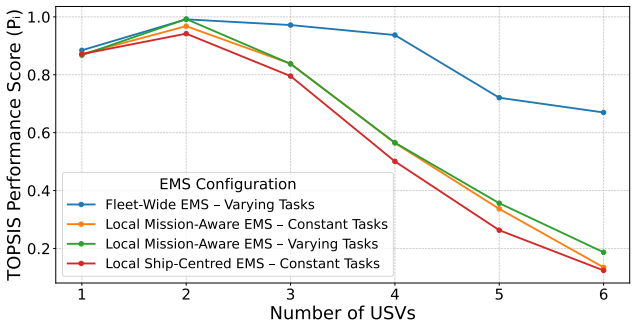

Figure 12: KPI TOPSIS scenario performance versus number of USVs.

7 Conclusion

This thesis set out to determine whether a nuclear-powered vessel could operate as a self-sustaining refuelling hub for a fleet of unmanned maritime vehicles. The completed model was evaluated for one to six USVs under three EMS configurations. The Local EMS supported small fleets but was not self-sustaining, while the Mission-Aware EMS improved efficiency through repositioning yet still experienced significant waiting times and declining fuel retention. The MILP-based Fleet-Wide EMS provided the most substantial improvement by coordinating refuelling timing, task order, and mothership positioning across the fleet, enabling six USVs to operate within mission limits and allowing five USVs to be supported sustainably.

Overall, the results show that small fleets can be managed without optimisation, but they do not fully utilise the mothership's fuel-production capability. Effective fleet-level coordination is therefore essential for unlocking the system's potential, demonstrating that the success of the nuclear refuelling ship concept relies not only on generation capacity, but on the integrated control that enables the fleet to operate as a unified, self-sustaining unit.

Recommendations and Future Work

1. Subsystem-level modelling and validation: Replace simplified input–output blocks with detailed thermodynamic and control models of the SOEC, DAC, and Fischer–Tropsch systems to assess true onboard feasibility.

2. Further development of the Fleet-Wide EMS: Explore how the EMS can be extended toward real-time optimisation to handle unpredictable scenarios, including the use of machine-learning methods to enable more autonomous, swarm-like behaviour among UXVs.

3. Identify optimal UXV combinations: Determine the range of UXV types that could operate within the mothership's logistical limits. Smaller platforms may reduce fuel-production requirements and allow the fleet to expand without increasing mothership size.

4. Multi-mothership operations: Extend the concept to coordinated fleets of refuelling motherships and study distributed refuelling strategies, inter-ship energy exchange, and cooperative EMS scheduling.

5. Alternatives to DAC: DAC remains the least mature and most space-intensive subsystem. Emerging offshore CO_2 storage reservoirs present a potential alternative source. If reservoirs become accessible for extraction, they could provide large CO_2 supply systems, thereby increasing fuel production on the Mothership.

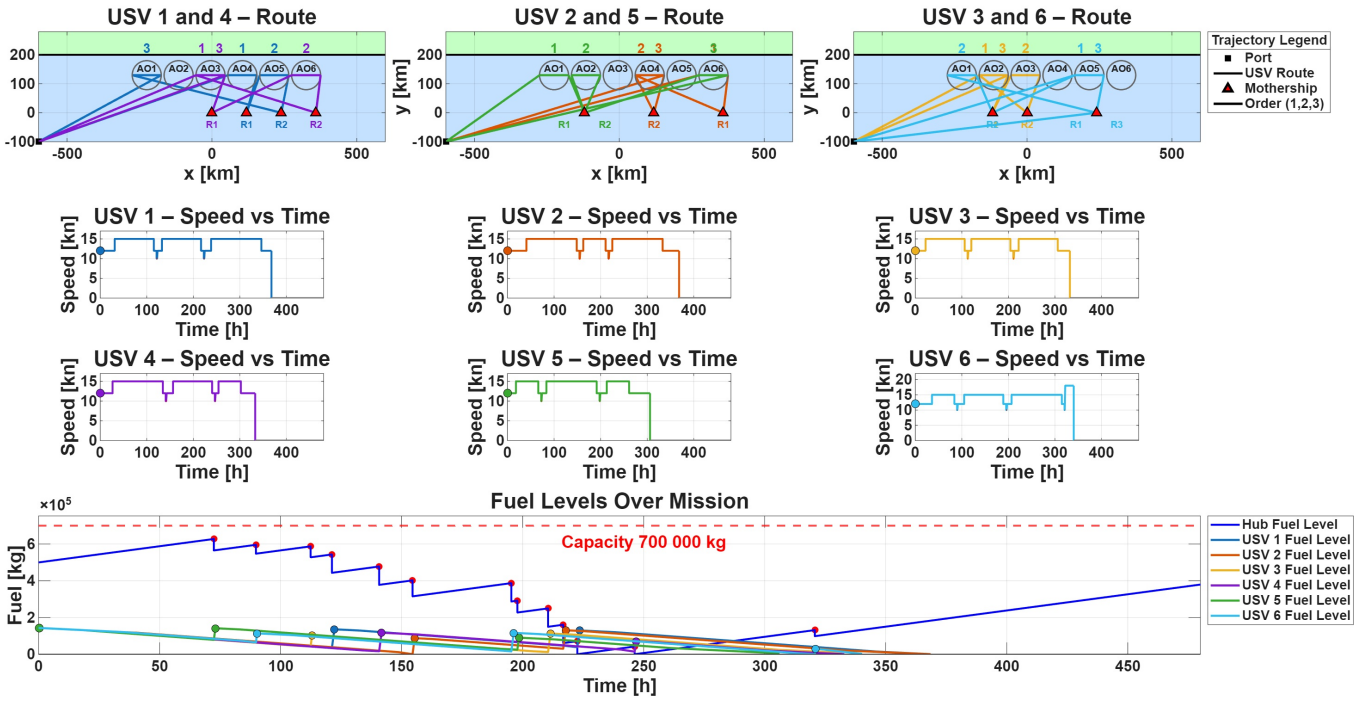

Figure 10: Fleet-Wide EMS with 6 USVs: route, speed, and fuel level plots.

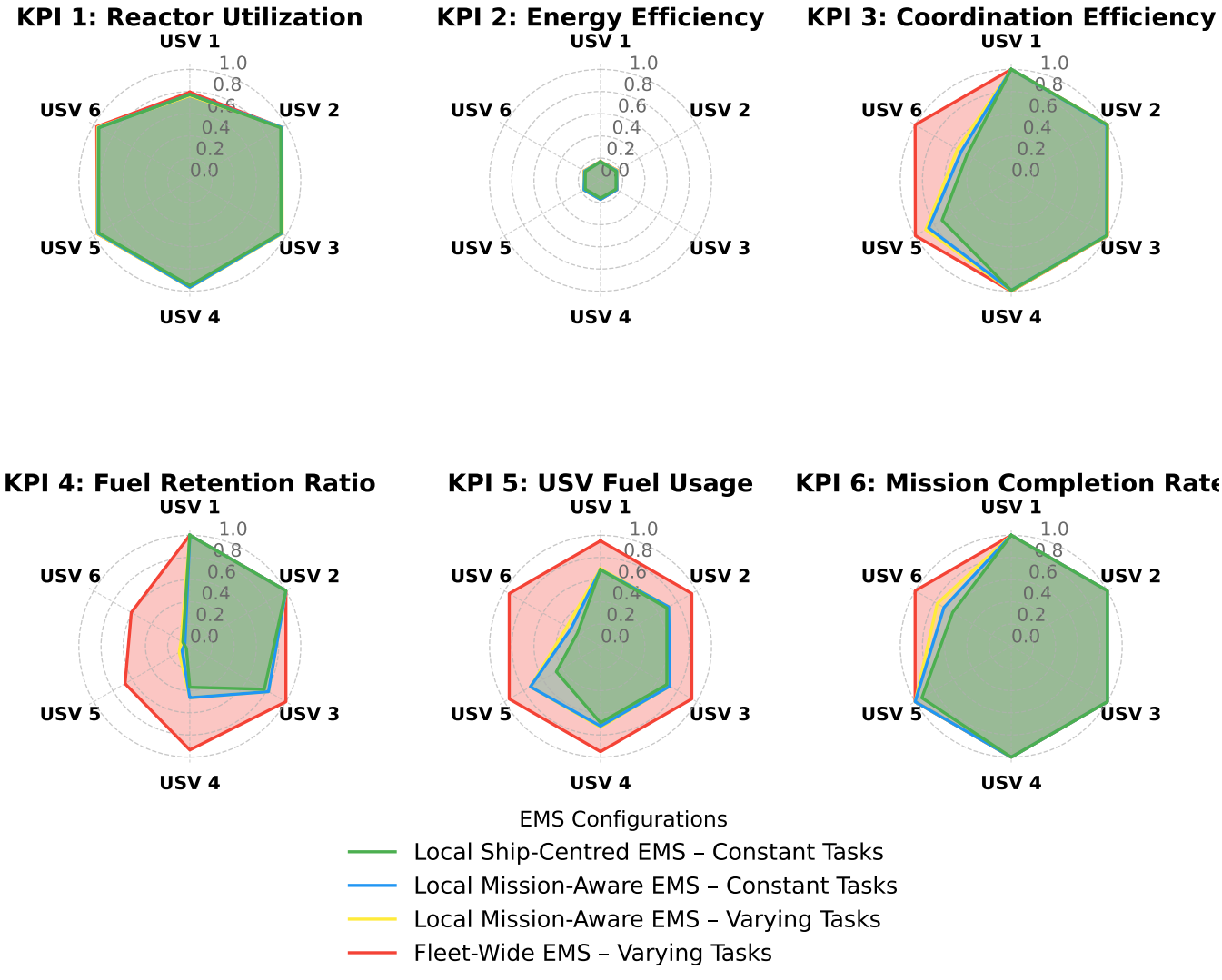

Figure 11: Spider plots showing KPI results per number of USVs for all four scenarios.

References

[1] Jacquelyn Schneider and Julia Macdonald. 'Looking Back to Look Forward: Autonomous Systems, Military Revolutions, and the Importance of Cost'. In: *Journal of Strategic Studies* 47.2 (2024), pp. 162–184. DOI: 10.1080/01402390.2022.2164570.

[2] Ronald O'Rourke. *Navy Large Unmanned Surface and Undersea Vehicles: Background and Issues for Congress*. Tech. rep. RL32418. Congressional Research Service, 2024. URL: https://crsreports.congress.gov/product/pdf/RL/RL32418.

[3] John C. Jackson et al. *Assessment of Deployment- and Mobilization-to-Dwell Policies for Active and Reserve Component Forces: An Examination of Current Policy Using Select U.S. Joint Force Elements*. Tech. rep. RR-A670-1. Santa Monica, CA: RAND Corporation, 2023. DOI: 10.7249/RRA670-1.

[4] Illia M. Diahovchenko et al. 'Resiliency-driven strategies for power distribution system development'. In: *Electric Power Systems Research* 197 (2021), p. 107327. ISSN: 0378-7796. DOI: https://doi.org/10.1016/j.epsr.2021.107327. URL: https://www.sciencedirect.com/science/article/pii/S0378779621003084.

[5] Robin Paul Bushore. 'Synthetic fuel generation capabilities of nuclear power plants with applications to naval ship technology.' PhD thesis. Massachusetts Institute of Technology, 1977.

[6] Alexandros Dimos et al. 'A Survey on UxV Swarms and the Role of Artificial Intelligence as a Technological Enabler'. In: *Drones* 9 (Oct. 2025), p. 700. DOI: 10.3390/drones9100700.

[7] William Edward Cummins and Regis Matzie. 'Design evolution of PWRs: Shippingport to generation III+'. In: *Progress in Nuclear Energy* 102 (2018). Shippingport 60th Anniversary: A Time to Take Stock of Nuclear Energy's Status, pp. 9–37. ISSN: 0149-1970. DOI: https://doi.org/10.1016/j.pnucene.2017.08.008.

[8] C. Wu and R. L. Kiang. 'Power Performance of a Nonisentropic Brayton Cycle'. In: *Journal of Engineering for Gas Turbines and Power* 113.4 (1991), pp. 501–504. DOI: 10.1115/1.2906268.

[9] 'A review of lithium-ion battery safety concerns: The issues, strategies, and testing standards'. In: *Journal of Energy Chemistry* 59 (2021), pp. 83–99. ISSN: 2095-4956. DOI: https://doi.org/10.1016/j.jechem.2020.10.017.

[10] Jurie Steyn and Christine Render. *Hydrogen as Energy Carrier*. Online resource. 2020. URL: https://www.researchgate.net/publication/339627476_Hydrogen_as_Energy_Carrier.

[11] Thomas Bacquart et al. 'Hydrogen for Maritime Application—Quality of Hydrogen Generated Onboard Ship by Electrolysis of Purified Seawater'. In: *Processes* 9.7 (2021), p. 1252. DOI: 10.3390/pr9071252.

[12] Marika Wieliczko and Ned Stetson. 'Hydrogen technologies for energy storage: A perspective'. In: *MRS Energy & Sustainability* 7 (2020), E41. DOI: 10.1557/mre.2020.43.

[13] Mahrokh Samavati et al. 'Synthetic Diesel Production as a Form of Renewable Energy Storage'. In: *Energies* 11 (May 2018), p. 1223. DOI: 10.3390/en11051223.

[14] R B Anderson. *Fischer-Tropsch synthesis*. 1984.

[15] S. Locke Bogart et al. 'Production of Liquid Synthetic Fuels from Carbon, Water, and Nuclear Power on Ships and at Shore Bases for Military and Potential Commercial Application'. In: *Proceedings of the 2006 International Congress on Advanced Power Plants (ICAPP 2006), Reno, NV*. 2006.

[16] Behdad Shadidi, Gholamhassan Najafi and Talal Yusaf. 'A Review of Hydrogen as a Fuel in Internal Combustion Engines'. In: *Energies* 14.19 (2021). DOI: 10.3390/en14196209.

[17] Kevin Brian Terry. 'Synthetic fuels for naval applications produced using shipboard nuclear power'. PhD thesis. Massachusetts Institute of Technology, 1995.

[18] John Michael Galle-Bishop, Charles W. Forsberg and Michael J. Driscoll. 'Nuclear tanker producing liquid fuels from air and water'. In: *Transactions of the American Nuclear Society* 104.1 (2011), pp. 589–590.

[19] Liam J. F. Comidy, Mark D. Staples and Steven R. H. Barrett. 'Technical, Economic, and Environmental Assessment of Liquid Fuel Production on Aircraft Carriers'. In: *Applied Energy* 256 (2019), p. 113810. DOI: 10.1016/j.apenergy.2019.113810.

[20] N. Kapoor and R. Pawling. 'Mobile Marine Fuel Generation Based on a Micro Nuclear Reactor'. In: *Proceedings of the International Naval Engineering Conference (INEC) 2024*. Institute of Marine Engineering, Science and Technology (IMarEST), 2024. DOI: 10.24868/11200.

[21] Truong M. N. Bui et al. 'An Energy Management Strategy for DC Hybrid Electric Propulsion System of Marine Vessels'. In: *2018 5th International Conference on Control, Decision and Information Technologies (CoDIT)*. IEEE, 2018, pp. 80–85. DOI: 10.1109/CoDIT.2018.8394800.

[22] JongHak Lee and JinSeok Oh. 'A Study on Load Monitoring Algorithms for EMS of Hybrid Electric Propulsion Ship'. In: *Journal of Advanced Marine Engineering and Technology* 48 (2024), pp. 402–413.

[23] Sidum Adumene et al. 'Advances in nuclear power system design and fault-based condition monitoring towards safety of nuclear-powered ships'. In: *Ocean Engineering* 251 (2022), p. 111156. ISSN: 0029-8018. DOI: https://doi.org/10.1016/j.oceaneng.2022.111156.

[24] Md Ibrahim Adham. 'Analysis and Optimal Planning of Nuclear-Renewable Hybrid Energy Systems for Ships'. MA thesis. Ontario Tech University, 2021. URL: https://hdl.handle.net/10155/1323.

[25] Xiuliang Zhao et al. 'Energy management strategies for fuel cell hybrid electric vehicles: Classification, comparison, and outlook'. In:

Energy Conversion and Management 270 (2022), p. 116179. ISSN: 0196-8904. DOI: https://doi.org/10.1016/j.enconman.2022.116179.

[26] D. Mitropoulou et al. 'Multi-objective Optimisation and Energy Management: Adapt Your Ship to Every Mission'. In: *Proceedings of the International Ship Control Systems Symposium (iSCSS)*. 2020. DOI: 10.24868/issn.2631-8741.2020.015.

[27] Ismar Klomp. 'Energy System Architecture for a Nuclear-Powered Refueling Vessel Designed to Support a Fleet of Unmanned Maritime Vehicles'. MA thesis. Delft, The Netherlands: Delft University of Technology, 2025.

[28] *Small Modular Reactors: Advances in SMR Developments 2024*. Non-serial Publications. Vienna: International Atomic Energy Agency, 2024. URL: https://www.iaea.org/publications/15790/small-modular-reactors-advances-in-smr-developments-2024.

[29] Jeffrey J. Powers and Brian D. Wirth. 'A review of TRISO fuel performance models'. In: *Journal of Nuclear Materials* 405.1 (2010), pp. 74–82. DOI: https://doi.org/10.1016/j.jnucmat.2010.07.030.

[30] Jerzy Gluch et al. 'Thermodynamic Efficiency of an Advanced 4th Generation VHTR Propulsion Engine for Large Container Ships'. In: *Polish Maritime Research* 31 (Dec. 2024), pp. 76–88. DOI: 10.2478/pomr-2024-0052.

[31] T. Wien and G. J. Meijn. 'Dynamic potential of naval nuclear power generation: modelling of a high-temperature reactor with a supercritical carbon dioxide power conversion cycle'. In: *Conference Proceedings of INEC*. 2024.

[32] Xing L. Yan. 'Chapter 3 - Very High Temperature ReactorThis book has a companion website hosting complementary materials.' In: *Handbook of Generation IV Nuclear Reactors (Second Edition)*. Second Edition. Woodhead Publishing Series in Energy. Woodhead Publishing, 2023, pp. 133–165. ISBN: 978-0-12-820588-4. DOI: https://doi.org/10.1016/B978-0-12-820588-4.00009-8.

[33] S. S. Gupta, P. Kumar and P. C. Gopi. 'Inventory Management and Control Options for Transient Operation of sCO2 Brayton Cycles'. In: *Proceedings of the ASME Turbo Expo 2025: Turbomachinery Technical Conference and Exposition*. Memphis, Tennessee, USA: ASME, 2025, V009T28A018. DOI: 10.1115/GT2025-153599.

[34] Mincho Hadjiski, Nencho Deliiski and Natalia Tumbarkova. 'Mathematical Description of the Latent Heat of Water Vaporization in Capillary Porous Materials'. In: 2019 (May 2020), pp. 1–9. DOI: 10.7546/itc-2019-0001.

[35] Sumudu Karunarathne et al. 'Review on CO2 removal from ocean with an emphasis on direct ocean capture (DOC) technologies'. In: *Separation and Purification Technology* 353 (2025), p. 128598. ISSN: 1383-5866. DOI: https://doi.org/10.1016/j.seppur.2024.128598.

[36] Omnya Al Yafiee et al. 'Direct air capture (DAC) vs. Direct ocean capture (DOC)–A perspective on scale-up demonstrations and environmental relevance to sustain decarbonization'. In: *Chemical Engineering Journal* 497 (2024), p. 154421. ISSN: 1385-8947. DOI: https://doi.org/10.1016/j.cej.2024.154421.

[37] Yujun Suo et al. 'Recent advances in cobalt-based Fischer-Tropsch synthesis catalysts'. In: *Journal of Industrial and Engineering Chemistry* 115 (2022), pp. 92–119. ISSN: 1226-086X. DOI: https://doi.org/10.1016/j.jiec.2022.08.026.

[38] Government of Canada, Department of National Defence. *Protecteur Class — Royal Canadian Navy*. 2025. URL: https://www.canada.ca/en/navy/corporate/fleet-units/surface/protecteur-class.html.

[39] Minhui Song et al. 'Design and Study of a Series Active Filter for the 10MW-Level High Power and High Stability DC Power Supply'. In: *IEEE Transactions on Applied Superconductivity* 32.6 (2022), pp. 1–5. DOI: 10.1109/TASC.2022.3172651.

[40] Christodoulos A. Floudas and Xiaoxia Lin. 'Mixed Integer Linear Programming in Process Scheduling: Modeling, Algorithms, and Applications'. In: *Annals of Operations Research* 139 (2005), pp. 131–162. DOI: 10.1007/s10479-005-3446-x.

[41] Majid Behzadian et al. 'A state-of-the-art survey of TOPSIS applications'. In: *Expert Systems with Applications* 39.17 (2012), pp. 13051–13069. ISSN: 0957-4174. DOI: https://doi.org/10.1016/j.eswa.2012.05.056.

8 Appendix A — Modelling and Simulation Framework

8.1 Simulink System Overview

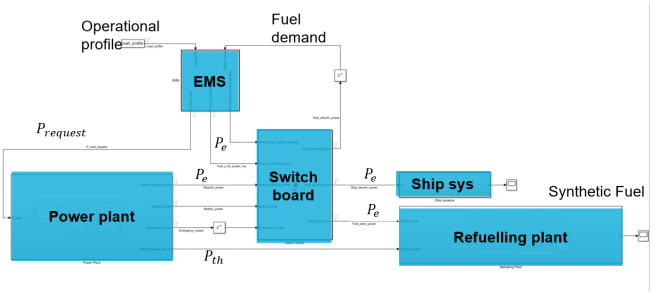

Figure 13: Overview of Simulink Energy Model

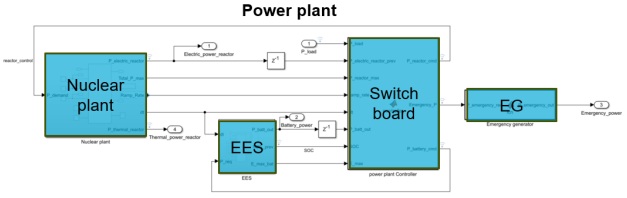

Figure 14: Simulink Power Plant Subsystem Design

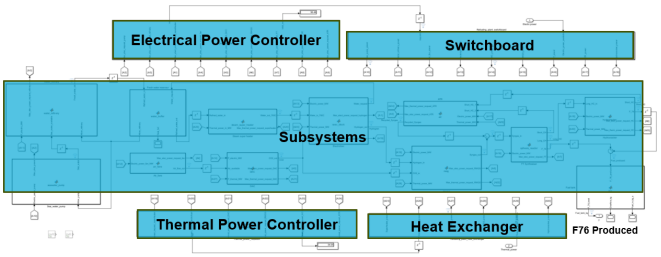

Figure 15: Simulink Fuel Production Plant Design

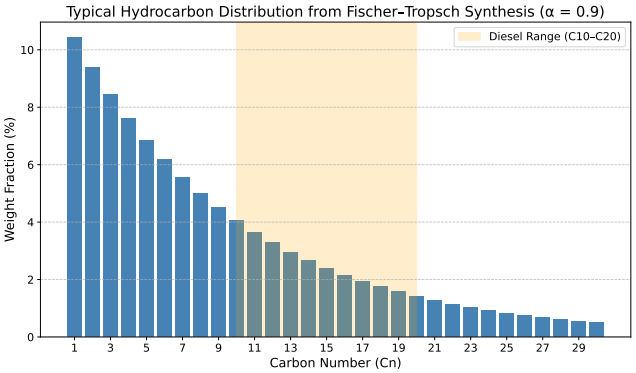

Figure 18: Fischer–Tropsch hydrocarbon distribution ($\alpha = 0.9$), based on [19].

Figure 18 illustrates the Anderson–Schulz–Flory (ASF) distribution for $\alpha = 0.9$, indicating that only the C_{10}–C_{20} fraction falls within the diesel range. The hydrocracker splits longer chains into usable diesel chains or smaller chains that are recycled into syngas by the ATR.

8.2 Operational profiles

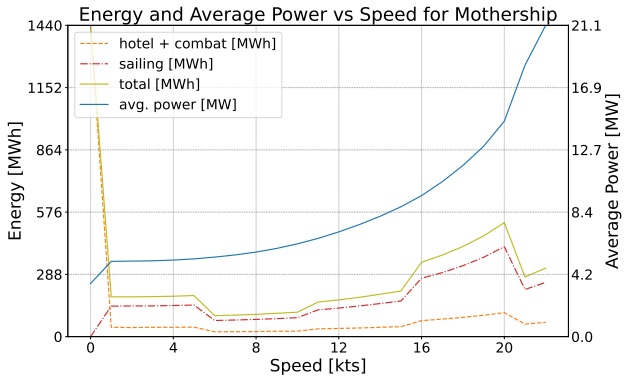

Figure 16: Operational profile of the mothership, derived from a generic Multi Purpose Support Ship (MPSS).

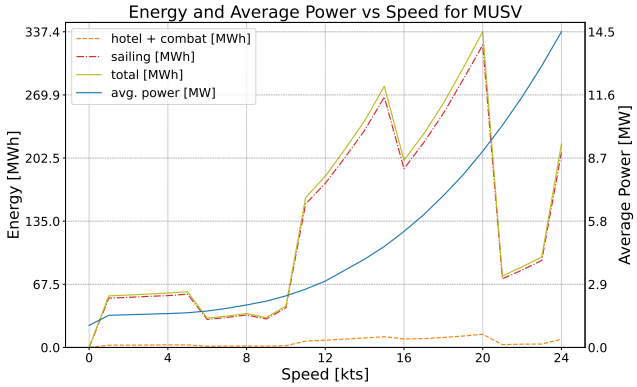

Figure 17: Energy spent versus speed (left axis) and average power at each speed (right axis).

Table 6: Symbols used in section 3

Symbol	Description
Reactor and ESS	
$P_{\text{th,max}}$, $P_{\text{e,max}}$	Max thermal and electrical power available after accounting for process heat.
$P_{\text{e,target}}$, $P_{\text{e,prev}}$	Requested and previous electrical output used for ramp-rate control.
η_{curr}, η_{prev}, η_{max}	Current, previous, and maximum reactor conversion efficiencies.
r	Reactor ramp-rate limit (fraction per minute).
SOE, E_{max}	Battery state of Energy and total capacity.
$P_{\text{max}}^{\text{dis}}$, $P_{\text{max}}^{\text{ch}}$	Max battery discharge and charge power.
η_{dis}, η_{ch}	Battery discharge and charge efficiency.
Ship Systems	
v_{knots}, $v_{\text{km/s}}$	Ship speed in knots and km/s.
$\mathbf{x}_k$, $\mathbf{x}_{\text{tgt}}$	Current ship position and target waypoint.
d_k, $\hat{\mathbf{d}}_k$	Distance to waypoint and its direction unit vector.
d_{tol}	Arrival tolerance radius (100 m).
Water Production (Pump + Purification)	
$\dot{m}_{\text{sw}}$, $\dot{m}_{\text{fw}}$	Seawater inflow and freshwater output mass flow.
$\dot{m}_{\text{sw,target}}$, $\dot{m}_{\text{fw,target}}$	Target flow based on pump power and purification availability.
r_{sw}, r_{fw}	Ramp-rate constants (pump and purification).
E_{spec}	Specific energy for purification (0.5 kWh kg^{-1}).
Superheater + SOEC	
T_{in}, T_{boil}, T_{target}	Inlet, boiling, and 700°C steam temperature.
$E_{\text{per,kg}}$	Total heat required per kg to reach 700°C.
$\dot{m}_{700^\circ\text{C}}$	Superheated steam flow.
r_{sh}	Superheater ramp-rate limit.
E_{elec}, E_{thermal}	Electrical and thermal specific energy for hydrogen production.
$\dot{m}_{\text{H}_2}$	Hydrogen mass-flow produced by SOEC.
Air Fan + Direct Air Capture	
$\dot{m}_{\text{air}}$	Airflow supplied to DAC.
$E_{\text{per flow}}$	Specific fan energy per airflow unit (40 W s kg^{-1}).
r_{fan}	Air-fan ramp-rate limit.
$\dot{m}_{\text{CO}_2}$	CO_2 capture rate.
$R_{\text{air/CO}_2}$	Air–to–CO_2 mass ratio.
RWGS	
$\dot{m}_{\text{CO}}$, $\dot{m}_{\text{H}_2\text{,left}}$	CO produced and hydrogen remaining after RWGS reaction.
$\dot{m}_{\text{syngas}}$	Total syngas output (CO + H_2).
$\dot{m}_{\text{max}}$	RWGS maximum syngas capacity.
Fischer–Tropsch Synthesis	
$\dot{m}_{\text{HC}}$	Total hydrocarbon output from FT reactor.
η_{conv}	Syngas conversion efficiency (0.92).
$\dot{m}_{\text{short}}$, $\dot{m}_{\text{F-76}}$, $\dot{m}_{\text{long}}$	Short, diesel-range, and long hydrocarbon fractions.
E_{FT}	Specific energy requirement for FT synthesis.
Autothermal Reformer	
$\dot{m}_{\text{short,tot}}$	Total short hydrocarbons sent to ATR.
$\dot{m}_{\text{ATR}}$	ATR syngas output.
Hydrocracker	
$\dot{m}_{\text{feed}}$	Long-chain hydrocarbon feed.
$\dot{m}_{\text{conv}}$	Converted fraction (90% of feed).